Zeitschrift: Helvetica Physica Acta

Band: 60 (1987)

Heft: 3

Artikel: Measurement of the deuteron tensorial and vectorial polarization : complete experimental reconstruction of the scattering amplitudes in the reaction pp d^+ at 447,515 and 580 MeV

Autor: Cantale, G. / Bach, P. / Degli-Agosti, S.

DOI: https://doi.org/10.5169/seals-115855

Helvetica Physica Acta, Vol. **60** (1987) 398–455

0018–0238/87/030398–58$1.50 + 0.20/0

Measurement of the deuteron tensorial and vectorial polarization. Complete experimental reconstruction of the scattering amplitudes in the reaction $pp \rightarrow d\pi^+$ at 447, 515 and 580 MeV

By G. Cantale, P. Bach, S. Degli-Agosti, Ph. Demierre, E. Heer, R. Hess, C. Lechanoine-Leluc, W. R. Leo[1]), Y. Onel, Ph. Sormani, D. Rapin and P. Y. Rascher

DPNC, University of Geneva, 1211 Geneva 4, Switzerland

and S. Jaccard

Schweizerisches Institut für Nuklearforschung, CH-5234 Villigen, Switzerland

(21. IV. 1986)

Abstract. Vectorial and tensorial deuteron polarization have been measured in the reaction $pp \rightarrow d\pi^+$ at 447, 515 and 580 MeV. From these measurements as well as earlier published data, the reaction scattering amplitudes have for the first time been reconstructed. They are compared with these from theoretical calculations. This analysis also provided indicative values for the dC effective analyzing powers for 150 to 350 MeV kinetic energy deuteron.

Introduction

To achieve a complete understanding of the nucleon-nucleon reaction, it has long been recognised that the study of the pion production channel $pp \rightarrow d\P$ is of greatest importance. To obtain this, detailed measurements of the spin dependence effects are necessary.

Experimental results were confined for years to cross-section or eventually analysing power measurements. But within the last 10 years, a renewed interest in this reaction coming in part (see Refs [1] and [2]) from controversial 'dibaryonic' structures stimulated detailed studies of the polarisation effects. A complete compilation of available $pp \rightarrow d\P$ data can be found in Refs. [3], [4], [5].

From a theoretical point of view, phase shift analyses as described in Refs [6] and [7] lead to a few possible resonances, but they all conclude that the data base is still insufficient to make a definitive statement.

---

[1]) Present address: IGA, Dept. of Physics, EPFL, 1015 Lausanne, Switzerland.

The $pp \rightarrow d\P$ reaction is described by 6 complex amplitudes. It is therefore necessary to measure polarisation parameters other than the usual asymmetries or correlation parameters as e.g. in Refs [8] and [9]. In particular direct deuteron polarisation measurements are necessary.

Three different techniques have been used up to now:

The first method consists in studying the reverse reaction $\P d \rightarrow pp$ where the deuteron target is polarised (see Ref. [10] for details): in this case only a single scattering experiment is needed. The main limitation of this method is the present technical status of polarised deuteron targets: at the moment, one can only have significant vectorial polarisation. A large technical development is being made at present at TRIUMF and at SIN to obtain a tensorial polarisation as large as 15%.

A second very elegant method is the one used in Ref. [11], where the scattered deuteron breaks up on a carbon target and the emerging proton polarisation is analysed in a polarimeter. About 90% of the deuteron's vector polarisation is transferred to the proton in the break up process; of course all tensor information is destroyed.

A third technique makes use of a polarimeter to measure the polarisation of the final state deuteron through a second scattering on carbon, e.g. [12], [13]. The principal drawback is the very sparse measured analysing powers for reaction involving polarised deuterons (Refs [14], [15], [16], [17]). This is the technique we have used for the following reasons: (1) in the group there was available a top quality polarimeter which was well understood because it had been extensively used in previous experiments (e.g. Refs [18], [19]); (2) we wanted to investigate the usefulness of a direct and systematic measurement of $d^{12}C$ analysing powers in the relevant range of deuteron kinetic energies (from 155 to 355 MeV); (3) last but not least, we were attracted by the possibility of measuring directly the different deuteron tensor polarisations in the $pp \rightarrow \pi d$ reaction, measurements which cannot be done with the two first techniques.

In 1981 when this work started, the following difficulties were encountered:

(1) No explicit and detailed $pp \rightarrow d\pi^+$ formalism for the observables and amplitudes was available: we, therefore, have worked out our own.
(2) No data on deuteron polarization were available; the only existing spin measurements were the correlation parameters.
(3) No knowledge of any deuteron analyzing power on any material was available in our energy range.
(4) The overall shape of the $pp \rightarrow d\pi^+$ amplitudes were unknown.

We will first describe the experimental method and specify the general observables we have measured without any theoretical assumptions. Unfortunately the ignorance of the $d^{12}C$ analysing powers forces us to perform a sophisticated analysis for the amplitude reconstruction as discussed in paragraph V and VI. At the same time $d^{12}C$ analysing powers were obtained. We hope, however, that direct analysing power measurement will be made in a near future at Saclay.

This paper is a condensed version of the PhD thesis of G. Cantale [71].

I. Theoretical considerations

1.1. *General formalism*

In these pages we shall use the conventions and notations given in Ref. [20], but for the reader it may be useful to refer to Refs [21], [22], [23], [24] to have a more complete understanding of tensorial formalism and polarisation experiments.

Let $|\psi\rangle$ be a general state in a $(2s+1)$-dimensional space with fixed momentum p. Let $|\mu\rangle$ be a basis in this space for a given frame, then we have

$$|\psi\rangle = \sum_{\mu} a_{\mu} |\mu\rangle \tag{1.1}$$

where $a_{\mu} = \langle \mu \mid \psi \rangle$ is called the amplitude.

The connection between two different frames (I and II) linked together by a rotation with Euler angles (α, β, γ) is given by

$$a^{\mathrm{I}}_{\mu} = \sum_{\mu'} D^{s}_{\mu\mu'}(\alpha, \beta, \gamma) a^{\mathrm{II}}_{\mu'} \tag{1.2}$$

where $D^{s}_{\mu\mu'}(\alpha, \beta, \gamma)$ are the usual rotation matrices, as defined in Ref. [25].

For a proton beam, if we have a number of particles $|\psi^i\rangle$, then we can define a density matrix

$$\rho_{\mu\mu'} = \sum_{i} w_i a^i_{\mu} a^{i*}_{\mu'} \tag{1.3}$$

where $\sum w_i = 1$ for normalisation.

From (1.3) we can deduce that

$$\rho_{\mu\mu'} = \rho^{*}_{\mu\mu'} \tag{1.4}$$

$$\mathrm{tr}\, \rho = \sum_{\mu} \rho_{\mu\mu} \tag{1.5}$$

and that the relation between rotated frames is given by

$$\rho^{\mathrm{I}}_{\mu\mu'} = \sum_{\nu\nu'} D^{s}_{\nu\mu}(\alpha, \beta, \gamma)^{*} D^{s}_{\nu'\mu'}(\alpha, \beta, \gamma) \rho^{\mathrm{II}}_{\nu\nu'} \tag{1.6}$$

We can now define the irreducible statistical tensors of rank k, $0 \leqslant k \leqslant 2s$, as

$$t_{kq} = (2s+1)^{1/2} \sum_{\mu\mu'} (-1)^{s-\mu} \langle s\mu', s-\mu \mid kq \rangle \rho_{\mu\mu'} \tag{1.7}$$

where $q = \mu' - \mu$, $-k \leqslant q \leqslant k$, and $\langle s\mu', s-\mu \mid kq \rangle$ are the Clebsch–Gordan coefficients and where the minus sign for μ comes from the Madison convention which we have adopted.

The hermiticity condition (1.4) gives us

$$t^{*}_{kq} = (-1)^{q} t_{k-q} \tag{1.8}$$

and it is easy to show that

$$t^{\mathrm{I}}_{kq} = \sum_{q'} D^{k}_{qq'}(\alpha, \beta, \gamma) t^{\mathrm{II}}_{kq'} \tag{1.9}$$

Here we see that, not only the rotational transformations are simpler than for the $\rho_{\mu\mu'}$, but also that the tensors of different ranks are not mixed.

We can also define the tensorial operators τ_{kq}

$$t_{kq} = \mathrm{tr}\,(\rho\tau_{kq}) = \sum_{\mu\mu'} (\tau_{kq})_{\mu\mu'} \rho_{\mu\mu'} \tag{1.10}$$

i.e.

$$(\tau_{kq})_{\mu\mu'} = (2s+1)^{1/2}(-1)^{s-\mu}\langle s\mu', s-\mu \mid kq\rangle \tag{1.11}$$

In such a way we have

$$(\tau_{00})_{\mu\mu'} = \delta_{\mu\mu'} \tag{1.12}$$

and

$$t_{00} = \mathrm{tr}\,(\rho) = 1. \tag{1.13}$$

For future use, we define as in Refs [22] and [26]

$$L_{kq} = \mathrm{Re}\,(t_{kq}) \qquad M_{kq} = \mathrm{Im}\,(t_{kq}) \tag{1.14}$$

As mentioned above, we adopt here the Madison convention [27], *i.e. the polarisation of a particle is such that the z-axis is along its momentum.*

If we now consider a two particle reaction such as $pp \to d\pi$, one can define a helicity frame of reference: the y-axis will be chosen perpendicular to the scattering plane. In such a reference system, the CM and laboratory axes remain the same for the beam and the target particles (see Fig. 1).

Let us now consider the general reaction $ab \to cd$. From (1.7) we can write

$$\rho_{\mu\mu'} = (2s+1)^{-1/2} \sum_{kq} (-1)^{s-\mu}\langle s\mu', s-\mu \mid kq\rangle t_{kq} \tag{1.15}$$

which, with (1.11), can be expressed in a matricial form:

$$\rho = \sum_{kq} t_{kq}\tau^{+}_{kq} \tag{1.16}$$

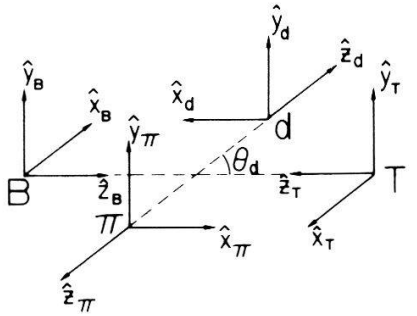

Figure 1
Definition of the helicity reference frame used here.

The initial density matrix ρ_i for the reaction will be written as

$$\rho_i = \rho_a \otimes \rho_b = \sum_{\substack{k_a q_a \\ k_b q_b}} t^a_{k_a q_a} t^b_{k_b q_b} (\tau^{a+}_{k_a q_a} \otimes \tau^{b+}_{k_b q_b}) \tag{1.17}$$

where $\otimes$ is the usual tensor product of spaces.

We define now the scattering matrix F as

$$\rho_f = F \rho_i F^+ \qquad FF^+ = F^+F, \quad (d\sigma/d\Omega)_0 = (2s+1)^{-1} \operatorname{tr}(FF^+) = I_0 \tag{1.18}$$

For a more explicit analysis of F we refer the reader to Section V; $(d\sigma/d\Omega)_0$ is the unpolarised cross section of the reaction (1.12). Using (1.12) we find then

$$\rho_f = FF^+ + \sum_{k_a>0, q_a} t^a_{k_a q_a} F(\tau^{a+}_{k_a q_a} \otimes \mathbb{1}_b) F^+ + \sum_{k_b>0, q_b} F(\mathbb{1}_a \otimes \tau^{b+}_{k_b q_b}) F^+ + \sum_{\substack{k_a, k_b>0 \\ q_a, q_b}} t^a_{k_a q_a} t^b_{k_b q_b} F(\tau^{a+}_{k_a q_a} \otimes \tau^{b+}_{k_b q_b}) F^+ \tag{1.19}$$

If we do measurement on the particle "c", we obtain

$$(d\sigma/d\Omega)_{\text{pol}} t^c_{k_c q_c} = \operatorname{tr}(\rho_f \tau^c_{k_c}) = (d\sigma/d\Omega)_0 \sum_{\substack{k_a k_b>0 \\ q_a q_b}} t^a_{k_a q_a} t^b_{k_b q_b} A^{k_a q_a k_b q_b}_{k_c q_c} \tag{1.20}$$

where

$$A^{k_a q_a k_b q_b}_{k_c q_c} = \operatorname{tr}[F(\tau^{a+}_{k_a q_a} \otimes \tau^{b+}_{k_b q_b}) F^+ (\tau^{c+}_{k_c q_c} \otimes \mathbb{1}_d)] / \operatorname{tr}(FF^+) \tag{1.21}$$

is the most general observable including polarisation measurement of the particle "c", and $(d\sigma/d\Omega)_{\text{pol}}$ is the polarised cross-section defined by $k_c = q_c = 0$.

If we apply the hermiticity condition (1.8), one obtains for our general observables

$$A^{k_a q_a k_b q_b}_{k_c q_c} = (-1)^{q_a + q_b + q_c} [A^{k_a - q_a k_b - q_b}_{k_c - q_c}]^* \tag{1.22}$$

Parity conservation gives (see Ref. [20])

$$A^{k_a q_a k_b q_b}_{k_c q_c} = (-1)^{k_a + k_b + k_c - q_a - q_b - q_c} A^{k_a - q_a k_b - q_b}_{k_c - q_c} \tag{1.23}$$

which combined with (1.22) gives

$$A^{k_a q_a k_b q_b}_{k_c q_c} = (-1)^{k_a + k_b + k_c} [A^{k_a q_a k_b q_b}_{k_c q_c}]^* \tag{1.24}$$

In addition, in the c.m. frame, the Pauli principle gives

$$A^{k_a q_a k_b q_b}_{k_c q_c}(\theta; b(a \to c)d) = (-1)^{q_a + q_b + q_c} A^{k_a q_a k_b q_b}_{k_c q_c}(\P - \theta, a(b \to c)d) \tag{1.25}$$

where θ represents the c.m. scattering angle of the particle "c".

1.2. $pp \rightarrow d\P$ Formalism

Now we will apply the results of Section 1.1 to our $pp \rightarrow d\pi$ case. *We shall name the particle "a" the beam (B) proton, the particle "b" the target (T) proton, "c" the deuteron (d) and, lastly, the particle "d" the pion* (¶). In such a way, the irreducible statistical tensor (1.7) for the beam polarisation and for the target will have only rank 1; that for the deuteron will present two possibilities, namely, rank 1 and rank 2; the pion is of course only a rank 0 particle. It is then possible to list all the observables (1.21) of the $pp \rightarrow d\P$ reaction, see Table 1. To make easier the writing of the observables we introduce more compacted symbols defined also in Table 1. There are *a priori* 144 observables if we use (1.24), but applying (1.23) and (1.25) we can reduce this number to 47 (see Table 2). Other linear relations between the observables, coming from parity rules, are derived in Ref. (24) p. 152; with these, we may simplify to only 36 linearly independent observables. Non linear equations permit to reduce this number to 11 physically independent observables.

Another set of observables, which may be of greater interest to the experimentalist, is the set of hybrid observables, where the beam and target polarisations are expressed in terms of cartesian polarisations p_x, p_y, p_z defined as follow

$$t_{10} = p_z \tag{1.26}$$

$$t_{1\pm1} = \mp(1/\sqrt{2})(p_x \pm ip_y) \tag{1.27}$$

Introducing (1.26) and (1.27) in (1.20) we can define in a straightforward way the following observables using a similar notation to that in Table 1:

$$A_{kq}^{xB} = -(1/\sqrt{2})(A_{kq}^{1B} - A_{kq}^{-1B}) \tag{1.28}$$

$$A_{kq}^{yB} = -(1/\sqrt{2})(A_{kq}^{1B} + A_{kq}^{-1B}) \tag{1.29}$$

$$A_{kq}^{zB} = A_{kq}^{0B} \tag{1.30}$$

Table 1
Explicit definitions of the $pp \rightarrow d\pi^+$ observables. The indices q, q' and q'' run from -1 to $+1$, and p from -2 to $+2$.

Observable	Symbol	Type	Name
$\left(\frac{d\sigma}{d\Omega}\right)_0$	I_0	Real	unpol. cross-sect.
A_{00}^{1q00}	A^{qB}	Imag.	analysing power
A_{00}^{001q}	A^{qT}	Imag.	asymmetry
$A_{00}^{1q'1q''}$	$A^{q'q''}$	Real	correlation
A_{1q}^{0000}	t_{1q}^0	Imag.	vectorial polar
A_{2p}^{0000}	t_{2p}^0	Real	tensorial polar
$A_{1q}^{1q'00}$	$A_{1q}^{q'B}$	Real	vect. pol. transfer
$A_{2p}^{1q'00}$	$A_{2p}^{q'B}$	Imag.	tens. pol. transfer
$A_{1q}^{001q'}$	$A_{1q}^{q'T}$	Real	vect. depolar.
$A_{2p}^{001q'}$	$A_{2p}^{q'T}$	Imag.	tens. depolar.
$A_{1q}^{1q'1q''}$	$A_{1q}^{q'q''}$	Imag.	vect. contribution
$A_{2p}^{1q'1q''}$	$A_{2p}^{q'q''}$	Real	tens. contribution

Table 2
Explicit list of the 47 left observables after having applied parity conservation and the Pauli principle. (The (s) or (a) letter indicates whether an observable is symmetric or antisymmetric.)

$I_0(\theta) = (d\sigma/d\Omega)|_0(\theta)$ (s)

$A^{1B}(\theta) = A^{-1B}(\theta) = -A^{1T}(\pi - \theta) = A^{-1T}(\pi - \theta)$

$A^{11}(\theta) = A^{-11}(\theta), \quad A^{1-1}(\theta) = A^{-11}(\theta), \quad A^{00}(\theta)$ (s)
$A^{10}(\theta) = -A^{-10}(\theta) = -A^{01}(\pi - \theta) = A^{0-1}(\pi - \theta)$

$t^0_{11}(\theta) = t^0_{1-1}(\theta)$ (a)

$t^0_{22}(\theta) = t^0_{2-2}(\theta), \quad t^0_{21}(\theta) = -t^0_{21}(\theta), \quad t^0_{20}(\theta)$ (s)

$A^{1B}_{11}(\theta) = A^{-1B}_{11}(\theta) = A^{1T}_{11}(\pi - \theta) = A^{-1T}_{11}(\pi - \theta),$
$A^{1B}_{10}(\theta) = -A^{1B}_{10}(\theta) = -A^{1T}_{10}(\pi - \theta) = A^{-1T}_{10}(\pi - \theta)$
$A^{1B}_{1-1}(\theta) = A^{1B}_{11}(\pi - \theta) = A^{1T}_{1-1}(\pi - \theta) = A^{-1T}_{11}(\pi - \theta),$
$A^{0B}_{11}(\theta) = -A^{0B}_{1-1}(\theta) = -A^{0T}_{11}(\pi - \theta) = A^{0T}_{1-1}(\pi - \theta)$
$A^{0B}_{10}(\theta) = A^{0T}_{10}(\pi - \theta)$

$A^{1B}_{22}(\theta) = A^{-1B}_{2-2}(\theta) = -A^{1T}_{22}(\pi - \theta) = -A^{-1T}_{2-2}(\pi - \theta),$
$A^{1B}_{21}(\theta) = -A^{-1B}_{2-1}(\theta) = A^{1T}_{21}(\pi - \theta) = -A^{-1T}_{21}(\pi - \theta),$
$A^{1B}_{2-2}(\theta) = A^{-1B}_{22}(\theta) = -A^{1T}_{2-2}(\pi - \theta) = -A^{-1T}_{22}(\pi - \theta),$
$A^{0B}_{22}(\theta) = -A^{0B}_{2-2}(\theta) = A^{0T}_{22}(\pi - \theta) = -A^{0T}_{2-2}(\pi - \theta)$
$A^{0B}_{21}(\theta) = A^{0B}_{21}(\theta) = -A^{0T}_{21}(\pi - \theta) = -A^{0T}_{2-1}(\pi - \theta)$

$A^{10}_{11}(\theta) = A^{-1-1}_{1-1}(\theta), \quad A^{10}_{11}(\theta) = -A^{-10}_{1-1}(\theta) = A^{01}_{11}(\pi - \theta) = -A^{0-1}_{11}(\pi - \theta)$
$A^{1-1}_{11}(\theta) = A^{-11}_{1-1}(\theta) = -A^{-11}_{11}(\pi - \theta) = -A^{1-1}_{1-1}(\pi - \theta)$
$A^{00}_{11}(\theta) = A^{00}_{1-1}(\theta), \quad A^{-11}_{10}(\theta) = -A^{1-1}_{10}(\theta), \quad A^{-1-1}_{11}(\theta) = A^{11}_{1-1}(\theta)$ (a)
$A^{0-1}_{11}(\theta) = -A^{01}_{1-1}(\theta) = A^{-10}_{11}(\pi - \theta) = -A^{10}_{1-1}(\pi - \theta),$
$A^{10}_{10}(\theta) = A^{-10}_{10}(\theta) = -A^{01}_{10}(\pi - \theta) = -A^{0-1}_{10}(\pi - \theta)$
$A^{11}_{10}(\theta) = -A^{-1-1}_{10}(\theta)$ (s)

$A^{11}_{22}(\theta) = A^{-1-1}_{2-2}(\theta), \quad A^{00}_{22}(\theta) = A^{00}_{2-2}(\theta), \quad A^{-1-1}_{22}(\theta) = A^{11}_{2-2}(\theta), \quad A^{1-1}_{20}(\theta) = A^{-11}_{20}(\theta)$ (s)
$A^{11}_{21}(\theta) = -A^{-1-1}_{2-1}(\theta), \quad A^{-1-1}_{21}(\theta) = -A^{11}_{2-1}(\theta),$ (a)
$A^{11}_{20}(\theta) = A^{-1-1}_{20}(\theta), \quad A^{00}_{20}(\theta)$ (s)
$A^{10}_{22}(\theta) = -A^{-1-1}_{22}(\theta) = -A^{01}_{22}(\pi - \theta) = A^{0-1}_{2-2}(\pi - \theta),$
$A^{1-1}_{22}(\theta) = A^{-11}_{2-2}(\theta) = A^{-11}_{22}(\pi - \theta) = A^{1-1}_{2-2}(\pi - \theta)$
$A^{0-1}_{22}(\theta) = -A^{01}_{2-2}(\theta) = -A^{-10}_{22}(\pi - \theta) = A^{10}_{2-2}(\pi - \theta),$
$A^{10}_{21}(\theta) = A^{-10}_{2-1}(\theta) = A^{01}_{21}(\pi - \theta) = A^{0-1}_{2-1}(\pi - \theta)$
$A^{1-1}_{21}(\theta) = -A^{-11}_{21}(\theta) = -A^{-11}_{21}(\pi - \theta) = A^{1-1}_{2-1}(\pi - \theta),$
$A^{0-1}_{21}(\theta) = A^{01}_{2-1}(\theta) = A^{-10}_{21}(\pi - \theta) = A^{10}_{21}(\pi - \theta)$
$A^{10}_{20}(\theta) = -A^{-10}_{20}(\theta) = -A^{01}_{20}(\pi - \theta) = A^{0-1}_{20}(\pi - \theta)$

$$A^{xx}_{kq} = (1/2)(A^{11}_{kq} - A^{1-1}_{kq} - A^{-11}_{kq} + A^{-1-1}_{kq}) \tag{1.31}$$

$$A^{yy}_{kq} = (-1/2)(A^{11}_{kq} + A^{1-1}_{kq} + A^{-11}_{kq} + A^{-1-1}_{kq}) \tag{1.32}$$

$$A^{zz}_{kq} = A^{00}_{kq} \tag{1.33}$$

$$A_{kq}^{xy} = (1/2)(A_{kq}^{11} + A_{kq}^{1-1} - A_{kq}^{-11} - A_{kq}^{-1-1}) \tag{1.34}$$

$$A_{kq}^{xz} = -(1/\sqrt{2})(A_{kq}^{10} - A_{kq}^{-10}) \tag{1.35}$$

$$A_{kq}^{yz} = -(1/\sqrt{2})(A_{kq}^{10} + A_{kq}^{-10}) \tag{1.36}$$

In general we will have only analysing powers, correlations, vectorial and tensorial polarisation and transfer coefficients (see Table 1) to measure. The polarisation of the outgoing particle in the CM reference frame will be (see notation of Ref. [22])

$$L_{11}^{\mathrm{CM}} = p_z A_{11}^{zB} + p_x A_{11}^{xB} \tag{1.37}$$

$$iM_{11}^{\mathrm{CM}} = (t_{11}^{0} + p_y A_{11}^{yB})/(1 + p_y A_{00}^{yB}) \tag{1.38}$$

$$L_{10}^{\mathrm{CM}} = p_z A_{10}^{zB} + p_x A_{10}^{xB}) \tag{1.39}$$

$$L_{22}^{\mathrm{CM}} = (t_{22}^{0} + p_y A_{22}^{yB})/(1 + p_y A_{00}^{yB}) \tag{1.40}$$

$$iM_{22}^{\mathrm{CM}} = p_z A_{22}^{zB} + p_x A_{22}^{xB} \tag{1.41}$$

$$L_{21}^{\mathrm{CM}} = (t_{21}^{0} + p_y A_{21}^{yB})/(1 + p_y A_{00}^{yB}) \tag{1.42}$$

$$iM_{21}^{\mathrm{CM}} = p_z A_{21}^{zB} + p_x A_{21}^{xB} \tag{1.43}$$

$$L_{20}^{\mathrm{CM}} = (t_{20}^{0} + p_y A_{20}^{yB})/(1 + p_y A_{00}^{yB}) \tag{1.44}$$

1.3. CM *vs* LAB *transformations*

The choice of the helicity frame described in Fig. 1 permits a simple relation between CM and LAB observables. As we mentioned, the CM and laboratory axes are the same for the beam and the target observables; this implies that all the observables which depend only on the incident and target particles spin are the same in the two frames:

$$A^{qq'}(\theta_{\mathrm{CM}})\,|_{\mathrm{CM}} = A^{qq'}(\theta_{\mathrm{CM}})\,|_{\mathrm{LAB}}. \tag{1.45}$$

In general all the upper level indices are unchanged in a CM LAB transformation.

For the outgoing particles, the two frames are related by a simple rotation around the y-axis, such that

$$t_{kq}^{d,\mathrm{LAB}} = \sum_{q'} D_{q'q}^{k}(0,\ \alpha,\ 0) t_{kq'}^{d,\mathrm{CM}} \tag{1.46}$$

where $\alpha = \theta_{\mathrm{LAB}} - \theta_{\mathrm{CM}} + \beta(\theta_{\mathrm{CM}})$ and $\beta(\theta_{\mathrm{CM}})$ is the Wigner correction defined as in Ref. [28] by:

$$\beta(\theta_{\mathrm{CM}}) = \arcsin\left\{|\vec{v}_1 \times \vec{v}_2|\left[\frac{1 + \gamma^{(1)} + \gamma^{(2)} + \gamma^{(3)}}{[1 + \gamma^{(1)}][1 + \gamma^{(2)}][1 + \gamma^{(3)}]}\right]\right\} \tag{1.47}$$

where $\gamma^{(i)} = \sqrt{1 - v_i^2/c^2}$. The index i refers to the three velocities relative to the scattered particle as defined in Fig. 2.

Using (1.47) and (1.20) or (1.27) we find that in general

$$A_{k_d q_d}^{k_B q_B k_T q_T}{}_{\mathrm{LAB}}(\theta_{\mathrm{CM}}) = \sum_{q_d'} D_{q_d' q_d}^{k_q}(0,\ \alpha,\ 0) A_{k_d q_d'}^{k_B q_B k_T q_T}{}_{\mathrm{CM}}(\theta_{\mathrm{CM}}) \tag{1.48}$$

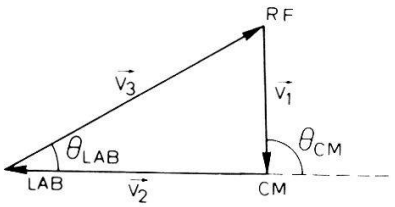

Figure 2
Definition, in the rest frame of the deuteron, of the vectors v_1 (opposite to the velocity of the outgoing particle in the CM frame) v_2 (the relative velocity between the laboratory and the CM frames) and v_3 (relative velocity between the rest and the laboratory frames).

where θ_{LAB} is as in (1.45). For the hybrid formalism

$$A^{\alpha\beta}_{k_d q_d \mathrm{LAB}}(\theta_{CM}) = \sum_{q'_d} D^{k_d}_{q'_d q_d}(0, \alpha, 0) A^{\alpha\beta}_{k_d q'_d \mathrm{CM}}(\theta_{CM}) \tag{1.49}$$

where $\alpha, \beta \in \{x, y, z\}$.

Relations (1.22) and (1.23) are exactly the same in both systems. Relations (1.25) will be written

$$A^{q'q''}_{kq\,\mathrm{LAB}}(\theta_{CM}) = (-1)^{q+q'+q''} \times \sum_{q'''} D^{k}_{qq'''}(0, \alpha + \alpha', 0) A^{q''q'}_{kq'''\,\mathrm{LAB}}(\theta') \tag{1.50}$$

where α is as in (1.46) and $\alpha' = \theta' - (\P - \theta_{CM}) + \beta(\P - \theta_{CM})$ with

$\theta' = \theta_{LAB}|_{\P} - \theta_{CM}$.

This last equation means that the observables in a given angular field are related among themselves simply by a rotation of an angle $\theta = \alpha + \alpha'$.

Otherwise the observables L^{CM}_{kq} and M^{CM}_{kq} have the following form in the LAB frame:

$$L^{LAB}_{22} = (1/2)[(1 + \cos^2\theta)L^{CM}_{22} + \sin 2\theta L^{CM}_{21} + (\sqrt{3/2})\sin^2(\theta/2)L^{CM}_{20}) \tag{1.51}$$

$$M^{LAB}_{22} = \cos\theta M^{CM}_{22} + \sin\theta M^{CM}_{21} \tag{1.52}$$

$$L^{LAB}_{21} = (-1/2)(\sin 2\theta L^{CM}_{22} + \cos 2\theta L^{CM}_{21} + (\sqrt{3/2})\sin 2\theta L^{CM}_{20}) \tag{1.53}$$

$$M^{LAB}_{21} = -\sin\theta M^{CM}_{22} + \cos\theta M^{CM}_{21} \tag{1.54}$$

$$L^{LAB}_{20} = (\sqrt{3/2})(\sin^2\theta L^{CM}_{22} - \sin 2\theta L^{CM}_{21}) + (1/2)(3\cos^2\theta - 1)L^{CM}_{20} \tag{1.55}$$

$$L^{LAB}_{11} = \cos\theta L^{CM}_{11} + (1/\sqrt{2})\sin\theta L^{CM}_{10} \tag{1.56}$$

$$M^{LAB}_{11} = M^{CM}_{11} \tag{1.57}$$

1.4. *Time reversal and $\P d \to pp$ reaction*

It can be of major interest to relate the $pp \to d\P$ reaction to its time reversal reaction $\P d \to pp$, since the two reactions have been studied intensively these last years; see, e.g., Ref. [10]. Time reversal implies (ref. [20])

$$\frac{d\sigma}{d\Omega}(\theta; p(p, d)\P) = \frac{|p_p|^2}{|p_d|^2}\frac{3}{4}\frac{d\sigma}{d\Omega}(\theta; d(\P, p)p) \tag{1.58}$$

where θ is the CM angle of the third particle (either d or p) as defined in equation (1.25) and

$$t_{k_d q_d}^{k_B q_B k_T q_T}(\theta; p(p, d)\P) = t_{k_B q_B k_T q_T}^{k_d q_d}(\P - \theta; d(\P, p)p) \tag{1.59}$$

Thus in particular

$$t_{11}^{0}(\theta; p(p, d)\P) = t_{0000}^{11}(\P - \theta; d(\P, p)p) \tag{1.60}$$

1.5. *Other formalisms*

a) *Spin correlation formalism.* We now would like to put the previously measured spin correlation observables by our group into the above formalism; see, e.g., Refs [29], [8], [30]. In these papers the frame used is as explained in Fig. 3a). To go from this frame to ours, one must exchange the pion with the deuteron, and turn the target frame by an angle $\varphi = \P$ around its $\hat{y}_T$ axis. This gives

$$A_{00}^{k_B q_B k_T q_T}(\theta_d) = (-1)^{k_T + q_B} E_{00}^{k_B q_B k_T q_T}(\theta_\P) \tag{1.61}$$

where E refers to these phenomenological observables and is in a spherical formalism; also $\theta_\P = \P - \theta_d$.

More explicitly, we have, using the previous notation for these observables:

$$A^{yB}(\theta_d) = -A_{n0}(\theta_\P) \tag{1.62}$$

$$A^{xz}(\theta_d) = A_{sk}(\theta_\P) \tag{1.63}$$

$$A^{zz}(\theta_d) = -A_{kk}(\theta_\P) \tag{1.64}$$

$$A^{xx}(\theta_d) = -A_{ss}(\theta_\P) \tag{1.65}$$

$$A^{yy}(\theta_d) = A_{nn}(\theta_\P) \tag{1.66}$$

b) *Foroughi's formalism.* We now want to connect with Refs [31], [32], [33] and through these with Ref. [24]. Foroughi's helicity reference frame is defined in Fig. 3b).

We see that one must again exchange the pion with the deuteron and, in

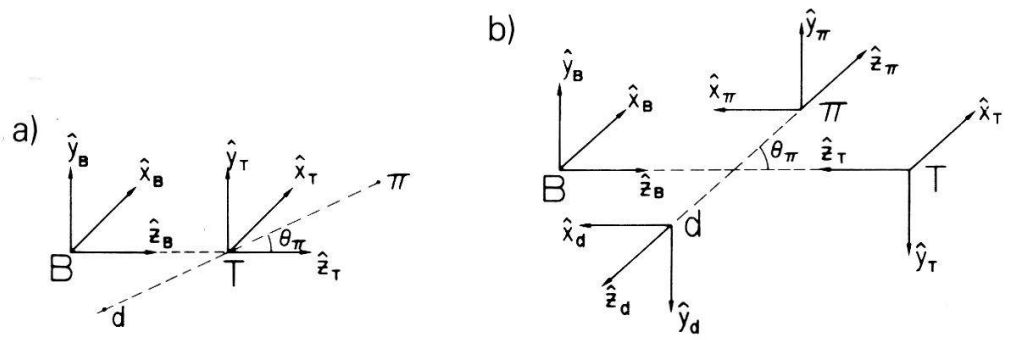

Figure 3
a) Reference frame used in spin correlation measurements [29] [8]. b) Helicity reference frame used in Refs [24] and [31].

addition, rotate the deuteron and the target frames by an angle $\varphi = ¶$ around $\hat{z}_d$, $\hat{z}_T$. This gives

$$A^{q_B q_T}(\theta_d) = (-1)^{q_B}(q_B q_T \mid k_d q_d)|_{\theta_¶} \tag{1.67}$$

where the right hand side of the equation is written in the Foroughi–Bourrely formalism. More explicitly:

$$A^{xx}(\theta_d) = -(xx \mid 00)|_{\theta_¶} \tag{1.68}$$

$$A^{yy}(\theta_d) = -(yy \mid 00)|_{\theta_¶} \tag{1.69}$$

$$A^{zz}(\theta_d) = (zz \mid 00)|_{\theta_¶} \tag{1.70}$$

$$A^{xz}(\theta_d) = -(xz \mid 00)|_{\theta_¶} \tag{1.71}$$

$$A^{y0}(\theta_d) = -(y0 \mid 00)|_{\theta_¶} \tag{1.72}$$

$$t^0_{kq}(\theta_d) = (00 \mid kq)|_{\theta_¶} \tag{1.73}$$

We checked the whole formalism and find that from (1.71) and (1.63) we can write

$$A_{sk}(\theta_¶) = -(xz \mid 00)|_{\theta_¶} \tag{1.74}$$

in contrast to Refs. [32] and [33].

c) *¶d → pp formalism.* Here we refer to Ref. [10]; in this article Boschitz's group present their data on the analysing power iT_{11} of the deuteron in the inverse reaction $¶d \to pp$; we can relate their experimental data to ours by (see equation (1.60))

$$t_{11}(\theta_d; p(p, \vec{d})¶) = T_{11}(\theta_¶; \vec{d}(¶, p)p) \tag{1.75}$$

d) *Blankleider's formalism.* In Ref. [34] predictions are made for the observables that we have measured. The authors use the same formalism as ours except for the description of asymmetries and correlation observables for which they use the spin correlation formalism (see Section 1.5a)).

1.6. *Application to the dA → X reaction*

Now, we will consider reactions of the type $A(d, d)A$ or $A(d, q)B$ where q is a charged particle; these reactions will be used to measure the polarisation of the deuteron. To achieve this goal, we will consider equation (1.20) using an incident polarised deuteron t^d_{kq}, but with no polarisation measurements on the outgoing particle $t^c_{kq} = t^c_{00} = 1$:

$$\frac{d\sigma}{d\Omega}(\theta; A(d, q)B)_{\text{pol}} = \frac{d\sigma}{d\Omega}(\theta; A(d, q)B)_0 \Big(\sum_{\substack{k_d > 0 \\ q_d}} t^d_{k_d q_d} C^{k_d q_d}(\theta; A(d, q)B) \Big) \tag{1.76}$$

We introduce here the new observable $C^{k_d q_d}$ as analysing power of the A analyser.

Until now, we have considered that the reference frame was the same for the incident particle d and the analyser A. However if the particle d is produced in a previous reaction, we can have an angle between the first reaction plane and the second; in this case $C^{k_d q_d}$ must be rotated around the $\hat{z}$ axis by φ:

$$C^{k_d q_d}(\varphi) = \sum_{q'_d} D^{k_d}_{q'_d q_d}(0, 0, \varphi) C^{k_d q'_d} = e^{-iq_d\varphi} C^{k_d q_d} \tag{1.77}$$

In the rotated frame, we will have

$$\frac{d\sigma}{d\Omega}(\theta, \varphi)_{\text{pol}} = \left(\frac{d\sigma}{d\Omega}(\theta)\right)_0 \left(\sum_{\substack{k_d>0 \\ q_d}} t^d_{k_d q_d} C^{k_d q_d}(\theta) e^{-iq\varphi}\right) \tag{1.78}$$

If we take into account the hermiticity and parity properties, we obtain finally

$$\frac{d\sigma}{d\Omega}(\theta, \varphi)_{\text{pol}} = \left(\frac{d\sigma}{d\Omega}(\theta)\right)_0 (1 + \pi^{20} L_{20} + (\pi^{11} M_{11} + \pi^{21} L_{21}) \cos\varphi + (-\pi^{11} L_{11} + \pi^{21} M_{21}) \sin\varphi + \pi^{22} L_{22} \cos 2\varphi + \pi^{22} M_{22} \sin 2\varphi) \tag{1.79}$$

where $\pi^{11} = 2iC^{11}$, $\pi^{2q} = 2C^{2q}$, $q = 0, 1, 2$ which we will call therefore the analysing powers of A on the deuteron: we remark that this definition is a factor of two larger than the one in Ref. [22] (see also equation 3.22).

II. Experimental apparatus

The experimental apparatus used in our measurements is basically the same as in Refs. [35], [19] and [30].

All the data presented here were accumulated during two periods at SIN in 1983.

During the first period (February–March 1983), we worked in a parasitic mode where the main unpolarised proton beam (590 MeV) was scattered at 8 deg lab from a thick Be target and entered into the pM1 channel with a polarisation of $p_B = 0.4165 \pm 0.0043$ (see Ref. [36]). A split magnet system allows a clean selection of the elastically scattered protons.

During the second period in October 1983 we worked at 515 MeV for a week and at 450 MeV for another week in a single user mode. In this mode, polarised protons coming from the SIN polarised ion source were accelerated up to 590 MeV and deflected into the pM1 channel. The polarisation of this accelerated beam was typically 81%; this beam polarisation was periodically monitored with a CH_2 target viewed by eight scintillation counters. Elastic proton–proton scattering coincidences were observed between one pair of forward detectors and its conjugate pair of recoil counters.

In order to lower the energy of the original beam to desired values a copper degrader was used. The depolarisation in the degrader and beam transport is negligible (Ref. [36] and [37]). The beam intensity at the target could be adjusted by a system of slits located at various points along the beam line.

The original direction of the polarisation for both the accelerated and scattered beam pointed downwards corresponding to the vertical $\hat{y}$-axis in the experimental area. With the scattered beam a 50 KGm superconducting solenoid placed in front of the last pair of deflecting magnets (ASK and ASL) allowed spin precession of 180 deg for full current. With the accelerated beam a fast periodical spin flip occurred at the ion source itself. To obtain a longitudinally polarised beam, the solenoid was set at half current to obtain a 90° precession. When used in front of ASK–ASL, these two magnets turned the spin vector into the longitudinal direction. To obtain a pure transversally polarised beam a second solenoid was installed down stream of the ASK–ASL magnet, just in front of the target. For the calibration of these two solenoids, see Refs. [19], [30] and [38].

The Oxford University group of J. Davies lent a LH_2 target to us from July 1982 until summer 1984. This liquid hydrogen target was cylindrical in shape, 10 cm long in the beam direction, 1.8 cm in radius, with 0.125 mm thick mylar walls (see Fig. 4 and Ref. [40]).

The background noise due to the mylar walls was directly measured in February 1983 with an empty target measurement and was found to be negligible, thus no dummy measurements were needed.

The detector layout is illustrated in Fig. 5. The position and profile of the incident beam was monitored by 2 small x–y MWPCs with 1 or 2 mm wire spacing.

The pion and the deuteron were simultaneously detected by two telescopes consisting of scintillators and MWPCs. They were mounted on two separate arms which could be rotated around the vertical axis $\hat{Y}$. The telescope detecting the pion consisted of three equidistant (10 cm) x–y MWPCs. Their wire planes were square and of side length 394, 512 and 512 mm with a wire spacing of 2 mm.

In the forward direction a scintillation counter (Y) was mounted which covered the entire recoil solid angle. In the backward direction two horizontal

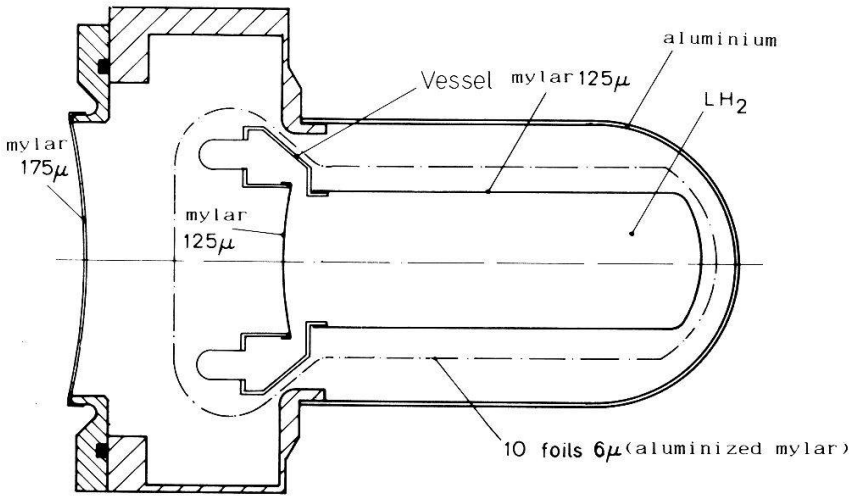

Figure 4
Scale drawing of the LH_2 hydrogen target.

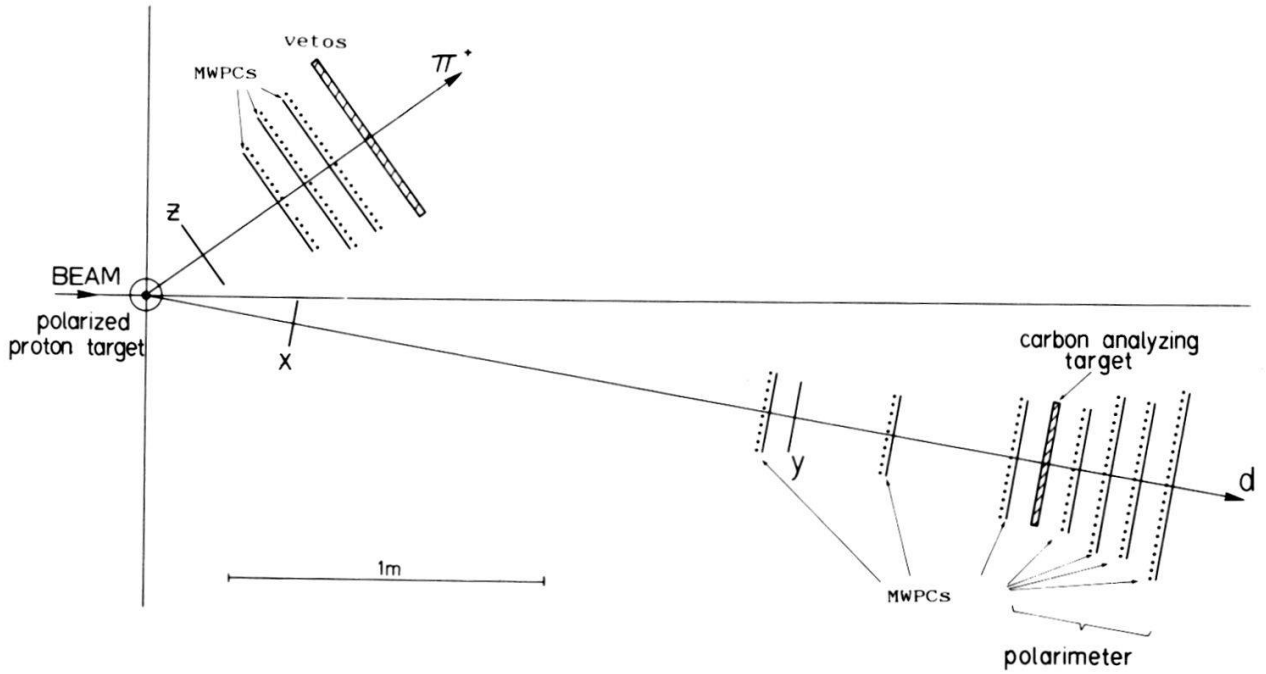

Figure 5
Scale drawing of the experimental system. The vetos on the telescope detecting the π were used to reduce the ϕ_H acceptance.

counters were used as VETOS to adapt the φ_H acceptance to the size of the polarimeter; to increase the detection efficiency a CH_2 plate of 5 mm thickness was used to stop possible elastically back-scattered protons when the detector arm was at 76°.

The scattering telescope consisted of 5 elements, in the following order: a scintillator (X), a 250 mm MWPC, a second scintillator (Z), and two MWPCs 250 and 394 mm square respectively. These two scintillators together with the counter Y of the recoil telescope permit one to define two time-of-flight (tofs) as $\tau_1 = Z - X$ and $\tau_2 = Z - Y$.

To analyse the polarisation of the scattered proton this scattered telescope is extended to a polarimeter consisting of a carbon target of 3 cm thickness (the density was 1.77 g/cm^3) and a telescope of 4 equidistant (10 cm) x–y MWPCs of 394,512,512 and 600 mm side length.

At each trigger all the coordinates were read and processed by a hardware coding unit and decision system. This second step decision is based on a single trajectory in each telescope and on a scattering in the polarimeter. If the event was accepted the information was then transferred to a 28 K minicomputer DPNC 811, which had been loaded with the reconstruction program (see next chapter). All the transfers were controlled by a PDP 11/20 computer.

Four types of events were recorded:

1. 'Straight tracks' for an off line-evaluation of the alignment parameters of the MWPCs; these events were taken without the carbon analysing target of the polarimeter.

2. 'Double scattering events': the actual measurements of the ε observables.

Taken for the 6 beam orientations ($\pm X, \pm Y, \pm Z$) at all the angular arm positions.

3. 'Straight tracks' as in type 1, but taken alternatively (about 20%) with scattered events of type 2 or 4 for an off-line determination of any possible residual misalignments.

4. 'Double scattering events' with an elastic proton at 40 deg. These events were used to give an upper limit for residual $2\varphi_c$ asymmetries due to possible geometrical misalignment of non uniform efficiencies in the MWPCs.

III. Experimental analysis

3.1. *On-line reconstruction and off-line analysis*

a) *Initial reconstruction of scattering events.* The event reconstruction, used to identify the $pp \rightarrow d\P$ reaction in the on-line or off-line analysis, is based on a well-established method in our group described in Refs [37], [40], [41], [43] and used in several experiments e.g. [42], [18], [44], [19] and [30]. Here we will only briefly summarise the principle.

For a given experimental set-up, at a given energy each measured event is completely characterised by the vertex coordinates (V_x, V_y, V_z), the c.m. polar and azimuthal angles, the vertically projected slope α_v of the incoming proton and α_h, the horizontal incidence angle of the incoming proton, but this last value is not measured. On the other hand the MWPCs give us 12 coordinates $\underline{X}$. If the parameters to be measured are called $\underline{P}$, there exists a relation

well-established method in our group described in Refs [37], [40], [43] and used in several experiments e.g. [42], [18], [44], [19] and [30]. Here we will only briefly summarise the principle.

$$\underline{X} = \underline{X}_0 + \left.\frac{\partial F}{\partial \underline{P}}\right|_{\underline{P}_0} (\underline{P} - \underline{P}_0) = \underline{X}_0 + D(\underline{P} - \underline{P}_0) \tag{3.2}$$

around the central value $\underline{P}_0$. If we introduce the reduced coordinates $\underline{x} = \underline{X} - \underline{X}_0$ $\underline{p} = \underline{P} - \underline{P}_0$ we obtain the design equation

$$\underline{x} = D\underline{p} \tag{3.3}$$

A linear least-square fit is then used to estimate the six reconstructed parameters:

$$\underline{p} = (D^T G D)^{-1} D^T G \underline{x} = R\underline{x} \tag{3.4}$$

where D^T is the transpose of the matrix D, and $G = C^{-1}$, where C is the covariance matrix of the measured coordinates; R is called the reconstruction matrix.

In order to check the quality of the reconstruction describing the goodness of

fit a parameter S^2 is defined by

$$S^2 = (\underline{x}_m - \underline{x}_r)^T G (\underline{x}_m - \underline{x}_r) \tag{3.5}$$

where $\underline{x}_m$ are the measured coordinates and

$$\underline{x}_r = DR\underline{x}_m \tag{3.6}$$

As we have a Gaussian distribution, the S^2 is a χ^2 with 6(12-6) degrees of freedom.

We have found that non-linearities occur mainly as functions of θ and ϕ and this implies an adjustment $\Delta\underline{x}$ of the coordinates:

$$\underline{x}_c = \underline{x}_m - \Delta\underline{x}(\theta, \phi) \tag{3.7}$$

The reconstruction matrix reduces the entire event reconstruction to a simple and fast matrix multiplication to be carried out on-line or off-line in the MINI computers: for the corrections, as table inputs, a first raw estimate (θ_r, ϕ_r) obtained of $\underline{x}_m$ by equation (3.4) was used. Events with θ_r and ϕ_r outside the table were rejected. The full reconstruction was then applied to the corrected coordinates $\underline{x}_c$ of the equation (3.7).

All this information ($\underline{X}$, R, correction table), prepared beforehand, was loaded into the MINI computers together with the reconstruction program, with a table containing the cuts to be applied to the reconstructed parameters. The TDC information was treated independently using a table with (θ_r, ϕ_r) entries as for the correction of the MWPC coordinates; the theoretical values of $\tau_1 = Z - X$ and $\tau_2 = Z - Y$ were computed.

In order to have TOF distributions independent of θ, ϕ for true $pp \to d$¶ events, we used the differences

$$\text{TOF1} = \tau_{1,\text{mes}} - \tau_{1,\text{th}} - \text{TDC's offsets} \tag{3.8}$$

$$\text{TOF2} = \tau_{2,\text{mes}} - \tau_{2,\text{th}} - \text{TDC's offsets} \tag{3.9}$$

where the TDC's offsets, obtained from a previous calibration measurement with the two detector telescopes placed directly in the beam, were subtracted in order to get a zero centered distribution. Since the above calculations involve only linear combinations of the TDCs and a search in a correction table, it is very convenient to compute TOF1 and TOF2 at the same time as the other parameters, taking advantage of the fast matrix multiplication, increasing the dimension of the reconstruction matrix R and of the table $\Delta\underline{x}$ (θ_r, ϕ_r).

The acceptance of this reconstruction in the on-line calculations was typically 30%, where the cuts were kept quite loose in order to allow some flexibility in imposing more stringent limits in the final off-line analysis.

b) *Second scattering events reconstruction.* The method used here is the same as that used in Ref. [19] for the $p^{12}C$ reaction extended to the case of $d^{12}C$ reaction. In this last reaction no attempt was made to identify inelastic scattering or stripping, although events with two or more charged particles behind the

carbon analyzer were rejected. For a more detailed analysis of this assumption see the next section.

Various calculations were done in the program in the following execution order:

α) The event is kept a) if the scattering angle θ_C is larger than 5° LAB *and* b) if the azimuthal $\varphi_C = 2¶$ acceptance of the polarimeter is guaranteed for this scattering angle (so-called polygonal cut)

β) Alignment procedure for the telescope similar to that of the first scattering, however more complex due to the fact that here we have 4 planes. Cuts were applied to the computed χ^2.

γ) Calculation of the polar angle θ_C. Cuts were made for events with $\theta_C < 5°$ or $\theta_C > 20°$.

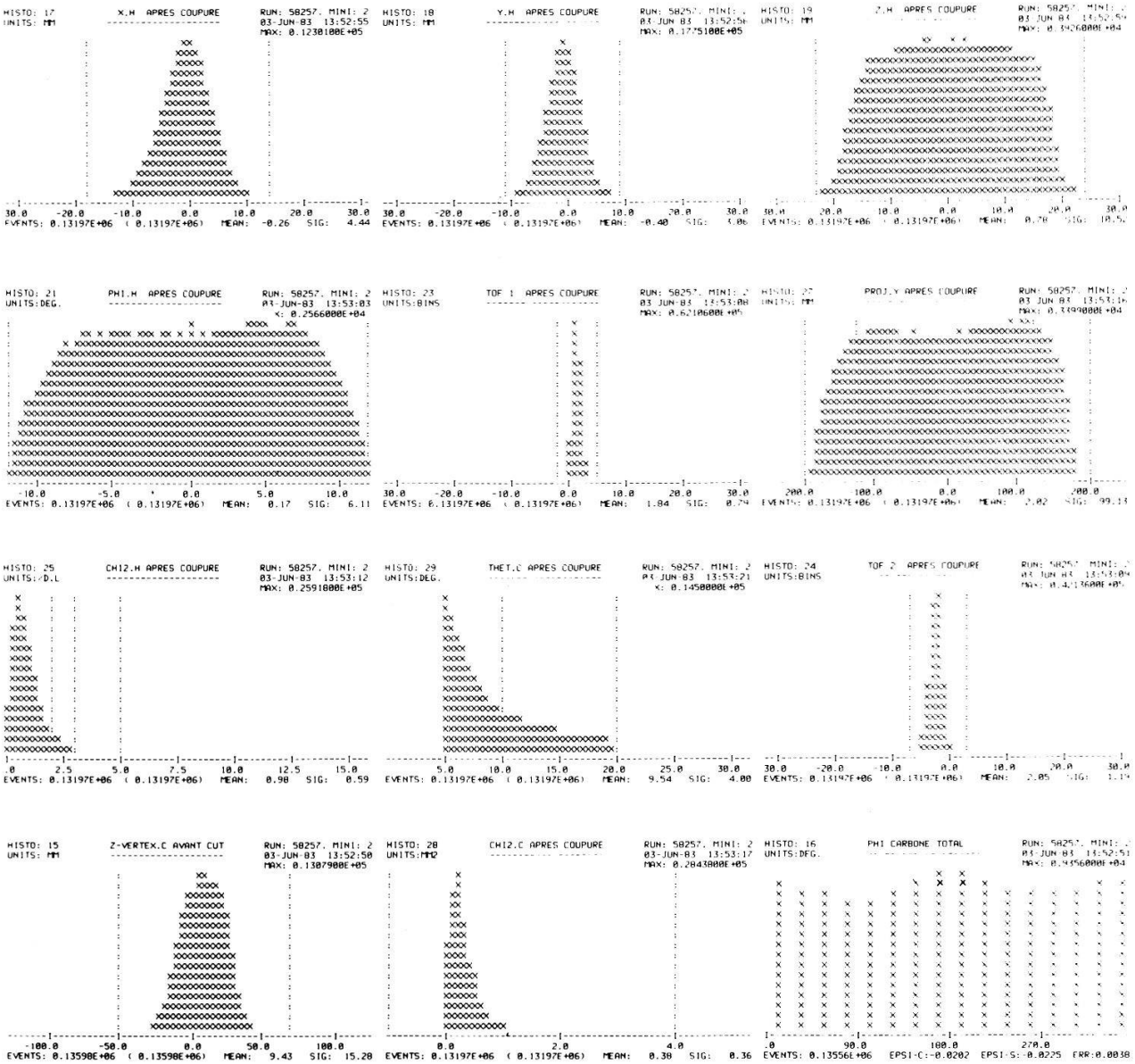

Figure 6
Typical distribution of the reconstructed events (LH_2 vertex in X, Y, and Z direction, ϕ_H, θ_c, time of flight distributions τ_1, τ_2, carbon vertex in Z, and χ^2 of the reconstructed tracks).

δ) Calculation of the minimum distance squared between incident and scattered track with a cut at 15 mm^2.

ε) Reconstruction of the vertex interaction, the cuts were applied in order to select the carbon region.

ξ) Calculation of the azimuthal angle ϕ_C.

On-line rejection levels were 20% for item α), 6% for item δ), 10% for item ε). The global on-line polarimeter rejection is of the order of 25%. Thus about 45% of the events pass the on-line reconstruction of the polarimeter.

Off-line rejection is less drastic we obtain 15% for item α), 0.1% for item β), 0.2% for item γ), 0.6% for item δ), 2% for item ε).

Two MINIs worked on-line with a number of 160–240 events per second together. Off-line we worked generally with four MINIs with a performance of 300 reconstructed events per second.

The off-line analysis was carried out in the same way as the on-line analysis. A PDP 11/34 replaced the 11/20 used on-line. The MINI computers, connected to the PDP via CAMAC, were loaded with essentially the same information for the reconstruction matrix. The values for the cuts to be applied were studied carefully on samples spread over the whole data set to be analysed. Displacement of the chambers were carefully studied from the straight track events mentioned earlier. Not only the transverse but also the rotational displacement was calculated. Figure 6 shows typical distribution of reconstructed events (Vertex in LH_2 and C target, ϕ_H, ϕ_C, tof and χ^2 for reconstructed tracks). The final multidimensional histogram which results from the off-line processing has the structure

$$8(\theta_H) \times 3(\phi_H) \times 15(\theta_C) \times 16(\phi_C) \tag{3.10}$$

Over this bin structure we can now estimate the observables defined in paragraph I.

3.2. *Data evaluation*

3.2.1. *Binning effects*

a) Two main reactions occur in the polarimeter:

$$\alpha: {}^{12}C(d, d)^{12}C \tag{3.11}$$

$$\beta: {}^{12}C(d, p)X. \tag{3.12}$$

From Ref. [46] we can estimate that the ratio of β- events (due to nuclear Coulomb break-up and small angle nuclear scattering) to α-events, with our 3 cm-thick carbon block, should be $<4\%$. Both reactions can be detected by our apparatus, and from paragraph I one obtains the two equations

$$\left(\frac{d\sigma^x}{d\Omega}(\theta_c, \phi_c)\right) = \left(\frac{d\sigma^x}{d\Omega}(\theta_c)\right)_0 (1 + \pi^{20,x} L_{20} + (\pi^{11,x} M_{11} + \pi^{21,x} L_{21}) \cos\phi$$
$$+ (-\pi^{11,x} L_{11} + \pi^{21,x} M_{21}) \sin\phi + \pi^{22,x} L_{22} \cos 2\phi + \pi^{22,x} M^{22,x} \sin 2\phi) \tag{3.13}$$

with $x = \alpha, \beta$, and where $d\sigma^x/d\Omega$ and $\pi^{kq,x}$ refer to the corresponding reaction; from (3.13) we obtain by simple addition

$$\left(\frac{d\sigma}{d\Omega}(\theta_c, \phi_c)\right)_{\text{pol}} = \left(\frac{d\sigma}{d\Omega}(\theta_c)\right)_0 (1 + \pi^{20}L_{20} + (\pi^{11}M_{11} + \pi^{21}L_{21})\cos\phi + (-\pi^{11}L_{11} + \pi^{21}M_{21})\sin\phi + \pi^{22}L_{22}\cos 2\phi + \pi^{22}M_{22}\sin 2\phi) \quad (3.14)$$

where

$$\left(\frac{d\sigma}{d\Omega}(\theta_c, \phi_c)\right)_{\text{pol}} = \left(\frac{d\sigma^\alpha}{d\Omega}(\theta_c, \phi_c)\right)_{\text{pol}} + \left(\frac{d\sigma^\beta}{d\Omega}(\theta_c, \phi_c)\right)_{\text{pol}}$$

$$\left(\frac{d\sigma}{d\Omega}(\theta_c, \phi_c)\right)_0 = \left(\frac{d\sigma^\alpha}{d\Omega}(\theta_c, \phi_c)\right)_0 + \left(\frac{d\sigma^\beta}{d\Omega}(\theta_c, \phi_c)\right)_0$$

and

$$\pi^{kq} = \frac{\left(\frac{d\sigma^\alpha}{d\Omega}\right)\pi^{kq,\alpha}}{\left(\frac{d\sigma^\alpha}{d\Omega} + \frac{d\sigma^\beta}{d\Omega}\right)_0} + \frac{\left(\frac{d\sigma^\beta}{d\Omega}\right)\pi^{kq,\beta}}{\left(\frac{d\sigma^\alpha}{d\Omega} + \frac{d\sigma^\beta}{d\Omega}\right)_0}$$

are the generalised cross-sections and analysing powers.

b) We now consider the influence of the binning introduced in the analysis for φ_C and θ_C in formula (3.10).

From formula (3.14), the number of $pp \to d\P$ events measured in the polarimeter is given by:

$$\begin{aligned} N(\theta_H, \theta_C, \phi_C) = N_0 \frac{d\sigma}{d\Omega}(\theta_C)\,\text{Acc}\,(\theta_C)[1 &+ \pi^{20}(\theta_H, \theta_C)L_{20}(\theta_H) \\ &+ (\pi^{11}(\theta_H, \theta_C)M_{11}(\theta_H) + \pi^{21}(\theta_H, \theta_C)L_{21}(\theta_H))\cos\phi_C \\ &+ (-\pi^{11}(\theta_H, \theta_C)L_{11}(\theta_H) + \pi^{21}(\theta_H, \theta_C)M_{21}(\theta_H))\sin\phi_C \\ &+ \pi^{22}(\theta_H, \theta_C)L_{22}(\theta_H)\cos 2\phi_C \\ &+ \pi^{22}(\theta_H, \theta_C)M_{22}(\theta_H)\sin 2\phi_C] \end{aligned} \quad (3.15)$$

where N_0 is a normalisation constant and $\text{Acc}\,(\theta_C)$ is the acceptance of the apparatus. This acceptance is supposed to be independent of ϕ_C due to the checks applied as described in item α) of Section 3.1. We suppose here that the θ_H-binning has a $\Delta\theta_H$ width for each bin, and that of θ_C, $\Delta\theta_C$: then the number of events in the ith bin of θ_H and in the jth bin of θ_C is given by

$$N(i, j, \phi_C) = \int_{\Delta\theta_H(i)\Delta\theta_C(j)} N(\theta_H, \theta_C, \phi_C)d\theta_H d\theta_C \quad (3.16)$$

$$\begin{aligned} = f_j[1 &+ \pi^{20}(i, j)L_{20}(i) \\ &+ (\pi^{11}(i, j)M_{11}(i) + \pi^{21}(i, j)L_{21}(i))\cos\phi_C \\ &+ (-\pi^{11}(i, j)L_{11}(i) + \pi^{21}(i, j)M_{21}(i))\sin\phi_C \\ &+ \pi^{22}(i, j)L_{22}(i)\cos 2\phi_C + \pi^{22}(i, j)M_{22}(i)\sin 2\phi_C] \end{aligned}$$

where

$$f_J = N_0 \int_{\Delta\theta_C(j)} \frac{d\sigma}{d\Omega}(\theta_C)\,\mathrm{Acc}\,(\theta_C)\,d\theta_C \tag{3.17}$$

$$\pi^{kq}(i,j) = \frac{\displaystyle\int_{\Delta\theta_C(j)} \frac{d\sigma}{d\Omega}(\theta_C)\,\mathrm{Acc}\,(\theta_C)\left[\int_{\Delta\theta_H(i)} \pi^{kq}(\theta_H, \theta_C)\,d\theta_H\right] d\theta_C}{\displaystyle\int_{\Delta\theta_C(j)} \frac{d\sigma}{d\Omega}(\theta_C)\,\mathrm{Acc}\,(\theta_C)\,d\theta_C} \tag{3.18}$$

We have also supposed that we may use the approximation $(dt_{kq}/d\theta_H)\,|_{\theta_H=\theta_H(i)} = 0$ over the bin interval $\Delta\theta_H/2$. $\theta_H(i)$ is the central value of the ith bin.

c) Now we investigate the effect of the polar angle ϕ_H on the incoming deuteron polarisation as seen by the polarimeter. From equation (1.8), we have

$$t_{kq}(\theta_H, \theta_C) = e^{-iq\phi_H} t_{kq}(\theta_H) \tag{3.19}$$

which obviously implies in the Mandl and Regge formalism

$$L_{kq}(\theta_H, \phi_H) = \cos(q\phi_H) L_{kq}(\theta_H) + \sin(q\phi_H) M_{kq}(\theta_H) \tag{3.20}$$

$$M_{kq}(\theta_H, \phi_H) = \cos(q\phi_H) M_{kq}(\theta_H) - \sin(q\phi_H) L_{kq}(\theta_H) \tag{3.21}$$

In our experiment, in fact, we have integrated with a symmetric range $\pm\delta\phi_H$ around ϕ_H, therefore, for a given set of bin i and j in θ_H and θ_C, we measured

$$\begin{aligned} n(\phi_C) &= \int_{-\delta\varphi_H}^{+\delta\varphi_H} N(\phi_H, \phi_C)\,d\phi_H \\ &= f(1 + T^{20}L_{20} + (T^{11}M_{11} + T^{21}L_{21})\cos\phi_C + (-T^{11}L_{11} + T^{21}L_{21})\sin\phi_C \\ &\quad + T^{22}L_{22}\cos 2\phi_C + T^{22}M_{22}\sin 2\phi_C) \end{aligned} \tag{3.22}$$

where $T^{kq} = \pi^{kq}(i,j)(\sin q\delta\phi_H / q\delta\phi_H)$, $L_{kq} = L_{kq}(i)$, $M_{kq} = M_{kq}(i)$ and $f = 2f_j\delta\phi_H$. *These T^{kq} are what we shall call from now on the effective analysing powers of the reaction $d^{12}C$.*

d) For a given pair of angular bins (i, j) of θ_H. θ_C we now have a 16 bin histogram in ϕ_C see equation (3.22). Unfortunately we do not have a sensitivity sufficient to measure directly f and $T^{20}L_{20}$, we are thus forced to consider the following experimental observables

$$\varepsilon_s = \frac{T^{11}L_{11} + T^{21}M_{21}}{1 + T^{20}L_{20}} \tag{3.23}$$

$$\varepsilon_c = \frac{-T^{11}M_{11} + T^{21}L_{21}}{1 + T^{20}L_{20}} \tag{3.24}$$

$$\varepsilon_{2c} = \frac{T^{22}L_{22}}{1 + T^{20}L_{20}} \tag{3.25}$$

$$\varepsilon_{2s} = \frac{T^{22}M_{22}}{1 + T^{20}L_{20}} \tag{3.26}$$

Equation (3.22) becomes

$$n(\phi_C) = f(1 + T^{20}L_{20})(1 + \varepsilon_c \cos\phi_C + \varepsilon_s \sin\phi_C + \varepsilon_{2c} \cos 2\theta_C + \varepsilon_{2s} \sin 2\phi_C) \tag{3.27}$$

and we see that the ε's are completely independent of the normalisation f. We can now write

$$n(\phi_C) = (2\P)^{-1}(A + B \sin\phi_C + C \cos\phi_C + D \sin 2\phi_C + E \cos 2\phi_C) \tag{3.28}$$

which implies that

$$\varepsilon_c = \frac{C}{A} \qquad \varepsilon_s = \frac{B}{A} \qquad \varepsilon_{2c} = \frac{E}{A} \qquad \varepsilon_{2s} = \frac{D}{A} \tag{3.29}$$

The fact that the ϕ_C-distribution is divided into 16 bins $(\phi_i - \Delta\phi_i, \phi_i + \Delta\phi_i)$ implies that one obtains a histogram distribution given by

$$n_i = \int_{\varphi_i - \Delta\varphi_i}^{\varphi_i + \Delta\varphi_i} n(\phi_C)\, d\phi_C = A\left(\frac{\Delta\phi_i}{\P}\right) + B\frac{\sin\Delta\phi_i}{\P}\sin\phi_i + \frac{C \sin\Delta\phi_i}{\P}\cos\phi_i + \frac{D \sin 2\Delta\phi_i}{2\P}\sin 2\phi_i + \frac{E \sin 2\Delta\phi_i}{2\P}\cos 2\phi_i \tag{3.30}$$

and because $\Delta\phi/\P = 1/16$ we obtain

$$n_i = (1/16)(A + B' \sin\phi_i + C' \cos\phi_i + D' \sin 2\phi_i + E' \cos 2\phi_i) \tag{3.31}$$

where

$$B' = 0.9936\, B \qquad C' = 0.9936\, C$$
$$D' = 0.9745\, D \qquad E' = 0.9745\, E \tag{3.32}$$

3.2.2. *Estimators*

If N_i are the experimental number of events found in the histogram we can perform a Fourier fit of these to calculate A, B', C', D', E' by minimizing

$$\chi^2 = \sum_{i=1}^{16} \frac{(n_i - N_i)^2}{\bar{N}} \tag{3.33}$$

where $\bar{N} = (1/16)N_{\text{tot}}$ and $N_{\text{tot}} = \sum_i N_i$. Then

$$\chi^2 = \frac{1}{16N_{\text{tot}}} \sum_i (A + B' \sin\phi_i + C' \cos\phi_i + D' \sin 2\phi_i + E' \cos 2\theta_i - 16N_i)^2 \tag{3.34}$$

and

$$\frac{\partial\chi^2}{\partial A} = 0 \Rightarrow A = \sum_i N_i = N_{\text{tot}} \tag{3.35}$$

$$\frac{\partial\chi^2}{\partial B'} = 0 \Rightarrow B' = 2\sum_i N_i \sin\phi_i \tag{3.36}$$

$$\frac{\partial \chi^2}{\partial C'} = 0 \Rightarrow C' = 2 \sum_i N_i \cos \phi_i \tag{3.37}$$

$$\frac{\partial \chi^2}{\partial D'} = 0 \Rightarrow D' = 2 \sum_i N_i \sin 2\phi_i \tag{3.38}$$

$$\frac{\partial \chi^2}{\partial E'} = 0 \Rightarrow E' = 2 \sum_i N_i \cos 2\phi_i \tag{3.39}$$

The evaluation of the errors gives us

$$\sigma_A^2 = \sum_i \left(\frac{\partial A}{\partial N_i}\right)^2 \sigma_{N_i}^2 = N_{\text{tot}} \tag{3.40}$$

$$\sigma_{B'}^2 = \sum_i \left(\frac{\partial B'}{\partial N_i}\right)^2 \sigma_{N_i}^2 = 2N_{\text{tot}} = \sigma_{C'}^2 = \sigma_{D'}^2 = \sigma_{E'}^2 \tag{3.41}$$

Finally, we obtain for our observed εs

$$\varepsilon_c = 1.0065\left(2 \sum_i N_i \cos \phi_i\right) \Big/ N_{\text{tot}} \tag{3.42}$$

$$\varepsilon_s = 1.0065\left(2 \sum_i N_i \sin \phi_i\right) \Big/ N_{\text{tot}} \tag{3.43}$$

$$\varepsilon_{2c} = 1.0262\left(2 \sum_i N_i \cos 2\phi_i\right) \Big/ N_{\text{tot}} \tag{3.44}$$

$$\varepsilon_{2s} = 1.0262\left(2 \sum_i N_i \sin 2\phi_i\right) \Big/ N_{\text{tot}} \tag{3.45}$$

where $\Delta\varepsilon_C = \sqrt{2/N_{\text{tot}}} = \Delta\varepsilon_s = \Delta\varepsilon_{2c} = \Delta\varepsilon_{2s}$.

3.2.3. *Residual asymmetries*

The mispositioning and geometrical construction deficiencies of the polarimeter give rise to errors on the reconstructed angles ϕ_C and θ_C leading to residual asymmetries ε. Straight tracks of type 3 events (see paragraph II) allow us to measure the mean geometrical deviations $\Delta_c = \langle \text{tg}\theta_C \cos \phi_C \rangle$, $\Delta_s = \langle \text{tg}\theta_C \sin \phi_C \rangle$ which correlate the measured (m) with the true (t) variables $\text{tg}\theta_C \cos \phi_C$ and $\text{tg}\theta_C \sin \phi_C$ (see Ref. [47] too):

$$\text{tg}\, \theta_m \cos \phi_m = \text{tg}\, \theta_t \cos \phi_t + \Delta_c \tag{3.46}$$

$$\text{tg}\, \theta_m \sin \phi_m = \text{tg}\, \theta_t \sin \phi_t + \Delta_s \tag{3.47}$$

For small angle value in θ_C and using (3.46), (3.47) one obtains

$$\theta_t = \theta_m \cos (\phi_t - \phi_m) - (\Delta_c \cos \phi_m + \Delta_s \sin \phi_m) \cos (\phi_t - \phi_m) + (\Delta_c \sin \phi_m - \Delta_s \cos \phi_m) \sin (\phi_t - \phi_m) \tag{3.48}$$

$$\theta_t \sin (\phi_t - \phi_m) = \Delta_c \sin \phi_m - \Delta_s \cos \phi_m \tag{3.49}$$

If ϕ_t is chosen near ϕ_m and θ_t near θ_m, one obtains the following expansion valid

to the second order approximation,

$$\theta_t^2 - [\theta_m - (\Delta_c \cos\phi_m + \Delta_s \sin\phi_m)]\theta_t - (1/2)(A_{cs}^2 \cos 2\phi_m - \Delta_{cs}^2 \sin 2\phi_m + S_{cs}^2) = 0 \quad (3.50)$$

where

$$A_{cs}^2 = (\Delta_c^2 - \Delta_s^2)/2 \qquad \Delta_{cs}^2 = \Delta_c \Delta_s \qquad S_{cs}^2 = (\Delta_c^2 + \Delta_s^2)/2$$

The solution of this equation gives

$$\theta_t = \theta_m - (\Delta_c \cos\phi_m + \Delta_s \sin\phi_m) + (2/\theta_m)(A_{cs}^2 \cos 2\phi_m + S_{cs}^2) \quad (3.51)$$

Then we have in second order

$$\frac{d\sigma}{d\Omega}(\theta_t) = \frac{d\sigma}{d\Omega}(\theta_m - (\Delta_c \cos\phi_m + \Delta_s \sin\phi_m) + (2/\theta_m)(A_{cs}^2 \cos 2\phi_m + S_{cs}^2))$$

$$= \frac{d\sigma}{d\Omega}(\theta_m)[1 + \delta_{cs}^s - \delta_c^1 \cos\phi_m - \delta_s^1 \sin\phi_m + \delta_{cs}^A \cos 2\phi_m + \delta_{cs}^s \sin 2\phi_m]$$

where

$$\delta_{cs}^s = [(2\sigma'/\theta_m\sigma) + (\sigma''/2\sigma)]S_{cs}^2 \quad (3.53)$$

$$\delta_c^1 = \frac{\sigma'}{\sigma}\Delta_c \qquad \delta_s^1 = \frac{\sigma'}{\sigma}\Delta_s \quad (3.54)$$

$$\delta_{cs}^A = [(2\sigma'/\theta_m\sigma) + (\sigma''/2\sigma)]A_{cs}^2 \quad (3.55)$$

$$\delta_{cs}^S = \frac{\sigma''}{2\sigma}\Delta_{cs}^2 \quad (3.56)$$

and

$$\sigma = \frac{d\sigma}{d\Omega}(\theta_m) \qquad \sigma' = \frac{\partial}{\partial\theta_m}\frac{d\sigma}{d\Omega} \qquad \sigma'' = \frac{\partial^2}{\partial\theta_m^2}\frac{d\sigma}{d\Omega}.$$

Multiplying $(d\sigma/d\Omega)(\theta_t)$ by $(1 + \varepsilon_c \cos\phi + \varepsilon_s \sin\phi + \varepsilon_{2c} \cos 2\phi + \varepsilon_{2s} \sin 2\phi)$ one obtains in second order

$$\varepsilon_c^t = \varepsilon_c^m + \delta_c^1 \quad (3.57)$$

$$\varepsilon_s^t = \varepsilon_s^m + \delta_s^1 \quad (3.58)$$

$$\varepsilon_{2c}^t = \varepsilon_{2c}^m - \delta_{cs}^A + (1/2)(\varepsilon_c^m \delta_c^1 - \varepsilon_s^m \delta_s^1 + (\delta_c^1)^2 - (\delta_s^1)^2 \quad (3.59)$$

$$\varepsilon_{2s}^t = \varepsilon_{2s}^m - \delta_{cs}^\Delta + (1/2)(\varepsilon_c^m \delta_s^1 - \varepsilon_s^m \delta_c^1 + 2\delta_c^1 \delta_s^1) \quad (3.60)$$

Using formula (3.15) it is easy to see that good approximations of σ'/σ, σ''/σ are given by

$$\frac{\sigma'}{\sigma} = \left\{\frac{\partial}{\partial\theta_C}\left(\int_0^{2\pi} N(\theta_H, \theta_C, \phi_C)\, d\phi_C\right)\right\} \Big/ \left(\int_0^{2\pi} N(\theta_H, \theta_C, \phi_C)\, d\phi_C\right) \quad (3.61)$$

$$\frac{\sigma''}{\sigma} = \left\{\frac{\partial^2}{\partial\theta_C^2}\left(\int_0^{2\pi} N(\theta_H, \theta_C, \phi_C)\, d\phi_C\right)\right\} \Big/ \left(\int_0^{2\pi} N(\theta_H, \theta_C, \phi_C)\, d\phi_C\right) \quad (3.62)$$

Direct calculation gives $\bar{\delta}_c^1 \sim 2‰$, $\bar{\delta}_s^1 \sim 0‰$, max $\delta_c^1 < 1\%$, max $\delta_s^1 < 5‰$. Second order corrections are $<10^{-4}$. Corrections given by (3.57) to (3.60) were directly calculated and applied to the determination of the εs presented in the following.

We can have other biasses or asymmetries in the apparatus due to non-uniform MWPC efficiencies in ϕ_C, residual misalignments and non-central passage through the polarimeter with asymmetric absorption and multiple scattering; all these effects imply an additive uncertainty for each ε.

3.2.4. *Beam polarisation effects*

For a given θ_H we have the following list of observables when we polarise the proton beam in the $\pm x$, $\pm y$, $\pm z$ directions

$$\begin{aligned}
&\varepsilon_c^m(+y) = \varepsilon_c^t(+y) + b_y^1 \\
&\varepsilon_c^m(\pm x/\pm z) = \varepsilon_c^t(\pm x/\pm z) + b_y^1 \qquad (3.63)\\
&\varepsilon_c^m(-y) = \varepsilon_c^t(-y) + b_y^1
\end{aligned}$$

$$\begin{aligned}
&\varepsilon_{2c}^m(+y) = \varepsilon_{2c}^t(+y) + b_y^2 \\
&\varepsilon_{2c}^m(\pm x/\pm z) = \varepsilon_{2c}^t(\pm x/\pm z) + b_y^2 \qquad (3.64)\\
&\varepsilon_{2c}^m(-y) = \varepsilon_{2c}^t(-y) + b_y^2
\end{aligned}$$

$$\begin{aligned}
&\varepsilon_s^m(+x/+z) = \varepsilon_s^t(+x/+z) + b_x^1 \\
&\varepsilon_s^m(\pm y) = b_x^1 \qquad (3.65)\\
&\varepsilon_s^m(-x/-z) = \varepsilon_s^t(-x/-z) + b_x^1
\end{aligned}$$

Table 3
Explicit relations between the measured asymmetries ε and the deuteron polarisation observables A_{kq}^{iB}, t_{kq}^0, and the dC analyzing powers T^{22}, T^{11}, T^{21} and T^{20}. The observables A_{kq}^{iB} ($i = x, y, z$) and t_{kq}^0 are intended here in the lab frame of the reaction.

$$\begin{aligned}
&\varepsilon_c(+y) = [T^{11}(-it_{11}^0 - ip_y A_{11}^{yB}) + T^{21}(t_{21}^0 + p_y A_{21}^{yB})]/[1 + p_y A^{yB} + T^{20}(t_{20}^0 + p_y A_{20}^{yB})]\\
&\varepsilon_c(-y) = [T^{11}(-it_{11}^0 + ip_y A_{11}^{yB}) + T^{21}(t_{21}^0 - p_y A_{21}^{yB})]/[1 - p_y A^{yB} + T^{20}(t_{20}^0 - p_y A_{20}^{yB})]\\
&\varepsilon_{2c}(+y) = [T^{22}(t_{22}^0 + p_y A_{22}^{yB})]/[1 + p_y A^{yB} + T^{20}(t_{20}^0 + p_y A_{20}^{yB})]\\
&\varepsilon_{2c}(-y) = [T^{22}(t_{22}^0 - p_y A_{22}^{yB})]/[1 - p_y A^{yB} + T^{20}(t_{20}^0 - p_y A_{20}^{yB})]\\
&\varepsilon_c(+x) = [-T^{11}it_{11}^0 + T^{21}t_{21}^0]/(1 + T^{20}t_{20}^0) = \varepsilon_c(0)\\
&\varepsilon_{2c}(+x) = T^{22}t_{22}^0/(1 + T^{20}t_{20}^0) = \varepsilon_{2c}(0)\\
&\varepsilon_c(0) = \varepsilon_c(-x) = \varepsilon_c(+z) = \varepsilon_c(-z)\\
&\varepsilon_{2c}(0) = \varepsilon_{2c}(-x) = \varepsilon_{2c}(+z) = \varepsilon_{2c}(-z)\\
&\varepsilon_s(+x) = p_x[-T^{11}A_{11}^{xB} - iT^{21}A_{21}^{xB}]/(1 + T^{20}t_{20}^0) = p_x\varepsilon_s(X)\\
&\varepsilon_s(+z) = p_z[-T^{11}A_{11}^{zB} - iT^{21}A_{21}^{zB}]/(1 + T^{20}t_{20}^0) = p_z\varepsilon_s(Z)\\
&\varepsilon_s(-x) = -p_x\varepsilon_s(X)\\
&\varepsilon_s(-z) = -p_z\varepsilon_s(Z)\\
&\varepsilon_{2s}(+x) = -p_x T^{22} iA_{22}^{xB}/(1 + T^{20}t_{20}^0) = p_x\varepsilon_{2s}(X)\\
&\varepsilon_{2s}(+z) = -p_z T^{22} iA_{22}^{zB}/(1 + T^{20}t_{20}^0) = p_z\varepsilon_{2s}(Z)\\
&\varepsilon_{2s}(-x) = -p_x\varepsilon_{2s}(X)\\
&\varepsilon_{2s}(-z) = -p_z\varepsilon_{2s}(Z)\\
&\varepsilon_s(+y) = \varepsilon_s(-y) = \varepsilon_{2s}(+y) = \varepsilon_{2s}(-y) = 0
\end{aligned}$$

$$\begin{aligned}
\varepsilon_{2s}^{m}(+x/+z) &= \varepsilon_{2s}^{t}(+x/+z) + b_x^2 \\
\varepsilon_{2s}^{m}(\pm y) &= b_x^2 \\
\varepsilon_{2s}^{m}(-x/-z) &= \varepsilon_{2s}^{t}(-x/-z) + b_x^2
\end{aligned} \tag{3.66}$$

b_x^2, b_x^1, b_y^1, b_y^2 are possible residual asymmetries.

3.2.5. *Experimental observables*

Of these 24 observables only 10 are independent (see Table 3). By minimisation it was then possible to calculate these 10 observables and b_x^1 and b_x^2. But no information is available on b_y^1 and b_y^2; these errors remain as uncertainties. However an indirect evaluation of b_y^2 was possible using pure $p^{12}C$ scattering and we found $b_x^2 = 5‰$; b_y^1 remains completely unknown, but estimated to be $<5‰$, see Ref. [19].

IV. Results of analysis

a) In this chapter we wish to summarise the results that we have obtained on the ε. All the corrections explained in Sections II and III were directly applied at each energy and at each angle. The results which we present here are integrated over all bins in θ_C (see from (3.10) and (3.18)). Thus the definition of the analysing powers is given by:

$$T^{kq}(i) = \frac{\sum_j \int_{\Delta\theta_C(j)} \frac{d\sigma}{d\Omega}(\theta_C)\,\mathrm{Acc}\,(\theta_C)\left[\int_{\Delta\theta_H(i)} \pi^{kq}(\theta_H, \theta_C)\,d\theta_H\right] d\theta_C}{\sum_j \int_{\Delta\theta_C(j)} \frac{d\sigma}{d\Omega}(\theta_C)\,\mathrm{Acc}\,(\theta_C)\,d\theta_C} \tag{4.1}$$

for the ith bin of θ_H.

We have 20 θ_H-bins at 580 MeV, 16 θ_H-bins at 515 and 447 MeV; this implies 480 ε at 580 MeV and 384 ε at 515 and at 447. After the minimisation explained in Ch. 3 §2 item *f*, we obtained 200 independent εs at 580 MeV and 160 at 515 and 447 MeV, i.e., a total of 520 new experimental points for the $pp \to d\P$ reaction.

We shall now present our data in Fig. 7 to 10 and Tables 4 to 10. In the figures there will be two fits, one shown as a continuous line and the other as a dashed line. At present we shall consider them as an overall guide; their specific meaning will be discussed in paragraph VI.

b) Figure 7 shows at 447, 515 and 580 MeV the polarisation asymmetries $\varepsilon_c(+y)$, $\varepsilon_c(-y)$, $\varepsilon_c(0)$ as defined in Table 3. We see that the spin effects are sufficiently large to be measured.

The small difference between $\varepsilon_c(+y)$ and $\varepsilon_c(-y)$ at 580 MeV compared to 515 and 447 MeV can be explained by the fact that the 580 MeV data were

Table 4
Numerical values at 447 MeV for the measured asymmetries $\varepsilon_c(+y)$, $\varepsilon_c(0)$, $\varepsilon_c(-y)$, $\varepsilon_{2c}(+y)$, $\varepsilon_{2c}(0)$ and $\varepsilon_{2c}(-y)$ as a function of the deuteron c.m. angle. The quoted errors are purely statistical.

$\theta_{\text{c.m.}}$	$\varepsilon_c(+y)$	$\varepsilon_c(0)$	$\varepsilon_c(-y)$	$\varepsilon_{2c}(+y)$	$\varepsilon_{2c}(0)$	$\varepsilon_{2c}(-y)$
52.50	-0.0679 ± 0.0068	-0.0200 ± 0.0030	0.0261 ± 0.0062	0.0281 ± 0.0067	0.0191 ± 0.0030	0.0086 ± 0.0061
57.50	-0.0535 ± 0.0055	-0.0232 ± 0.0024	0.0236 ± 0.0051	0.0283 ± 0.0054	0.0217 ± 0.0024	0.0190 ± 0.0050
62.50	-0.0568 ± 0.0053	-0.0232 ± 0.0024	0.0156 ± 0.0050	0.0440 ± 0.0052	0.0288 ± 0.0023	0.0172 ± 0.0049
67.50	-0.0481 ± 0.0052	-0.0274 ± 0.0024	0.0115 ± 0.0052	0.0291 ± 0.0052	0.0351 ± 0.0024	0.0206 ± 0.0051
72.50	-0.0538 ± 0.0053	-0.0278 ± 0.0025	0.0043 ± 0.0056	0.0457 ± 0.0052	0.0379 ± 0.0025	0.0355 ± 0.0055
77.50	-0.0386 ± 0.0060	-0.0177 ± 0.0029	0.0153 ± 0.0065	0.0485 ± 0.0059	0.0401 ± 0.0028	0.0483 ± 0.0064
82.50	-0.0239 ± 0.0075	-0.0160 ± 0.0036	0.0064 ± 0.0084	0.0336 ± 0.0073	0.0340 ± 0.0036	0.0467 ± 0.0083
87.50	-0.0105 ± 0.0115	-0.0012 ± 0.0056	-0.0120 ± 0.0132	0.0014 ± 0.0113	0.0321 ± 0.0055	0.0150 ± 0.0131
93.75	-0.0112 ± 0.0064	-0.0002 ± 0.0034	-0.0183 ± 0.0079	0.0321 ± 0.0064	0.0335 ± 0.0033	0.0221 ± 0.0078
101.25	0.0165 ± 0.0052	-0.0040 ± 0.0026	-0.0162 ± 0.0059	0.0172 ± 0.0051	0.0220 ± 0.0026	0.0261 ± 0.0058
108.75	0.0157 ± 0.0047	0.0028 ± 0.0023	-0.0116 ± 0.0049	0.0156 ± 0.0046	0.0070 ± 0.0023	0.0053 ± 0.0048
116.25	0.0206 ± 0.0043	0.0004 ± 0.0020	-0.0144 ± 0.0041	0.0087 ± 0.0042	0.0065 ± 0.0020	0.0034 ± 0.0041
123.75	0.0145 ± 0.0040	0.0035 ± 0.0018	-0.0060 ± 0.0037	0.0068 ± 0.0039	0.0009 ± 0.0018	-0.0005 ± 0.0036
131.25	0.0092 ± 0.0039	0.0028 ± 0.0018	-0.0006 ± 0.0035	0.0007 ± 0.0038	0.0012 ± 0.0017	-0.0035 ± 0.0034
138.75	0.0071 ± 0.0055	0.0054 ± 0.0025	0.0034 ± 0.0049	0.0085 ± 0.0054	0.0000 ± 0.0025	0.0045 ± 0.0048
146.25	-0.0272 ± 0.0288	-0.0231 ± 0.0135	0.0208 ± 0.0254	-0.0045 ± 0.0277	0.0304 ± 0.0131	-0.0210 ± 0.0247

Table 5
Same as Table 4 but at 515 MeV.

$\theta_{c.m.}$[deg]	$\varepsilon_c(+y)$	$\varepsilon_c(0)$	$\varepsilon_c(-y)$	$\varepsilon_{2c}(+y)$	$\varepsilon_{2c}(0)$	$\varepsilon_{2c}(-y)$
52.50	-0.0679 ± 0.0062	-0.0155 ± 0.0030	0.0091 ± 0.0057	0.0261 ± 0.0062	0.0231 ± 0.0030	0.0111 ± 0.0056
57.50	-0.0721 ± 0.0050	-0.0270 ± 0.0024	0.0030 ± 0.0045	0.0428 ± 0.0049	0.0311 ± 0.0024	0.0232 ± 0.0045
62.50	-0.0725 ± 0.0048	-0.0297 ± 0.0024	-0.0013 ± 0.0045	0.0380 ± 0.0047	0.0390 ± 0.0024	0.0377 ± 0.0044
67.50	-0.0707 ± 0.0049	-0.0338 ± 0.0025	-0.0066 ± 0.0046	0.0509 ± 0.0048	0.0430 ± 0.0025	0.0413 ± 0.0046
72.50	-0.0625 ± 0.0050	-0.0374 ± 0.0026	-0.0120 ± 0.0049	0.0519 ± 0.0049	0.0501 ± 0.0026	0.0483 ± 0.0048
77.50	-0.0518 ± 0.0055	-0.0253 ± 0.0029	0.0026 ± 0.0054	0.0497 ± 0.0053	0.0574 ± 0.0029	0.0560 ± 0.0054
82.50	-0.0356 ± 0.0066	-0.0282 ± 0.0037	-0.0202 ± 0.0067	0.0483 ± 0.0065	0.0532 ± 0.0036	0.0541 ± 0.0066
87.50	-0.0146 ± 0.0095	-0.0269 ± 0.0055	-0.0029 ± 0.0098	0.0678 ± 0.0093	0.0452 ± 0.0055	0.0412 ± 0.0097
93.75	0.0105 ± 0.0077	-0.0049 ± 0.0041	-0.0105 ± 0.0089	0.0324 ± 0.0077	0.0358 ± 0.0041	0.0446 ± 0.0088
101.25	0.0136 ± 0.0058	0.0013 ± 0.0030	-0.0097 ± 0.0063	0.0334 ± 0.0057	0.0213 ± 0.0030	0.0063 ± 0.0063
108.75	0.0228 ± 0.0051	0.0012 ± 0.0026	-0.0171 ± 0.0053	0.0118 ± 0.0051	0.0072 ± 0.0026	0.0009 ± 0.0053
116.25	0.0215 ± 0.0046	0.0016 ± 0.0022	-0.0089 ± 0.0045	0.0088 ± 0.0045	-0.0042 ± 0.0022	-0.0080 ± 0.0045
123.75	0.0126 ± 0.0041	-0.0048 ± 0.0020	-0.0092 ± 0.0039	-0.0027 ± 0.0041	-0.0073 ± 0.0019	-0.0058 ± 0.0039
131.25	0.0178 ± 0.0038	-0.0042 ± 0.0018	-0.0094 ± 0.0036	-0.0034 ± 0.0038	-0.0012 ± 0.0018	-0.0043 ± 0.0035
138.75	0.0078 ± 0.0044	-0.0041 ± 0.0021	-0.0030 ± 0.0041	-0.0020 ± 0.0043	-0.0004 ± 0.0021	0.0015 ± 0.0040
146.25	-0.0037 ± 0.0118	0.0065 ± 0.0058	0.0018 ± 0.0111	0.0142 ± 0.0115	-0.0060 ± 0.0056	0.0053 ± 0.0109

Table 6
Same as Table 4 but at 580 MeV.

$\theta_{c.m.}$[deg]	$\varepsilon_c(+y)$	$\varepsilon_c(0)$	$\varepsilon_c(-y)$	$\varepsilon_{2c}(+y)$	$\varepsilon_{2c}(0)$	$\varepsilon_{2c}(-y)$
52.50	-0.0338 ± 0.0026	-0.0135 ± 0.0013	-0.0007 ± 0.0028	0.0449 ± 0.0026	0.0407 ± 0.0013	0.0405 ± 0.0028
57.50	-0.0501 ± 0.0024	-0.0199 ± 0.0012	-0.0118 ± 0.0026	0.0500 ± 0.0024	0.0511 ± 0.0012	0.0470 ± 0.0026
62.50	-0.0510 ± 0.0026	-0.0265 ± 0.0012	-0.0120 ± 0.0028	0.0642 ± 0.0026	0.0608 ± 0.0012	0.0574 ± 0.0028
67.50	-0.0434 ± 0.0028	-0.0271 ± 0.0013	-0.0182 ± 0.0030	0.0677 ± 0.0028	0.0695 ± 0.0013	0.0676 ± 0.0030
72.50	-0.0475 ± 0.0030	-0.0307 ± 0.0014	-0.0221 ± 0.0033	0.0802 ± 0.0030	0.0796 ± 0.0014	0.0780 ± 0.0033
77.50	-0.0434 ± 0.0032	-0.0302 ± 0.0015	-0.0229 ± 0.0035	0.0801 ± 0.0032	0.0844 ± 0.0015	0.0876 ± 0.0035
82.50	-0.0271 ± 0.0034	-0.0220 ± 0.0016	-0.0194 ± 0.0037	0.0832 ± 0.0033	0.0833 ± 0.0016	0.0880 ± 0.0037
87.50	-0.0245 ± 0.0042	-0.0172 ± 0.0019	-0.0098 ± 0.0046	0.0772 ± 0.0041	0.0762 ± 0.0019	0.0722 ± 0.0045
92.50	-0.0095 ± 0.0052	-0.0081 ± 0.0027	-0.0114 ± 0.0057	0.0670 ± 0.0052	0.0635 ± 0.0027	0.0628 ± 0.0056
97.50	0.0064 ± 0.0042	0.0008 ± 0.0022	-0.0118 ± 0.0045	0.0500 ± 0.0041	0.0533 ± 0.0022	0.0406 ± 0.0045
102.50	0.0164 ± 0.0040	0.0067 ± 0.0021	0.0012 ± 0.0043	0.0336 ± 0.0039	0.0344 ± 0.0020	0.0355 ± 0.0042
107.50	0.0125 ± 0.0037	0.0055 ± 0.0019	-0.0092 ± 0.0039	0.0297 ± 0.0036	0.0247 ± 0.0019	0.0197 ± 0.0039
112.50	0.0150 ± 0.0034	0.0023 ± 0.0017	-0.0040 ± 0.0036	0.0156 ± 0.0033	0.0135 ± 0.0017	0.0117 ± 0.0035
117.50	0.0014 ± 0.0031	-0.0004 ± 0.0016	-0.0066 ± 0.0033	0.0126 ± 0.0031	0.0099 ± 0.0016	0.0075 ± 0.0032
122.50	0.0078 ± 0.0029	0.0015 ± 0.0015	-0.0063 ± 0.0030	0.0069 ± 0.0028	0.0063 ± 0.0014	0.0035 ± 0.0030
127.50	0.0092 ± 0.0027	-0.0012 ± 0.0014	-0.0090 ± 0.0028	0.0081 ± 0.0026	0.0104 ± 0.0013	0.0091 ± 0.0027
132.50	0.0122 ± 0.0025	-0.0018 ± 0.0013	-0.0066 ± 0.0026	0.0208 ± 0.0024	0.0123 ± 0.0013	0.0095 ± 0.0026
137.50	0.0063 ± 0.0024	0.0002 ± 0.0012	-0.0064 ± 0.0025	0.0243 ± 0.0023	0.0172 ± 0.0012	0.0159 ± 0.0024
142.50	0.0047 ± 0.0023	0.0033 ± 0.0012	-0.0033 ± 0.0025	0.0220 ± 0.0023	0.0206 ± 0.0012	0.0179 ± 0.0024
147.50	0.0066 ± 0.0028	0.0046 ± 0.0014	0.0020 ± 0.0030	0.0288 ± 0.0027	0.0224 ± 0.0014	0.0247 ± 0.0029

Table 7
Numerical values for the measured asymmetry $\varepsilon_s(X)$ at 447, 515 and 580 MeV as a function of the deuteron c.m. scattering angle. The quoted errors are purely statistical.

$\theta_{c.m.}$[deg]	447 MeV	515 MeV	580 MeV
52.50	-0.0325 ± 0.0083	0.0095 ± 0.0075	-0.0425 ± 0.0044
57.50	-0.0357 ± 0.0066	-0.0043 ± 0.0068	-0.0465 ± 0.0039
62.50	-0.0228 ± 0.0058	0.0013 ± 0.0061	-0.0310 ± 0.0041
67.50	-0.0252 ± 0.0068	-0.0018 ± 0.0069	-0.0282 ± 0.0044
72.50	-0.0175 ± 0.0068	-0.0105 ± 0.0069	-0.0228 ± 0.0047
77.50	-0.0102 ± 0.0078	0.0186 ± 0.0070	-0.0073 ± 0.0049
82.50	-0.0064 ± 0.0098	-0.0003 ± 0.0094	-0.0039 ± 0.0051
87.50	-0.0075 ± 0.0143	0.0042 ± 0.0141	-0.0109 ± 0.0063
92.50			-0.0232 ± 0.0097
93.75	0.0096 ± 0.0094	0.0212 ± 0.0101	
97.50			-0.0327 ± 0.0076
101.25	0.0222 ± 0.0070	0.0266 ± 0.0073	
102.50			-0.0296 ± 0.0072
107.50			-0.0497 ± 0.0066
108.75	0.0221 ± 0.0066	0.0296 ± 0.0060	
112.50			-0.0546 ± 0.0060
116.25	0.0187 ± 0.0056	0.0301 ± 0.0059	
117.50			-0.0436 ± 0.0055
122.50			-0.0474 ± 0.0050
123.75	0.0087 ± 0.0050	0.0278 ± 0.0055	
127.50			-0.0365 ± 0.0047
131.25	0.0160 ± 0.0048	0.0278 ± 0.0044	
132.50			-0.0236 ± 0.0044
137.50			-0.0262 ± 0.0042
138.75	0.0074 ± 0.0067	0.0088 ± 0.0054	
142.50			-0.0242 ± 0.0041
146.25	-0.0252 ± 0.0359	0.0065 ± 0.0147	
147.50			-0.0165 ± 0.0049

measured with a beam polarisation of 0.4165 while for 515 and 447 MeV data the beam polarisation was 0.8108.

c) Figure 8 tells us that $2\phi_C$ asymmetries exist and are measurable while practically no spin dependence on the beam polarisation is observed. This dependence on the beam polarisation is observed. This implies a small value of A_{22}^{yB}. The shape of the distributions are very similar to those predicted by Ref [17]. The difference in absolute value between the three figures is essentially due to the fast increase of the analysing power T^{22}. Figures 7 and 8 give also a global view of the energy dependence of $\varepsilon_c(0)$ and $\varepsilon_{2c}(0)$.

d) Figures 9 and 10 give $\varepsilon_s(X)$, $\varepsilon_s(Z)$, $\varepsilon_{2s}(X)$ and $\varepsilon_{2s}(Z)$ as defined in Table 3, because they are completely independent of p_B. From Fig. 9 and 10 and from item c), we see that A_{22}^{xB} and A_{22}^{zB} are not large. As Ref. [55] indicates, the tensor spin transfer A_{22}^{yB}, A_{22}^{zB}, A_{22}^{xB} are small.

In general we note similarities with the predictions of Ref. [55]. Tables 4 to 10 complete these plots.

Table 8
Same as Table 7 but for the asymmetry $\varepsilon_{2s}(X)$.

$\theta_{c.m.}$[deg]	447 MeV	515 MeV	580 MeV
52.50	0.0189 ± 0.0081	0.0193 ± 0.0079	−0.0031 ± 0.0043
57.50	0.0141 ± 0.0065	0.0234 ± 0.0056	−0.0163 ± 0.0039
62.50	0.0232 ± 0.0062	0.0260 ± 0.0063	−0.0123 ± 0.0041
67.50	0.0225 ± 0.0054	0.0192 ± 0.0058	−0.0176 ± 0.0044
72.50	0.0282 ± 0.0067	0.0137 ± 0.0063	−0.0121 ± 0.0046
77.50	0.0243 ± 0.0077	0.0245 ± 0.0077	−0.0185 ± 0.0048
82.50	0.0262 ± 0.0096	0.0187 ± 0.0092	−0.0159 ± 0.0050
87.50	−0.0073 ± 0.0141	0.0288 ± 0.0140	0.0055 ± 0.0062
92.50			−0.0087 ± 0.0096
93.75	0.0171 ± 0.0093	0.0067 ± 0.0108	
97.50			−0.0150 ± 0.0076
101.25	0.0296 ± 0.0067	0.0125 ± 0.0081	
102.50			−0.0032 ± 0.0071
107.50			−0.0077 ± 0.0065
108.75	0.0168 ± 0.0053	0.0106 ± 0.0072	
112.50			−0.0008 ± 0.0059
116.25	0.0118 ± 0.0048	0.0030 ± 0.0056	
117.50			−0.0129 ± 0.0054
122.50			−0.0040 ± 0.0050
123.75	0.0102 ± 0.0050	0.0203 ± 0.0046	
127.50			−0.0102 ± 0.0046
131.25	0.0119 ± 0.0043	0.0057 ± 0.0048	
132.50			−0.0090 ± 0.0043
137.50			−0.0081 ± 0.0041
138.75	0.0096 ± 0.0060	0.0054 ± 0.0052	
142.50			−0.0101 ± 0.0040
146.25	0.0188 ± 0.0297	0.0168 ± 0.0148	
147.50			−0.0058 ± 0.0047

V. Theory of amplitude reconstruction

5.1. *Scattering amplitudes*

We will continue using the notations and conventions of Ref. [20].

The most general expression for the scattering amplitudes in the $pp \to d\P$ reaction is given by

$$F_\gamma^{\alpha\beta}(\theta) = C\langle \vec{P}_d\gamma, \vec{P}_\P | T | \vec{P}_B\alpha, \vec{P}_T\beta \rangle \tag{5.1}$$

where $\gamma = \pm 1, 0$ is the helicity of the deuteron, $\alpha, \beta = \pm 1/2$ are the helicities of the two incident protons, $\vec{P}_d$, $\vec{P}_\P$, $\vec{P}_B$, $\vec{P}_T$ are respectively the momenta of the deuteron, pion, beam proton and target proton. T is the T-matrix, whose elements are on the energy shell with the momentum conservation and whose relation with the S-matrix is then given by (Ref. [48])

$$S_{fi} = \delta_{fi} - 2\P i\delta(E_f - E_i)\delta(\vec{P}_f - \vec{P}_i)T_{fi} \tag{5.2}$$

and S is such that $S^+S = SS^+ = 1$.

Table 9
Same as Table 7 but for the asymmetry $\varepsilon_s(Z)$.

$\theta_{c.m.}$[deg]	447 MeV	515 MeV	580 MeV
52.50	-0.0930 ± 0.0086	-0.1064 ± 0.0074	-0.1173 ± 0.0044
57.50	-0.0788 ± 0.0070	-0.0940 ± 0.0068	-0.0995 ± 0.0041
62.50	-0.0627 ± 0.0063	-0.0776 ± 0.0060	-0.0779 ± 0.0044
67.50	-0.0649 ± 0.0072	-0.0569 ± 0.0069	-0.0633 ± 0.0048
72.50	-0.0517 ± 0.0072	-0.0484 ± 0.0069	-0.0356 ± 0.0052
77.50	-0.0339 ± 0.0083	-0.0132 ± 0.0070	-0.0242 ± 0.0055
82.50	-0.0227 ± 0.0105	-0.0103 ± 0.0094	-0.0102 ± 0.0059
87.50	-0.0091 ± 0.0155	0.0060 ± 0.0139	-0.0020 ± 0.0072
92.50			0.0039 ± 0.0092
93.75	-0.0091 ± 0.0093	0.0098 ± 0.0107	
97.50			-0.0116 ± 0.0074
101.25	-0.0046 ± 0.0070	0.0081 ± 0.0076	
102.50			-0.0164 ± 0.0070
107.50			-0.0193 ± 0.0065
108.75	-0.0008 ± 0.0066	-0.0048 ± 0.0063	
112.50			-0.0178 ± 0.0059
116.25	0.0006 ± 0.0056	-0.0123 ± 0.0061	
117.50			-0.0275 ± 0.0055
122.50			-0.0291 ± 0.0050
123.75	-0.0106 ± 0.0051	0.0018 ± 0.0056	
127.50			-0.0220 ± 0.0046
131.25	0.0005 ± 0.0049	-0.0106 ± 0.0046	
132.50			-0.0275 ± 0.0044
137.50			-0.0194 ± 0.0041
138.75	0.0061 ± 0.0070	0.0025 ± 0.0057	
142.50			-0.0079 ± 0.0041
146.25	0.0153 ± 0.0398	-0.0009 ± 0.0151	
147.50			-0.0098 ± 0.0050

With the plane wave normalisation

$$\langle \vec{P}' \mid \vec{P} \rangle = (2\P\rangle)^3 \delta^3(\vec{P} - \vec{P}') \tag{5.3}$$

and the conventional formula

$$\frac{d\sigma}{d\Omega} = \tfrac{1}{4} \sum_{\alpha\beta\gamma} |F_\gamma^{\alpha\beta}|^2 \tag{5.4}$$

one obtains for the normalisation constant C of (5.1)

$$C = \frac{-1}{2\P} (P_f/P_i)^{1/2} (\mu_i(P_i)\mu_f(P_f))^{1/2} \tag{5.5}$$

where

$$\begin{aligned}
&\vec{P}_i = \tfrac{1}{2}(\vec{P}_B - \vec{P}_T) \quad P_i = |\vec{P}_i| \\
&\vec{P}_f = \tfrac{1}{2}(\vec{P}_d - \vec{P}_\P) \quad P_f = |\vec{P}_f| \\
&\mu_i(P_i) = \frac{(P_i^2 + m_B^2)^{1/2}(P_i^2 + m_T^2)^{1/2}}{(P_i^2 + m_B^2)^{1/2} + (P_i^2 + m_T^2)^{1/2}} \\
&\mu_f(P_f) = \frac{(P_f^2 + m_B^2)^{1/2}(P_f^2 + m_T^2)^{1/2}}{(P_f^2 + m_B^2)^{1/2} + (P_f^2 + m_T^2)^{1/2}}
\end{aligned} \tag{5.6}$$

Table 10
Same as Table 7 but for the asymmetry $\varepsilon_{2s}(Z)$.

$\theta_{c.m.}$[deg]	447 MeV	515 MeV	580 MeV
52.50	0.0213 ± 0.0084	0.0246 ± 0.0078	0.0147 ± 0.0044
57.50	0.0041 ± 0.0069	0.0179 ± 0.0056	0.0124 ± 0.0040
62.50	0.0247 ± 0.0066	0.0130 ± 0.0062	0.0186 ± 0.0044
67.50	0.0222 ± 0.0059	0.0152 ± 0.0058	0.0247 ± 0.0047
72.50	0.0288 ± 0.0071	0.0154 ± 0.0063	0.0183 ± 0.0051
77.50	0.0164 ± 0.0082	0.0292 ± 0.0077	0.0129 ± 0.0054
82.50	0.0287 ± 0.0103	0.0131 ± 0.0091	0.0068 ± 0.0058
87.50	−0.0099 ± 0.0153	0.0140 ± 0.0137	0.0049 ± 0.0071
92.50			0.0077 ± 0.0091
93.75	0.0185 ± 0.0092	−0.0043 ± 0.0113	
97.50			0.0049 ± 0.0073
101.25	0.0189 ± 0.0067	0.0079 ± 0.0084	
102.50			0.0118 ± 0.0069
107.50			−0.0039 ± 0.0064
108.75	0.0032 ± 0.0053	0.0071 ± 0.0074	
112.50			−0.0020 ± 0.0058
116.25	0.0030 ± 0.0049	0.0012 ± 0.0058	
117.50			0.0057 ± 0.0054
122.50			0.0078 ± 0.0049
123.75	0.0027 ± 0.0050	0.0045 ± 0.0049	
127.50			0.0033 ± 0.0045
131.25	0.0172 ± 0.0043	−0.0030 ± 0.0050	
132.50			0.0023 ± 0.0043
137.50			0.0035 ± 0.0040
138.75	0.0107 ± 0.0063	−0.0012 ± 0.0055	
142.50			−0.0026 ± 0.0040
146.25	−0.0298 ± 0.0333	0.0234 ± 0.0151	
147.50			0.0024 ± 0.0048

Taking all the possible combinations of α, β, γ in (5.1) yields to 12 complex amplitudes. However, applying parity conservation to the reaction, we find that

$$F_{\gamma}^{\alpha\beta}(\theta) = -(-1)^{\alpha+\beta+\gamma} F_{-\gamma}^{-\alpha-\beta}(\theta) \tag{5.7}$$

where the minus sign reflects the negative intrinsic parity of the pion. This reduces to six the number of independent amplitudes, i.e.

$$\begin{aligned} A &= F_1^{1/2\,1/2} = -F_{-1}^{-1/2\,-1/2} & B &= F_0^{1/2\,1/2} = F_0^{-1/2\,-1/2} \\ C &= F_{-1}^{1/2\,1/2} = -F_1^{-1/2\,-1/2} & D &= F_0^{-1/2\,1/2} = -F_0^{1/2\,-1/2} \\ E &= F_1^{-1/2\,1/2} = F_{-1}^{1/2\,-1/2} & F &= F_1^{1/2\,-1/2} = F_{-1}^{-1/2\,1/2} \end{aligned} \tag{5.8}$$

On the other hand, since the two initial particles are identical we can use the symmetry–antisymmetry relations arising from the Pauli principle to obtain

$$F_{\gamma}^{\alpha\beta}(\theta) = (-1)^{\alpha-\beta+\gamma} F_{\gamma}^{\beta\alpha}(¶ - \theta) \tag{5.9}$$

where θ is the CM scattering angle. More explicitly the amplitudes become

$$\begin{aligned} &A(\theta) = -A(¶ - \theta) \qquad B(\theta) = B(¶ - \theta) \qquad C(\theta) = -C(¶ - \theta) \\ &D(\theta) = D(¶ - \theta) \qquad E(\theta) = F(¶ - \theta) \end{aligned} \tag{5.10}$$

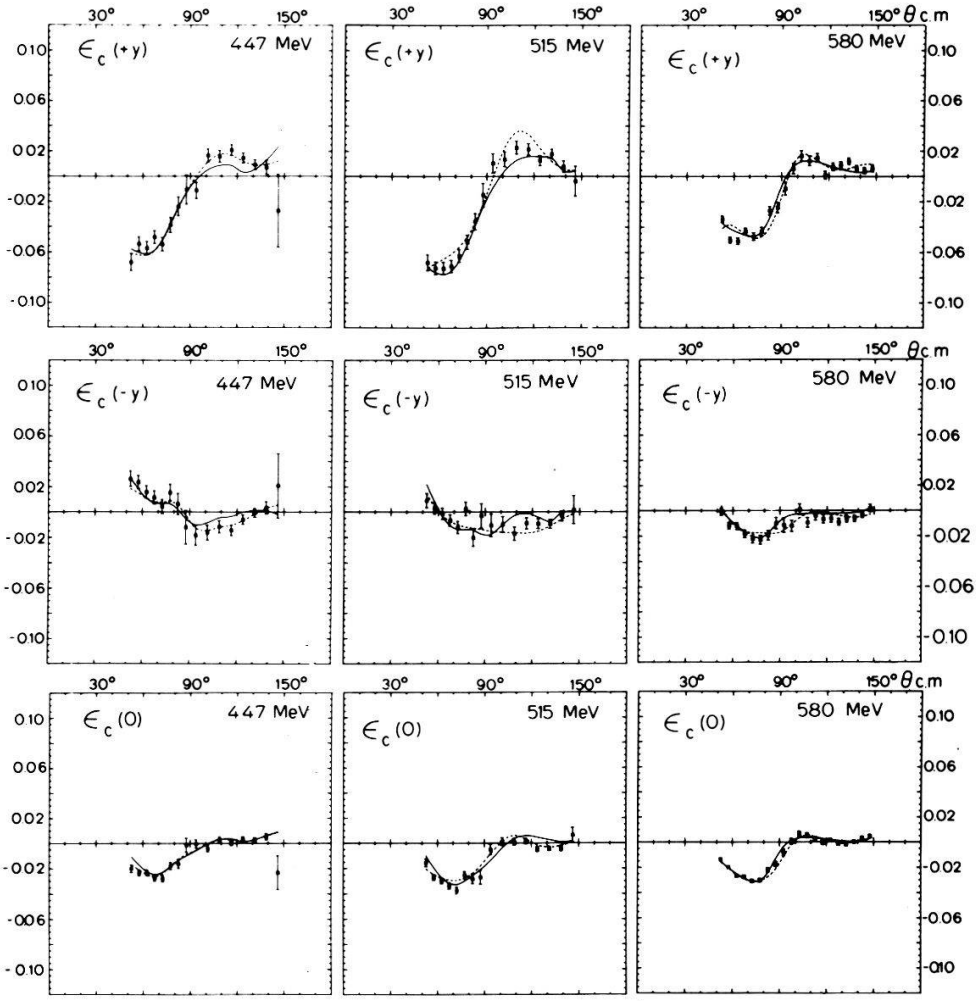

Figure 7
Plots of the measured asymmetries $\varepsilon_c(+y)$, $\varepsilon_c(-y)$ and $\varepsilon_c(0)$ as a function of the deuteron c.m. scattering angle for the 3 energies 447, 515 and 580 MeV. The full and dotted lines are discussed in paragraph VI.

We can derive now the explicit relations between amplitudes and observables. If we define $I_0 = (d\sigma/d\Omega)_0$, one obtains for the spherical observables (equation 1.21):

$$4I_0 = \sum_{\alpha\beta\gamma} |F_\gamma^{\alpha\beta}|^2 \tag{5.11}$$

$$4I_0 A^{q'T} = \sum_{\alpha\gamma\beta\beta'} F_\gamma^{\alpha\beta} F_\gamma^{\alpha\beta'*} [(-1)^{1/2-\beta'} \sqrt{2}\, \langle 1/2\beta', 1/2-\beta \mid 1q' \rangle] \tag{5.12}$$

$$4I_0 A^{q''B} = \sum_{\beta\gamma\alpha\alpha'} F_\gamma^{\alpha\beta} F_\gamma^{\alpha'\beta*} [(-1)^{1/2-\alpha} \sqrt{2} \langle 1/2\alpha', 1/2-\alpha \mid 1q' \rangle] \tag{5.13}$$

$$4I_0 A^{q'q''} = \sum_{\gamma\alpha\alpha'\beta\beta'} F_\gamma^{\alpha\beta} F_\gamma^{\alpha'\beta'*} [(-1)^{\alpha+\beta} 2 \langle 1/2\alpha', 1/2-\alpha \mid 1q' \rangle \times \langle 1/2\beta', 1/2-\beta \mid 1q'' \rangle] \tag{5.14}$$

$$4I_0 t_{kq}^0 = \sum_{\alpha\beta\gamma\gamma'} F_\gamma^{\alpha\beta} F_{\gamma'}^{\alpha\beta*} [(-1)^{1-\gamma} \sqrt{3} < 1\gamma', 1\gamma \mid kq \rangle] \tag{5.15}$$

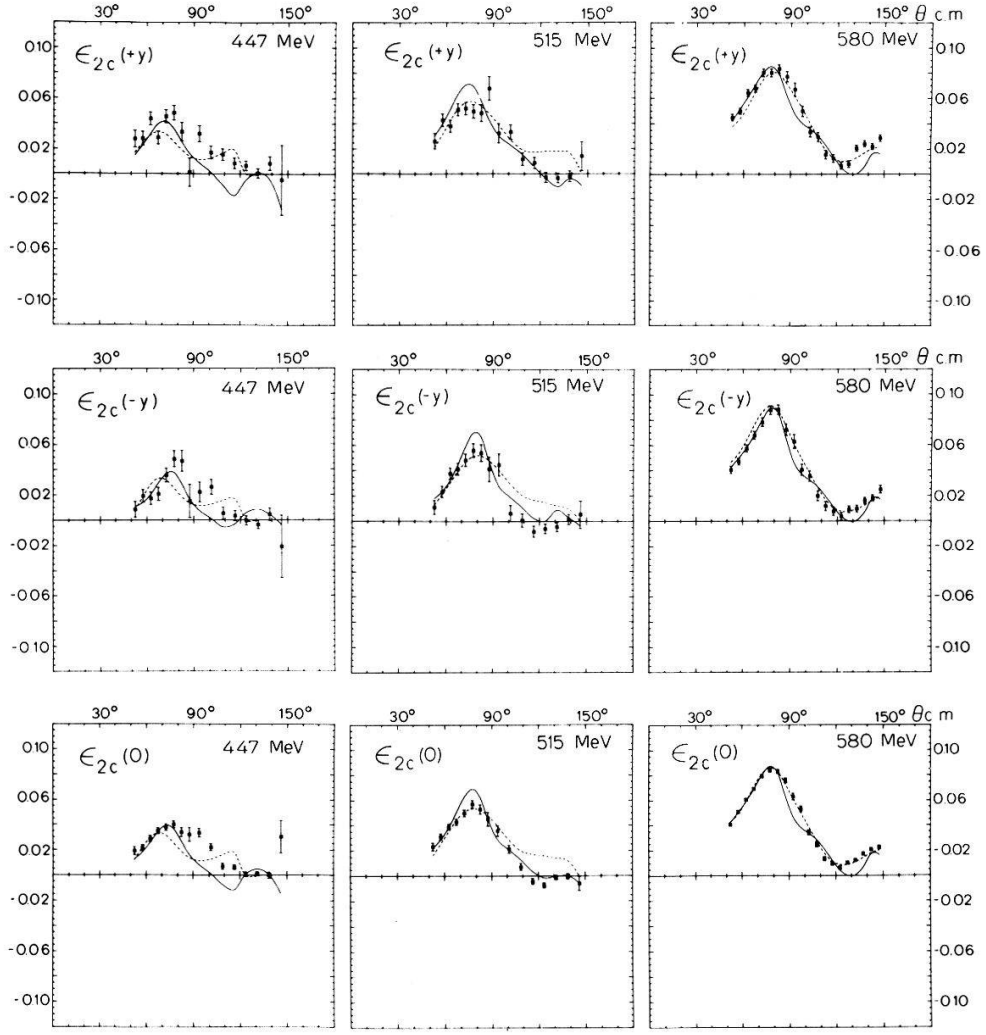

Figure 8
Same as Fig. 7 but for the asymmetries $\varepsilon_{2c}(+y)$, $\varepsilon_{2c}(-y)$ and $\varepsilon_{2c}(0)$.

$$4I_0 A_{kq}^{q''T} = \sum_{\alpha\beta\beta'\gamma\gamma'} F_\gamma^{\alpha\beta} F_{\gamma'}^{\alpha\beta'*} [(-1)^{1/2-\beta}\sqrt{2}\langle 1/2\beta', 1/2-\beta \mid 1q''\rangle$$

$$\times(-1)^{1-\gamma}\sqrt{3}<1\gamma', 1-\gamma \mid kq\rangle] \tag{5.16}$$

$$4I_0 A_{kq}^{q'B} = \sum_{\beta\alpha\alpha'\gamma\gamma'} F_\gamma^{\alpha\beta} F_{\gamma'}^{\alpha'\beta*} [(-1)^{1/2-\alpha}\sqrt{2}\langle 1/2\alpha', 1/2-\alpha \mid 1q'\rangle$$

$$\times(-1)^{1-\gamma}\sqrt{3}<1\gamma', 1-\gamma \mid kq\rangle] \tag{5.17}$$

$$4I_0 A_{kq}^{q'q''} = \sum_{\alpha\alpha'\beta\beta'\gamma\gamma'} F_\gamma^{\alpha\beta} F_{\gamma'}^{\alpha'\beta'*} [(-1)^{\alpha+\beta} 2\langle 1/2\alpha', 1/2-\alpha \mid 1q'\rangle$$

$$\times<1/2\beta', 1/2\beta \mid 1q''\rangle(-1)^{1-\gamma}\sqrt{3}<1\gamma', 1-\gamma \mid kq\rangle] \tag{5.18}$$

where the $\langle j_1 m_1, j_2 m_2 \mid kq\rangle$ are Clebsch–Gordon coefficients.

We give in Table 11 the explicit relations for the observables we use, as a function of the amplitudes A, B, C, D, E, F which are defined in (5.8). On the other hand, we give in Table 12 the formulae for the hybrid observables, as defined in equations (1.28) to (1.36).

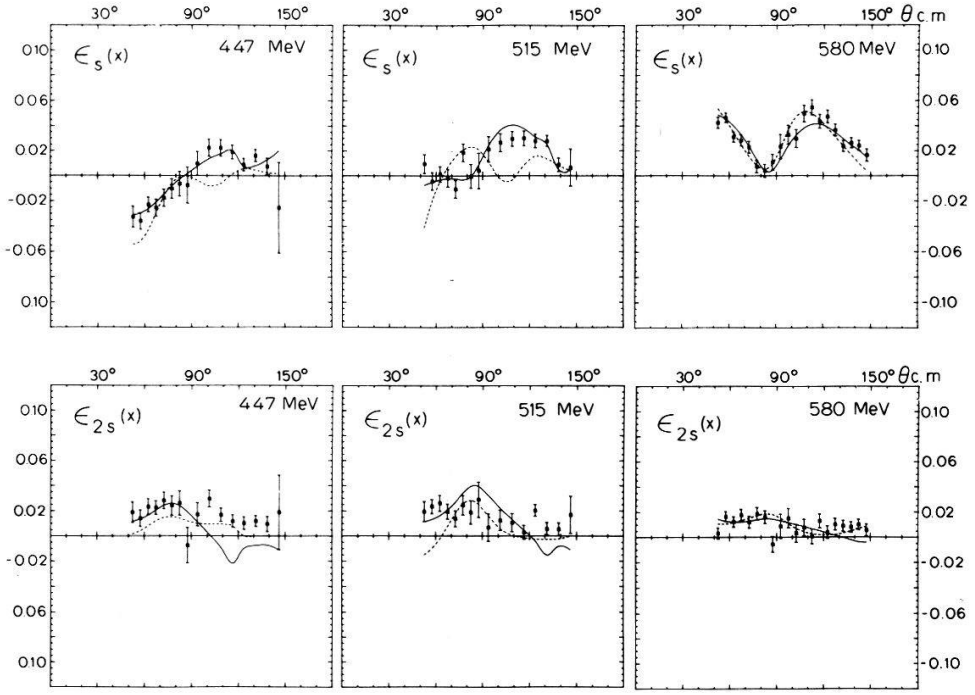

Figure 9
Same as Fig. 7 but for the asymmetries $\varepsilon_s(X)$ and $\varepsilon_{2s}(X)$.

5.2. *Partial wave decomposition*

In the helicity representation, the partial wave decomposition takes the form

$$F_\gamma^{\alpha\beta}(\theta) = \sum_J \frac{2J+1}{4\P} f_\gamma^{\alpha\beta}(J) d^J_{\alpha-\beta,\gamma}(\theta) \tag{5.19}$$

where J denotes the total angular momentum, and the d-function are defined as in Ref. [49].

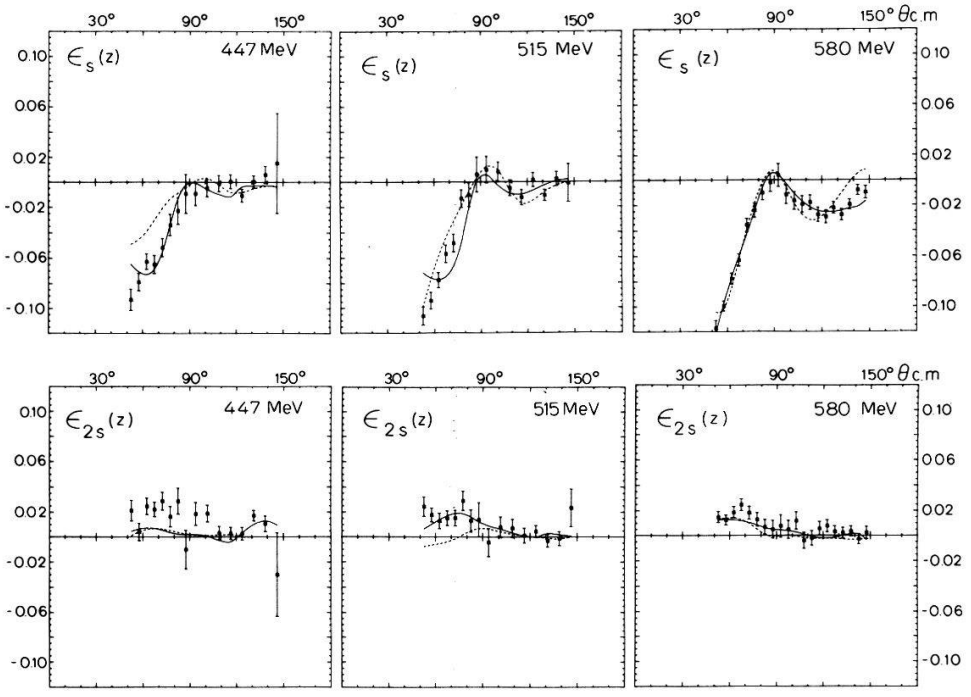

Figure 10
Same as Fig. 7 but for the asymmetries $\varepsilon_s(Z)$ and $\varepsilon_{2s}(Z)$.

Table 11
Explicit relation between the observables in spherical tensor representation and the amplitudes as defined in equation 5.8.

$I_0 = (1/2)(|A|^2 + |B|^2 + |C|^2 + |D|^2 + |E|^2 + |F|^2)$
$I_0 A^{1B} = (i/\sqrt{2})\,\mathrm{Im}\,(AE^* + CF^* + BD^*)$
$I_0 A^{1T} = (i/\sqrt{2})\,\mathrm{Im}\,(-AF^* - CE^* + BD^*)$
$I_0 A^{10} = (-1/\sqrt{2})\,\mathrm{Re}\,(AE^* + CF^* + BD^*)$
$I_0 A^{11} = (1/2)(|B|^2 - 2\,\mathrm{Re}\,(AC^*))$
$I_0 A^{1-1} = (1/2)(|D|^2 - 2\,\mathrm{Re}\,(EF^*))$
$I_0 A^{00} = (1/2)(|A|^2 + |B|^2 + |C|^2 - |D|^2 - |E|^2 - |F|^2)$
$I_0 t^0_{11} = (i\sqrt{6}/4)\,\mathrm{Im}\,(AB^* + BC^* - DE^* + DF^*)$
$I_0 t^0_{22} = (\sqrt{3}/2)\,\mathrm{Re}\,(AC^* + EF^*)$
$I_0 t^0_{21} = (\sqrt{6}/4)\,\mathrm{Re}\,(-AB^* + BC^* - DE^* + DF^*)$
$I_0 t^0_{20} = (\sqrt{2}/4)(|A|^2 + |B|^2 + |E|^2 + |F|^2) - (\sqrt{2}/2)(|B|^2 + |D|^2)$
$I_0 A^{1B}_{11} = (\sqrt{3}/2)\,\mathrm{Re}\,(AD^* + BF^*)$
$I_0 A^{1B}_{1-1} = (-\sqrt{3}/2)\,\mathrm{Re}\,(BE^* + CD^*)$
$I_0 A^{1B}_{10} = (\sqrt{3}/2)\,\mathrm{Re}\,(-AE^* + CF^*)$
$I_0 A^{1B}_{22} = (\sqrt{6}/2)i\,\mathrm{Im}\,(AF^*)$
$I_0 A^{1B}_{2-2} = (\sqrt{6}/2)i\,\mathrm{Im}\,(CE^*)$
$I_0 A^{1B}_{21} = (\sqrt{3}/2)i\,\mathrm{Im}\,(-AD^* + BF^*)$
$I_0 A^{1B}_{2-1} = (\sqrt{3}/2)i\,\mathrm{Im}\,(BE^* - CD^*)$
$I_0 A^{1B}_{20} = (1/2)i\,\mathrm{Im}\,(AE^* + CF^* - 2BD^*)$
$I_0 A^{0B}_{11} = (-\sqrt{6}/4)\,\mathrm{Re}\,(AB^* + BC^* - DE^* - DF^*)$
$I_0 A^{0B}_{10} = (\sqrt{6}/4)(|A|^2 - |C|^2 - |E|^2 + |F|^2)$
$I_0 A^{0B}_{21} = (\sqrt{6}/4)i\,\mathrm{Im}\,(AB^* - BC^* + DE^* + DF^*)$
$I_0 A^{0B}_{22} = (\sqrt{3}/2)i\,\mathrm{Im}\,(-AC^* + EF^*)$

Table 12
Explicit relation between the hybrid observables and the amplitudes as defined in equation 5.8.

$I_0 A^{yB} = \mathrm{Im}\,(AE^* + CF^* + BD^*)$
$I_0 A^{xz} = \mathrm{Re}\,(AE^* + CF^* + BD^*)$
$I_0 A^{xx} = (1/2)(|B|^2 - |D|^2 - 2\,\mathrm{Re}\,(AC^*) + 2\,\mathrm{Re}\,(EF^*))$
$I_0 A^{yy} = (-1/2)(|B|^2 + |D|^2 - 2\,\mathrm{Re}\,(AC^*) - 2\,\mathrm{Re}\,(EF^*))$
$I_0 A^{zx} = \mathrm{Re}\,(AF^* + CE^* - BD^*)$
$I_0 A^{yB}_{11} = i(\sqrt{6}/4)\,\mathrm{Re}\,(-AD^* - BF^* + BE^* + CD^*)$
$I_0 A^{yB}_{22} = (\sqrt{3}/2)\,\mathrm{Im}\,(AF^* + CE^*)$
$I_0 A^{yB}_{21} = (\sqrt{6}/4)\,\mathrm{Im}\,(-AD^* + BF^* - BE^* + CD^*)$
$I_0 A^{yB}_{20} = (\sqrt{2}/2)\,\mathrm{Im}\,(AE^* + CF^* - 2BD^*)$
$I_0 A^{xB}_{11} = (-\sqrt{6}/4)\,\mathrm{Re}\,(AD^* + BF^* + BE^* + CD^*)$
$I_0 A^{xB}_{10} = (-\sqrt{6}/2)\,\mathrm{Re}\,(-AE^* + CF^*)$
$I_0 A^{xB}_{22} = -i(\sqrt{3}/2)\,\mathrm{Im}\,(AF^* - CE^*)$
$I_0 A^{xB}_{21} = -i(\sqrt{6}/4)\,\mathrm{Im}\,(-AD^* + BF^* + BE^* - CD^*)$

If we apply on (5.19) parity conservation (5.7) and Pauli principle (5.9) with

$$d^J_{mn}(\theta) = (-1)^{m-n} d^J_{-m-n}(\theta) \tag{5.20}$$

we find the two following relations

$$f^{\alpha\beta}_{\gamma}(J) = f^{-\alpha-\beta}_{-\gamma}(J) \tag{5.21}$$

$$f^{\alpha\beta}_{\gamma}(J) = (-1)^{J+\alpha-\beta} f^{\beta\alpha}_{\gamma}(J) \tag{5.22}$$

It is then easy to give the explicit series

$$A(\theta) = \sum_{k=1}^{\infty} \frac{4k+1}{4\P} a_{2k} d^{2k}_{01}(\theta) \tag{5.23}$$

$$B(\theta) = \sum_{k=0}^{\infty} \frac{4k+1}{4\P} b_{2k} d^{2k}_{00}(\theta) \tag{5.24}$$

$$C(\theta) = \sum_{k=1}^{\infty} \frac{4k+1}{4\P} c_{2k} d^{2k}_{0-1}(\theta) \tag{5.25}$$

$$D(\theta) = \sum_{k=0}^{\infty} \frac{4k+3}{4\P} d_{2k+1} d^{2k+1}_{-10}(\theta) \tag{5.26}$$

$$E(\theta) = \sum_{J=1}^{\infty} \frac{2J+1}{4\P} e_J d^J_{-11}(\theta) \tag{5.27}$$

$$F(\theta) = \sum_{J=1}^{\infty} \frac{2J+1}{4\P} (-1)^{J+1} e_J d^J_{11}(\theta) \tag{5.28}$$

See the synoptical Table 13 for $J \leq 4$.

The connection between our partial waves and the more usual $l-s$ coupled states in the non-relativistic limit is given by (see Refs. [20], [50])

$$f^{\alpha\beta}_{\gamma}(J) = \sum_{l_i s_i l_f s_f} \langle J l_f s_f \mid J\gamma 0\rangle \langle J l_i s_i \mid J\alpha\beta\rangle l^{l_i s_i}_{l_f s_f}(J) \tag{5.29}$$

where $\langle Jls \mid J\alpha\beta\rangle$ is the Clebsch–Gordon product

$$(-1)^{s-s_b+\alpha} \langle s_a \alpha,\, s_b - \beta \mid s\alpha - \beta\rangle \langle s\beta - \alpha,\, J\alpha - \beta \mid l0\rangle.$$

Table 13
Coefficients of the partial wave decompositions of the amplitudes with $J < 5$.

	J				
Amplitude	0	1	2	3	4
A	0	0	5/4¶	0	9/4¶
B	1/4¶	0	5/4¶	0	9/4¶
C	0	0	5/4¶	0	9/4¶
D	0	3/4¶	0	7/4¶	0
E	0	3/4¶	5/4¶	7/4¶	9/4¶
F	0	3/4¶	−5/4¶	7/4¶	−9/4¶

The $l^{l_i s_i}_{l_f s_f}(J)$ are the partial waves in the spin-orbit $(l-s)$ representation normalised as the $f^{\alpha\beta}_{\gamma}(J)$.

If we apply the parity conservation and the Pauli principle on the $l^{l_i s_i}_{l_f s_f}(J)$, one obtains the two well-known relations:

$$l^{l_i s_i}_{l_f s_f}(J) = -(-1)^{l_i + l_f} l^{l_i s_i}_{l_f s_f}(J) \tag{5.30}$$

$$l^{l_i s_i}_{l_f s_f}(J) = 0 \quad \text{if} \quad (-1)^{l_i + s_i} = -1 \tag{5.31}$$

where the minus sign in (5.30) reflects the negative pion parity. These two last formulae give all the possible transitions in the $pp \to d\P$ system: they are listed in Table 14.

Writing explicitly equation (5.29) one obtains Table 15. From this table we can deduce that the B amplitude is purely singlet, the D and E amplitudes are purely triplet and A and C mix singlet and triplet states in such a way that $A + C$ is purely singlet and $C - A$ purely triplet.

To end this section, we remember that, to relate the partial waves (5.19) to the measured observables, one has to use the relations given in Table 11 and 12, to convert them from CM to LAB as in equation (1.49) and lastly to insert all these equations in equations (3.23) to (3.26).

5.3. *Other formalisms*

a) *Foroughi's formalism.* We refer to Fig. 3 for the definition of Foroughi's helicity reference frames. The application of the transformation described in section 1.5 gives us (right hand side defined as in Ref. [31] to [33]):

$$F^{\alpha\beta}_{\gamma}(\theta_d) = (-1)^{3/2+\alpha+2\beta} i H_{\gamma,\alpha\beta}(\theta_\P) \tag{5.32}$$

i.e.

$$A = -iM_1 \tag{5.33}$$

Table 14
Allowed $l-s$ transitions in a $pp \to d\pi^+$ system.

Transition	$J^\P$	l_i	s_i	l_f	s_f
$^1S_0 \to p_0$	0^+	0	0	1	1
$^3P_1 \to s_1$	1^-	1	1	0	1
$^3P_1 \to d_1$	1^-	1	1	2	1
$^3P_2 \to d_2$	2^-	1	1	2	1
$^1D_2 \to p_2$	2^+	2	0	1	1
$^1D_2 \to f_2$	2^+	2	0	3	1
$^3F_2 \to d_2$	2^-	3	1	2	1
$^3F_3 \to d_3$	3^-	3	1	2	1
$^3F_3 \to g_3$	3^-	3	1	4	1
$^3F_4 \to g_4$	4^-	3	1	4	1
$^1G_4 \to f_4$	4^+	4	0	3	1
$^1G_4 \to h_4$	4^+	4	0	5	1
$^3H_4 \to g_4$	4^-	5	1	4	1

Table 15
Connection between the partial waves as defined in equation 5.19 with the $l-s$ partial waves in $J<5$.

$J=0$ $b_0 = f_0^{1/2\,1/2}(0) = (-1/\sqrt{2})({}^1S_0 \to p_0)$

$J=1$ $d_1 = -f_0^{1/2\,-1/2}(1) = \sqrt{1/6}\,({}^3P_1 \to s_1) - \sqrt{1/3}\,({}^3P_1 \to d_1)$

$e_1 = f_{-1}^{1/2\,-1/2}(1) = (-\sqrt{1/6})({}^3P_1 \to s_1) - \sqrt{1/12}\,({}^3P_1 \to d_1)$

$J=2$ $a_2 = f_1^{1/2\,1/2}(2) = \sqrt{1/2}\,[\sqrt{3/10}({}^1D_2 \to p_2) + \sqrt{1/5}\,({}^1D_2 \to f_2)]$
$-\sqrt{1/10}\,({}^3P_2 \to d_2) + \sqrt{3/20}({}^3F_2 \to d_2)$

$b_2 = f_0^{1/2\,1/2}(2) = \sqrt{1/5}\,({}^1D_2 \to p_2) - \sqrt{3/10}\,({}^1D_2 \to f_2)$

$c_2 = f_{-1}^{1/2\,1/2}(2) = \sqrt{1/2}\,[\sqrt{3/10}\,({}^1D_2 \to p_2) + \sqrt{1/5}\,({}^1D_2 \to f_2)]$
$+\sqrt{1/10}\,({}^3P_2 \to d_2) - \sqrt{3/20}\,({}^3F_2 \to d_2)$

$e_2 = f_{-1}^{1/2\,-1/2}(2) = \sqrt{1/2}\,[\sqrt{3/10}\,({}^3P_2 \to d_2) + \sqrt{1/5}\,({}^3F_2 \to d_2)]$

$J=3$ $d_3 = -f_0^{1/2\,1/2}(3) = \sqrt{3/14}\,({}^3F_3 \to d_3) - \sqrt{2/7}\,({}^3F_3 \to g_3)$

$e_3 = f_{-1}^{1/2\,-1/2}(3) = -\sqrt{1/7}\,({}^3F_3 \to d_3) - \sqrt{3/28}\,({}^3F_3 \to g_3)$

$J=4$ $a_4 = f_1^{1/2\,1/2}(4) = [\sqrt{5/36}\,({}^1G_4 \to f_4) + \sqrt{1/9}\,({}^1G_4 \to h_4)]$
$-\sqrt{1/9}\,({}^3F_4 \to g_4) + \sqrt{5/36}\,({}^3H_4 \to g_4)$

$b_4 = f_0^{1/2\,1/2}(4) = \sqrt{2/9}\,({}^1G_4 \to f_4) - \sqrt{5/18}\,({}^1G_4 \to h_4)$

$c_4 = f_{-1}^{1/2\,1/2}(4) = [\sqrt{5/36}\,({}^1G_4 \to f_4) + \sqrt{1/9}\,({}^1G_4 \to h_4)]$
$+\sqrt{1/9}\,({}^3F_4 \to g_4) - \sqrt{5/36}\,({}^3H_4 \to g_4)$

$e_4 = f_{-1}^{1/2\,-1/2}(4) = \sqrt{5/36}\,({}^3F_4 \to g_4) + \sqrt{1/9}\,({}^3H_4 \to g_4)$

$$B = -iS \tag{5.34}$$

$$C = -iM_4 \tag{5.35}$$

$$D = iT_6 \tag{5.36}$$

$$E = iT_3 \tag{5.37}$$

$$F = -iT_2 \tag{5.38}$$

Helicity partial waves amplitudes are related by

$$f_\gamma^{\alpha\beta}(J) = (-1)^{3/2+J+2\alpha+\beta}\,4\pi\,h^J_{\gamma,\alpha\beta} \tag{5.39}$$

And the $l-s$ waves by:

$$l^{l_i s_i}_{l_f 1}(J) = 4¶(-1)^{J-s_i} s^{J s_i}_{l_i l_f} \tag{5.40}$$

See Table 16a also.

b) *Locher's formalism.* Here we refer to Refs [4], [6], [51], [52]: in these papers the same convention as in Ref. [31] is used but with different normalisations. One then obtains

$$F_\gamma^{\alpha\beta}(\theta_d) = i(-1)^{3/2+\alpha+2\beta} C\, M^S_{\gamma,\alpha\beta}(\theta_\pi) \tag{5.41}$$

with

$$C = \frac{m}{4¶}\sqrt{\frac{k}{sp}}$$

i.e.

$$A = -iC\phi_1 \tag{5.42}$$

$$B = -iC\phi_2 \tag{5.43}$$

$$C = -iC\phi_3 \tag{5.44}$$

$$D = iC\phi_5 \tag{5.45}$$

$$E = -iC\phi_6 \tag{5.46}$$

$$F = -iC\phi_4 \tag{5.47}$$

Helicity partial wave amplitudes are related by

$$f_\gamma^{\alpha\beta}(J) = (-1)^{3/2+J+2\alpha+\beta}\, 2\pi i\, C\, M^J_{\gamma,\alpha\beta} \tag{5.48}$$

and the $l-s$ waves by

$$l^{l_i s_i}_{l_f 1}(J) = (-1)^{l_i}\, 2¶i\, C\, M^J_{l_i s_i l_f} \tag{5.49}$$

where m, s, p, k are the proton mass, the usual Mandelstam variable, the proton and the pion CM momenta, respectively.

See Tables 16b and 17 also.

c) *Bugg's and Watari's formalism.* Here we refer essentially to [5], [53], [54] for Bugg and to [55] for Watari.

Both use the same normalisation and same sign conventions (Ref. [6]), the connection with our definitions is given by

$$l^{l_i s_i}_{l_f 1}(J) = i(-1)^{l_i}\left(\frac{-4¶}{p}\right)a_J \tag{5.50}$$

Table 16
Relation between our helicity partial waves and Foroughi's helicity partial waves in a), and in b) with Locher's ones. Both have $J<5$. Q is defined as $=(im/2)\sqrt{k/sp}$.

a)	b)
$a_2 = -2¶(MS(2)+MT(2))$	$a_2 = -Q\phi_1^2$
$a_4 = -2¶(MS(4)+MT(4))$	$a_4 = -Q\phi_1^4$
$b_0 = -4¶S(0)$	$b_0 = -Q\phi_2^0$
$b_2 = -4¶S(2)$	$b_2 = -Q\phi_2^2$
$b_4 = -4¶S(4)$	$b_4 = -Q\phi_2^4$
$c_2 = -2¶(MS(2)-MT(2))$	$c_2 = -Q\phi_3^2$
$c_4 = -2¶(MS(4)-MT(4))$	$c_4 = -Q\phi_3^4$
$d_1 = 4¶T_6(1)$	$d_1 = Q\phi_5^1$
$d_3 = 4¶T_6(3)$	$d_3 = Q\phi_5^3$
$e_1 = 4¶T_3(1)$	$e_1 = -Q\phi_6^1$
$e_2 = -4¶T_3(2)$	$e_2 = Q\phi_6^2$
$e_3 = 4¶T_3(3)$	$e_3 = -Q\phi_6^3$
$e_4 = 4¶T_3(4)$	$e_4 = Q\phi_6^4$

Table 17
Relation between our $l-s$ partial waves, Locher's and Bugg's ones. Q' is defined as $=(-4\pi/P)$ and Q as $=(im/2)\sqrt{k/sp}$.

Transition	This work	Locher	Bugg
$^1S_0 \to p_0$	$l_1^{00}(0)$	QM_{011}^0	$Q'a_0$
$^3P_1 \to s_1$	$l_0^{11}(1)$	$-QM_{110}^1$	$-Q'a_1$
$^3P_1 \to d_1$	$l_2^{11}(1)$	$-QM_{112}^1$	$-Q'a_3$
$^3P_2 \to d_2$	$l_2^{11}(2)$	$-QM_{112}^2$	$-Q'a_4$
$^1D_2 \to p_2$	$l_1^{20}(2)$	QM_{201}^2	$Q'a_2$
$^1D_2 \to f_2$	$l_3^{20}(2)$	QM_{203}^2	$Q'a_7$
$^3F_2 \to d_2$	$l_2^{31}(2)$	$-QM_{312}^2$	$-Q'a_5$
$^3F_3 \to d_3$	$l_2^{31}(3)$	$-QM_{312}^3$	$-Q'a_6$
$^3F_3 \to g_3$	$l_4^{31}(3)$	$-QM_{314}^3$	$-Q'a_9$
$^3F_4 \to g_4$	$l_4^{31}(4)$	$-QM_{314}^4$	$-Q'a_{10}$
$^1G_4 \to f_4$	$l_3^{40}(4)$	QM_{403}^4	$Q'a_8$
$^1G_4 \to h_4$	$l_5^{40}(4)$	QM_{405}^4	$Q'a_{13}$
$^3H_4 \to g_4$	$l_4^{51}(4)$	$-QM_{514}^4$	$-Q'a_{11}$

where $J=\{J, l_i, s_i, l_f\}$ and a_J extends the Mandl and Regge definitions (Ref. [22]). See Table 17 too.

For amplitudes and observables Bugg uses the same conventions as Foroughi (see Ref. [31] and Ref. [5]).

d) *Blankleider's formalism.* We refer here to [34], [56], [57] for Blankleider, to Refs [22], [58] for, respectively, Mandl and Regge and Dolnick and to [5] to establish the connection; then, we will have

$$l_{l_f 1}^{l_i s_i}(J) = i(-1)^{l_i+s_i}\sqrt{\frac{2\P}{5}}\sqrt{\frac{1}{2l_i+1}}a_J \tag{5.51}$$

where $J=\{J, l_i, s_i, l_f\}$ and a_J represent the Blankleider's $l-s$ partial waves.

VI. Experimental amplitude determination

6.1. *How to obtain a complete experimental set*

6.1.1. *Theoretical approach*

In the following paragraph in order to solve the bilinear equations of the amplitudes we summarise the results of Refs. [59] to [62].

Let us consider a scattering process involving four particles ($\mu=1, 2, 3, 4$), each of them with angular momentum j_μ. The process is then completely described by $N=\sum_\mu (2j_\mu+1)$ amplitudes $F_{m_1 m_2 m_3 m_4}$.

Any experimental quantity is given, as discussed in the precedent chapter, by the linear combinations of products of type $F_{m_1 m_2 m_3 m_4} F^*_{m_1' m_2' m_3' m_4'}$: we have therefore N^2 linearly independent measurements at a given energy and angle. In

fact only $2N-1$ real quantities are necessary to uniquely determine the N^2 measurements because at each angle $(F_{m_1m_2m_3m_4}F^*_{m_1'm_2'm_3'm_4'})^* = F_{m_1'm_2'm_3'm_4'}F^*_{m_1m_2m_3m_4}$ and the overall phase cannot be determined.

Let S_1 be the set containing some particles, and let S_2 be a second similar set; let E_{S_i} be the general space of the particles in the set S_i; let α and β be two new signs to denote all the possible combination of the quantum number m_i, for $i \in S_1$ and $i \in S_2$, respectively; then we can examine the two following cases.

A) Let S_1 and S_2 be such that $S_1 \cap S_2 = \varnothing$; then the set of the amplitudes $F_{m_1m_2m_3m_4} = F_{\alpha\beta}$ can be written as a mapping $F: E_{S_2} \to E_{S_1}$, where F is a non squared matrix; then the most general measurement involving unpolarised particles S_2, is of the form

$$A^{(S_1)}_{\alpha\alpha'} = \sum_{\beta} F_{\alpha\beta}F^*_{\alpha'\beta} \tag{6.1}$$

i.e. in a matrix representation:

$$A^{(S_1)} = FF^+ \tag{6.2}$$

Conversely, if S_1 is the set of the unpolarised particles, we shall have:

$$A^{(S_2)}_{\beta\beta'} = \sum_{\alpha} F_{\beta\alpha}F^*_{\beta'\alpha} \tag{6.3}$$

i.e.

$$A^{(S_2)} = F^+F \tag{6.4}$$

$A^{(S_i)}$ give us the maximum information available from such measurements.

We see immediately that if F is a solution of (6.2) and (6.4) simultaneously, then $F' = UF$ is also a solution if F is unitary and $[U, A^{(S_2)}] = 0$; such a unitary matrix exists and forms a continuous set since $A^{(S_2)}$ is hermitian.

This implies the following necessity statement: if no phase shift analysis is performed, the set of measurements given by $S_1 \cup S_2$ is insufficient to determine the scattering amplitudes if $S_1 \cap S_2 = \phi$.

B) However, Ref. [60] has proved the following theorem: if there are no more than four particles with non-zero spin in a reaction, then it is possible to completely determine the amplitudes up to a free phase from measurements involving the polarisation of no more than two particles at a time.

We come here to a very important assertion (Thm 10.1 Ref. [60]): for the case of three non-zero spin particles, if we define $S_{(ab)}$ the set containing the particles a and b, and similarly $S_{(bc)}$, we can say that $\{A^{(S_{(ab)})}, A^{(S_{(bc)})}\}$ completely determine the amplitudes, and no discrete ambiguities are possible if all measurements of this set are performed.

Even if parity rules are applied, this assertion remains true (cfr. Lemma 3.1 Ref. [60]). One exception is examined in Ref. [61], but it is irrelevant in our case.

This means that, if in the $pp \to d\P^+$ reaction we performed all the correlation measurements between the protons, and all the transfer polarisation measure-

ments for instance between the beam proton and the scattered deuteron, we would obtain a complete set of experiments in the sense that we can unambiguously determine the scattering amplitudes of the reaction up to a free phase.

One must remark that the uniqueness of the determination of the amplitudes depends not only on the set of performed measurements but also on the actual values of the amplitudes and of the experimental data, as well, of course, on the error bars of the measurements; conversely, even if the amplitudes are not singular, a singularity might lie near them, which can imply large errors in the determination of some amplitudes even if the experiments are exact.

6.1.2. *Our experimental approach*

In the $pp \to d\P^+$ reaction we have eleven real parameters to determine at each angle, and we have measured 17 experimental quantities, i.e. the cross-section, 6 correlations and asymmetries and 10 εs; but we do not know the 4 analysing powers: this means that we have to solve 17 equations with 15 unknown parameters, so we have too little redundancy. But this unpleasant situation can be improved by the following remarks:

1) In Section 6.2 we shall give reasons to believe that $T^{20} \approx 0$. In this case $\varepsilon_c(+y)$ becomes redundant with $\varepsilon_c(-y)$ and $\varepsilon_{2c}(+y)$ redundant with $\varepsilon_{2c}(-y)$ (see equations (3.23) to (3.26) and (1.37) to (1.44); this means that we have only 15 independent experiments for 14 unknown parameters.

2) If we accept the impulse approximation, we can impose $T^{21} = 0$: in this case we shall have only 13 unknown parameters.

3) Fortunately, using equations (1.51) to (1.57), equations (1.37) to (1.44), equation (1.50), equations (3.23) to (3.26) and equation (5.10), at a given θ_{CM} we can also correlate the εs measured in $\theta' = \theta_{\mathrm{LAB}}(\pi - \theta_{\mathrm{CM}})$ with the set of observables calculated at $\theta = \theta_{\mathrm{LAB}}(\theta_{\mathrm{CM}})$. This means that in half of the CM angular range one has 27 experiments for 11 amplitudes + 4 analysing powers at deuteron LAB energy $\theta_{\mathrm{LAB}}(\theta_{\mathrm{CM}}) + 4$ analysing powers at $\theta_{\mathrm{LAB}}(\pi - \theta_{\mathrm{CM}})$. Thus there are 19 parameters to be determined.

Moreover if we also suppose that $T^{20} = 0$, we then have 23 independent experiments for 17 parameters as discussed above in 1). All further analysis will be performed using this last approach [i.e. putting $T^{20} = 0$ and assuming that all observables are symmetric about 90 °CM].

The difficult problems we shall encounter are that we do not have starting values for the minimisation, we do not have a symmetric range around 90°, which reduces the effective range for the amplitude reconstruction, and lastly the data of the correlation experiments are not measured at the same θ.

6.1.3. *Overall phase*

To end this section it is interesting to recall what is known about the overall indeterminate phase. In fact this phase is exactly defined at each angle by

unitarity, i.e. by solving the following integral equation system:

$$F_{\substack{\alpha\to\alpha' \\ \sigma\to\sigma'}}(k\to k') + F^*_{\substack{\alpha'\to\alpha \\ \sigma'\to\sigma}}(k'\to k) = \sum_{\beta\tau}\int dk''\, F_{\substack{\alpha\to\beta \\ \sigma\to\tau}}(k\to k'') \times F^*_{\substack{\beta\to\alpha' \\ \tau\to\sigma'}}(k''\to k') \quad (6.5)$$

where F is a generalised scattering amplitude and α, α', β indicate the channels of the reaction (e.g. $\alpha, \alpha', \beta \in \{pp, d\P^+, p\P^+n, pp\P^\circ\}$ for us); k, k', k'' are the momenta of the reactions, σ, σ', τ describe the spin status of each channel (see Ref. [63]). It can be demonstrated that there exists a solution. In fact this system of equations shows how some channels are correlated with the others.

But, inside one given reaction, this overall phase definition remains insignificant at each angle (see formula (1.19). We decide then to fix the overall phase such that the phase of A (see equation (5.10)) will be zero at each angle, and this without loss of generality.

6.2. $d^{12}C$ *analysing powers*

The first difficulty encountered in this analysis is the fact that hardly anything is known about the analysing powers of dX reactions. Our present knowledge in the 155 to 355 MeV energy range can easily be summarised.

At lower energies (about 30 to 50 MeV) one finds the reaction $^3\mathrm{He}(d, p)^4\mathrm{He}$ well studied and useful, for example, to study the t_{20} deuteron tensor polarisation (see, e.g., Ref. [64]).

Closer to our energy domain studies of Refs. [65], [66] and [17] made in 1956, 1959 and 1984, respectively, are available. Reference [65] studied the energy range between 94 to 157 MeV and did not find any tensor component of the deuteron polarisation in scattering off the nuclei C, Al, Cu, Li. However, Ref. [66] studied deuterons of 410 and 420 MeV scattered from Be and C, and the tensor components of polarisation were determined to be appreciably different from zero (for example at about 10° $iT_{11} \sim 40\%$, $T_{22} \sim -20\%$, $T_{21} \sim 20\%$, $T_{20} \sim -40\%$ in the notation of the Ref. [66]). More recently, Ref. [17] found at 191 MeV $T_{20} \sim 0\%$, $T_{22} \sim -2\%$ and at 395 MeV $T_{20} \sim -8\%$ and $T_{22} \sim -22\%$ (these last values in the notation of Ref. [17]).

Unfortunately, all these measurements are irrelevant to our experimental conditions, but they seem to indicate that:

a) there exists a rapid increase of the tensor analysing powers with deuteron incident energy: at low energy it is expected to be close to zero, but above 200 MeV appears to be significantly different from zero.

b) the impulse approximation is not a good model for this reaction (only iT_{11} is satisfactorily reproduced in Ref. [66]).

c) no information is really given about T^{21}; it is reasonable to assume that $T^{20} < 8\%$, i.e. not really measurable in our experiment because its contribution is then of the same order of magnitude as the statistical errors.

d) from the comparison between data and calculations in Ref. [66] we can conclude that T^{11} in $d^{12}C$ scattering has a similar behaviour as the analysing power A_y in $p^{12}C$ scattering.

We shall use for our analysing powers (defined in equation (4.1)) the following formalism in analogy with Ref. [45], for the $p^{12}C$ reaction:

$$T^{kq}(E_{\mathrm{LAB}}) = (AA_{kq} + BA_{kq}\delta + CA_{kq}\delta^2 + DA_{kq}\delta^3 + EA_{kq}\delta^4) \\ /(1 + CE_{kq} \exp\{-[(\delta - AE_{kq})/BE_{kq}]\}) \quad (6.6)$$

where $\delta = (E_{\mathrm{LAB}} - 251.35\,\mathrm{MeV})/100$ (251.35 MeV is the center of our energy range), and AE, BE, CE, AA, BA, CA, DA, EA are the coefficients to be determined in an energy dependent analysis.

6.3. *The partial wave analysis*

The second difficult problem we meet is the choice of the starting points for the minimisation procedure. It is a crucial problem due to the complicated shape of our χ^2 function, as we have to deal with linear combinations of products of unknown parameters (amplitudes and analysing powers). We found that purely random starting points often gave secondary minima which led to crazy results: for instance the connection between one angle and the next one was not easy to establish for the amplitudes and, moreover, a coherent energy dependence for the analysing powers was practically impossible to obtain.

We therefore decided to first study the $pp \to d\P^+$ reaction globally, using the data at the three energies all together, making use of a partial wave energy-independent analysis with $J \leq 4$ (see equations (5.23) to (5.28)) with a global constraint on the analysing powers such that they have the energy-dependence as given by equation (6.6). This will provide us with reasonable starting values for the direct amplitude reconstruction.

To do this we used the data of Refs. [67], [68], [9] for the differential cross-section, of Refs. [29], [8] for the correlation parameters, and the measured ε. These give a total of 860 experimental points with the following distribution:

Energy	Spin-correlation and cross-section	ε
447 MeV	108	160
515 MeV	92	160
580 MeV	140	200

We have analysed these data using a gradient method in the context of the MINUIT routine (Ref. [69]) according to the following procedure:

a) As a first step we minimise the partial waves (with $J \leq 4$) only on the correlations parameters and the cross-sections separately for each energy and using random starting points: after convergence we ended with a set of 10 different minima at each energy with a very good χ^2 value.

b) As a second step, we fixed the partial waves at each energy to the values found in a), and we fitted only the ε at all the three energies together and

imposing the energy dependent analysing powers of equation (6.6): the aim was to obtain a certain number of starting points for the analysing powers parameters.

c) In the third and last step, all the parameters were left free: but, due to MINUIT constraints, we cannot operate with more than 55 parameters at a time.

In fact we have 25 parameters at each energy to describe the partial wave dependence (with $J \leq 4$) and 22 parameters to describe the analysing powers, i.e. 97 parameters in total.

After convergence one finds 2 independent minima: solution 1 (sol. 1) with $\chi^2 = 3007$, and solution 2 (sol. 2) with $\chi^2 = 2737$. In fact, in (sol. 1), 49 points contribute with 1380 to the χ^2, and, in sol. 2, 48 points contribute with 930. If we remove these points one finds for sol. 1 a $\chi^2 = 1627$ for 811 points and 97 parameters, which gives a $\chi^2/d.f. = 2.28$, and for sol. 2 $\chi^2 = 1807$ for 812 points, i.e. $\chi^2/d.f. = 2.53$.

These numbers are just given as an indication of the quality of the fit, no further fitting was done after removal of the points which gave a big contribution to the χ^2.

For the sol. 1 these large contributions to the χ^2 are essentially given by the backward region of $\varepsilon_c(+y)$, $\varepsilon_{2s}(X)$, $\varepsilon_{2c}(\pm y)$, $\varepsilon_{2c}(0)$ at 447 MeV, and by the backward region of $\varepsilon_{2c}(\pm y)$, $\varepsilon_{2c}(0)$ at 580 MeV.

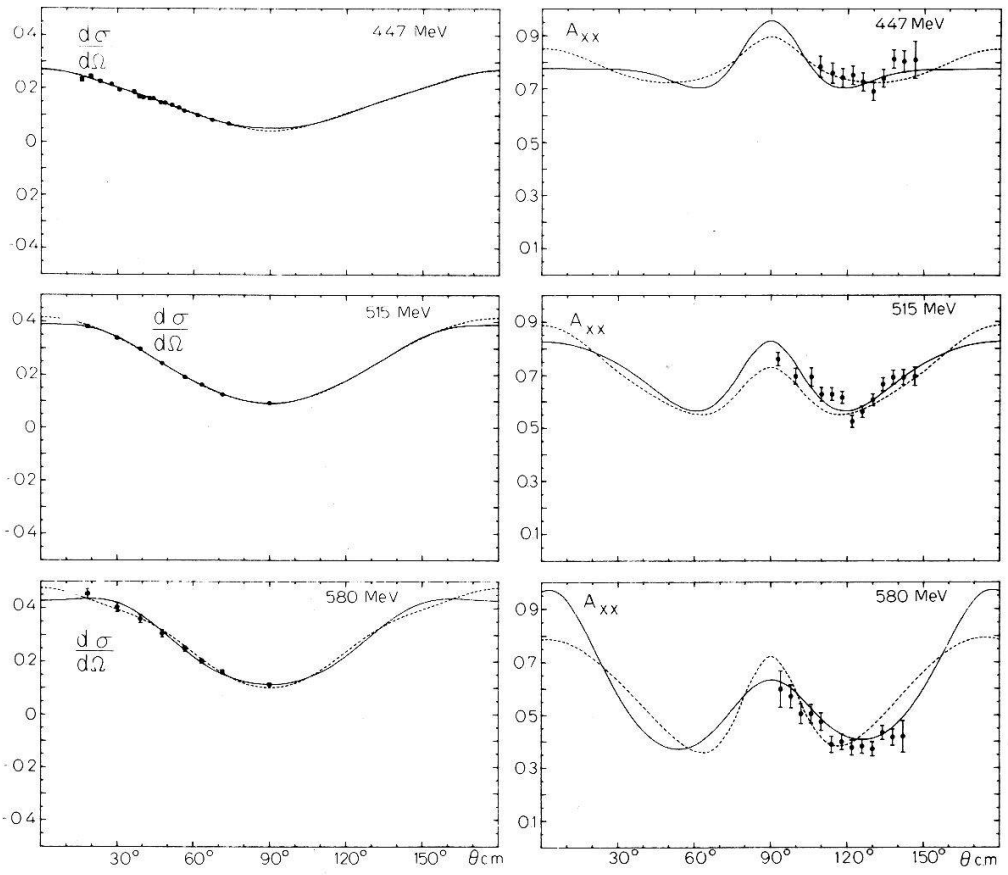

Figure 11
Plot of used differential cross-section and correlation parameter A_{xx}[29][8] at 447, 515 and 580 MeV as a function of the deuteron c.m. scattering angle. The full and dotted lines are the 2 solutions obtained in the partial wave decomposition analysis with $J < 5$ (sol. 1 and sol. 2 respectively).

For sol. 2 the highest contributions are given by the backward $\varepsilon_{2c}(\pm y)$, $\varepsilon_{2c}(0)$, $\varepsilon_s(X)$, the forward $\varepsilon_s(Z)$ at 447 MeV, the backward $\varepsilon_{2c}(\pm y)$, $\varepsilon_{2c}(0)$ and all the $\varepsilon_s(X)$ at 515 MeV.

Figures 7 to 10 show how the two solutions fit the various ε, the continuous line representing sol. 1 and the dashed one sol. 2.

Figures 11 to 13 show how the same solutions fit the cross-sections and the correlations parameters. Open circles for the A_{xz} parameters at 515 and 580 MeV are taken from Ref. [68] but these were not used in the analysis.

In Table 18 are listed the values of the partial waves for sol. 1 and sol. 2. One notices that Im b_0 has been fixed to 0, but not the two other partial waves contributing to the B amplitude as allowed by the general considerations developed in Section 6.1.3, to allow more freedom to find the right minimum. But the calculated amplitude values which are given in Figs 14 to 16 (continuous line sol. 1, short dashed line sol. 2) have the phase of A defined equal to be zero at each angle: this is possible because of the overall phase freedom at each angle. This provides an easy way to compare the phase values at different angles.

We are insensitive to T^{20} value, due essentially to the fact that the ε are small in absolute value, which implies that the corrections in the denominator of these ε (see equations (3.23) to (3.36)) are of the same order of magnitude as the statistical errors.

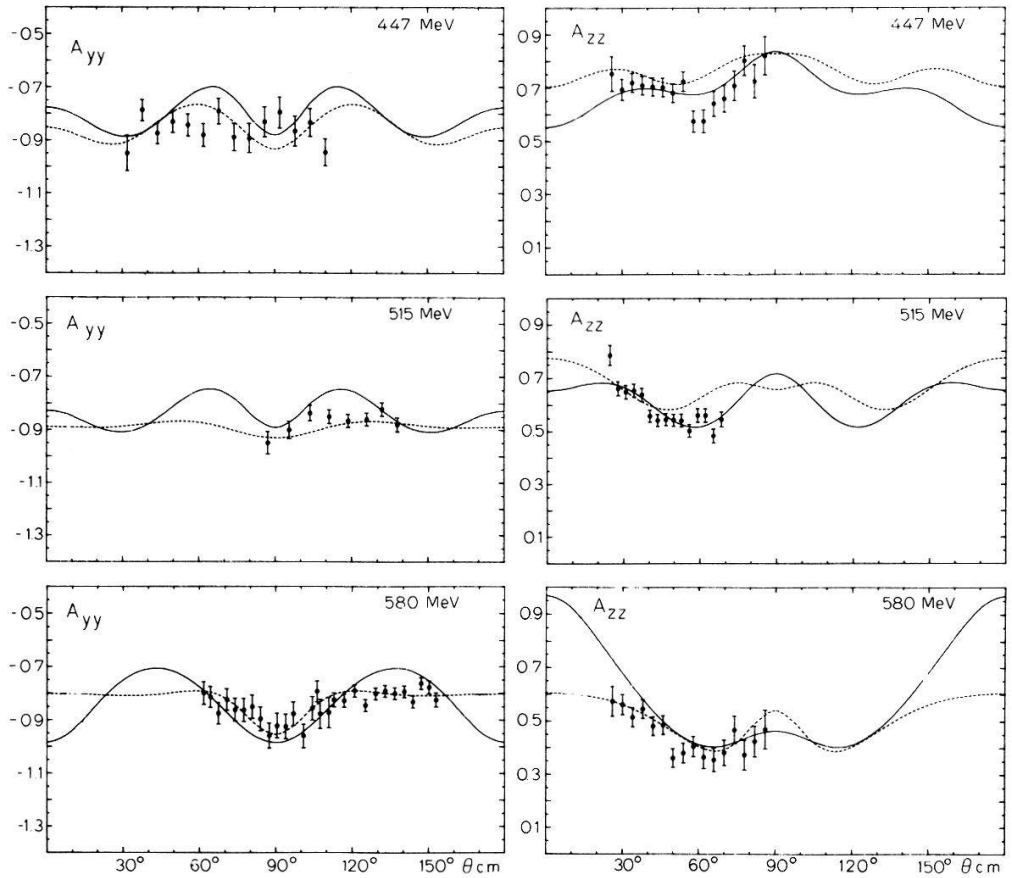

Figure 12
Same as Fig. 11 but for the correlation parameters A_{yy} and A_{zz} [29][8].

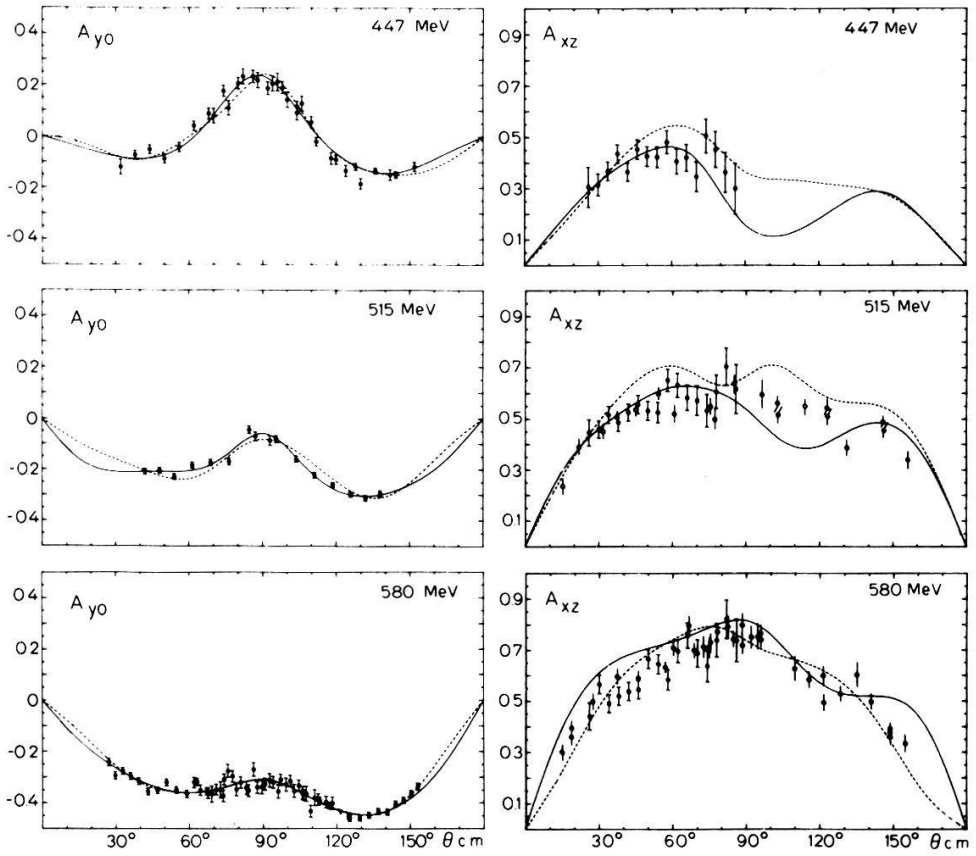

Figure 13
Same as Fig. 11 but for the correlation parameters A_{xz} and asymmetry A_{y0} [29] [8]. The open circles are from Ref. [68] but were not used in the analysis.

6.4. *Direct amplitude reconstruction*

Using the symmetry relations around 90° cm as described in paragraph 6.1.2, one can now perform an angle independant amplitude reconstruction at each energy using as starting points the two solutions (sol. 1–sol. 2) found previously. In fact the angular point close to 90° cm (i.e. 87.5° cm) was treated in a somewhat different way for the following reasons: a) there is an ambiguity in the analyzing powers definitions at 90° cm at a given proton energy due to simplification of the equations, b) the deuteron kinetic energy differs only by about 6 MeV between the two data set symmetrized around 90° cm (namely 87.5° cm and 92.5° cm). We therefore have assumed equal analyzing powers at these two angles, providing an extra 3 degrees of freedom in the fit.

Before starting the fit, some of the experimental data values had to be recalculated for exactly symmetric θ_d values around 90° cm. At 447 and 515 MeV, we have done a linear interpolation of the ε_s' values centered on the wanted angle value, the statistical errors being also interpolated. For the cross-sections and spin correlation measurements, an interpolation was made based on free partial wave analysis performed without introducing the ε's measurements; the errors are calculated as for those on the ε's.

The amplitude analysis was then performed on these values using as starting

Table 18
Numerical values for the partial waves for the 2 solutions sol. 1 and sol. 2 at 447, 515 and 580 MeV for completeness. But we believe that sol. 1 is the good one to consider.

		447 MeV	515 MeV	580 MeV
Sol. 1	RE a_2	0.508 ± 0.044	0.138 ± 0.111	0.400 ± 0.330
	IM a_2	1.521 ± 0.030	2.047 ± 0.026	2.529 ± 0.056
	RE a_4	0.300 ± 0.026	0.395 ± 0.027	0.148 ± 0.041
	IM a_4	-0.139 ± 0.018	-0.011 ± 0.037	0.180 ± 0.020
	RE b_0	1.709 ± 0.038	1.663 ± 0.096	0.540 ± 0.107
	IM b_0	0.000 ± 0.000	0.000 ± 0.000	0.000 ± 0.000
	RE b_2	0.569 ± 0.037	0.213 ± 0.065	0.314 ± 0.260
	IM b_2	1.011 ± 0.040	1.554 ± 0.055	2.081 ± 0.032
	RE b_4	0.368 ± 0.020	0.482 ± 0.037	0.235 ± 0.037
	IM b_4	-0.321 ± 0.021	-0.066 ± 0.025	0.034 ± 0.023
	RE c_2	0.101 ± 0.049	0.022 ± 0.093	0.039 ± 0.138
	IM c_2	1.056 ± 0.018	1.371 ± 0.020	0.985 ± 0.017
	RE c_4	0.369 ± 0.031	0.504 ± 0.033	0.162 ± 0.022
	IM c_4	0.014 ± 0.021	0.176 ± 0.042	-0.076 ± 0.030
	RE d_1	-0.396 ± 0.025	-0.633 ± 0.022	-0.316 ± 0.078
	IM d_1	-0.472 ± 0.022	-0.214 ± 0.038	0.386 ± 0.040
	RE d_3	-0.081 ± 0.018	-0.204 ± 0.036	-0.477 ± 0.094
	IM d_3	-0.368 ± 0.014	-0.607 ± 0.018	-0.701 ± 0.065
	RE e_1	0.570 ± 0.021	0.661 ± 0.037	0.633 ± 0.088
	IM e_1	0.167 ± 0.040	0.575 ± 0.051	0.680 ± 0.082
	RE e_2	-0.058 ± 0.022	-0.223 ± 0.028	-0.337 ± 0.043
	IM e_2	0.201 ± 0.022	0.058 ± 0.019	-0.340 ± 0.040
	RE e_3	0.123 ± 0.013	0.086 ± 0.031	-0.261 ± 0.066
	IM e_3	-0.222 ± 0.017	-0.423 ± 0.013	-0.455 ± 0.045
	RE e_4	0.013 ± 0.015	0.020 ± 0.015	0.035 ± 0.017
	IM e_4	0.149 ± 0.013	0.161 ± 0.013	0.083 ± 0.016
Sol. 2	RE a_2	0.296 ± 0.039	0.366 ± 0.033	-2.271 ± 0.027
	IM a_2	0.214 ± 0.032	0.034 ± 0.038	0.129 ± 0.032
	RE a_4	0.266 ± 0.031	0.045 ± 0.024	-0.067 ± 0.019
	IM a_4	-0.042 ± 0.022	0.114 ± 0.023	0.090 ± 0.032
	RE b_0	5.287 ± 0.056	6.909 ± 0.025	4.867 ± 0.055
	IM b_0	0.000 ± 0.000	0.000 ± 0.000	0.000 ± 0.000
	RE b_2	0.595 ± 0.024	0.763 ± 0.013	0.514 ± 0.024
	IM b_2	-0.388 ± 0.080	-0.201 ± 0.075	-0.118 ± 0.032
	RE b_4	-0.080 ± 0.018	-0.022 ± 0.008	0.391 ± 0.017
	IM b_4	-0.223 ± 0.029	-0.151 ± 0.029	0.135 ± 0.007
	RE c_2	-0.284 ± 0.046	-0.342 ± 0.042	-1.020 ± 0.019
	IM c_2	-0.156 ± 0.035	-0.007 ± 0.034	-0.324 ± 0.021
	RE c_4	0.215 ± 0.030	0.201 ± 0.034	-0.166 ± 0.012
	IM c_4	0.120 ± 0.026	-0.138 ± 0.018	-0.007 ± 0.020
	RE d_1	-0.624 ± 0.023	-1.417 ± 0.018	-1.076 ± 0.011
	IM d_1	-0.061 ± 0.012	0.394 ± 0.020	0.054 ± 0.010
	RE d_3	-0.214 ± 0.019	-0.341 ± 0.013	0.069 ± 0.014
	IM d_3	0.125 ± 0.012	0.195 ± 0.017	-0.166 ± 0.011
	RE e_1	0.111 ± 0.044	-0.001 ± 0.038	-0.809 ± 0.030
	IM e_1	-0.102 ± 0.044	-0.385 ± 0.030	0.856 ± 0.021
	RE e_2	0.240 ± 0.040	0.091 ± 0.034	0.444 ± 0.024
	IM e_2	0.356 ± 0.026	0.330 ± 0.021	-0.562 ± 0.017
	RE e_3	0.162 ± 0.019	0.210 ± 0.018	0.417 ± 0.017
	IM e_3	-0.058 ± 0.018	-0.140 ± 0.017	-0.106 ± 0.013
	RE e_4	0.167 ± 0.018	0.192 ± 0.018	0.035 ± 0.013
	IM e_4	0.092 ± 0.018	-0.002 ± 0.019	-0.046 ± 0.008

values for the amplitudes and analysing powers the values found in sol. 1 and sol. 2. As a result, only one viable solution was found: either both points converged to the same minimum or one was clearly better than the other. A study, also showed that the analysis was highly insensitive to the T^{20} analyzing power. Imposing T^{20} to zero did not, in fact, increase the χ^2/d.f. significantly and this allowed us to decrease the number of unknowns to 17. A summary of the χ^2 values obtained at each angle in this condition is given in Table 19.

In order to facilitate comparison with other calculations, the amplitudes are given in a polar representations e.g. $A = |A| \exp(i\phi_A)$ where the phases are taken relative to A. At each angle an overall phase remains impossible to be determined by any polarization experiment. This phase is fixed by the convention $\phi_A = 0$. Figures 14 to 16 show the results for the 6 amplitudes as solid points. The dashed lines are theoretical calculations based on relativistic perturbation theory by M. Locher (Refs. [4] and [70]) at 450, 508 and 578 MeV, and these appear to be in good agreement. In general one observes a very smooth energy dependence behaviour for the moduli as well as for the norms. Numerical values for the phases and moduli are given in Tables 20–21.

Results for the 3 carbon analyzing powers have been regrouped in ≃20 MeV energy bin size. These are shown in Fig. 17 as black circles. The open circles are results from Ref. [17] in our formalism and for the same deuteron angular range (5°–20° lab). The numerical values are listed in Table 22.

As a final remark, we note that if T^{21} is imposed to zero, as suggested by our results, the χ^2 value increases by a factor 2, but the amplitudes remain stable. We can conclude from this analysis that the spin correlation parameters impose severe constraints on the search for a minimum χ^2.

6.5. *Triplet state contribution*

From the comparison of our results with Locher's prediction, one can make the following remarks using Table 15.

Table 19
Summary of the χ^2 contribution as a function of the deuteron scattering angle, separately for the three energies 447, 515 and 580 MeV. For the 87.5° point marked as *, the number of degree of freedom was 13 instead of 10.

$\theta_{c.m.}$[deg]	447 MeV	515 MeV	580 MeV
52.5	12	22	18
57.5	8	38	29
62.5	26	15	18
67.5	20.3	17	11
72.5	16	9	12
77.5	9.2	7.6	6.3
82.5	8.9	1.3	11
87.5*	20.5	14.8	28.0
Total χ^2	120.9	124.7	133.3
χ^2/d.f.	1.46	1.50	1.61

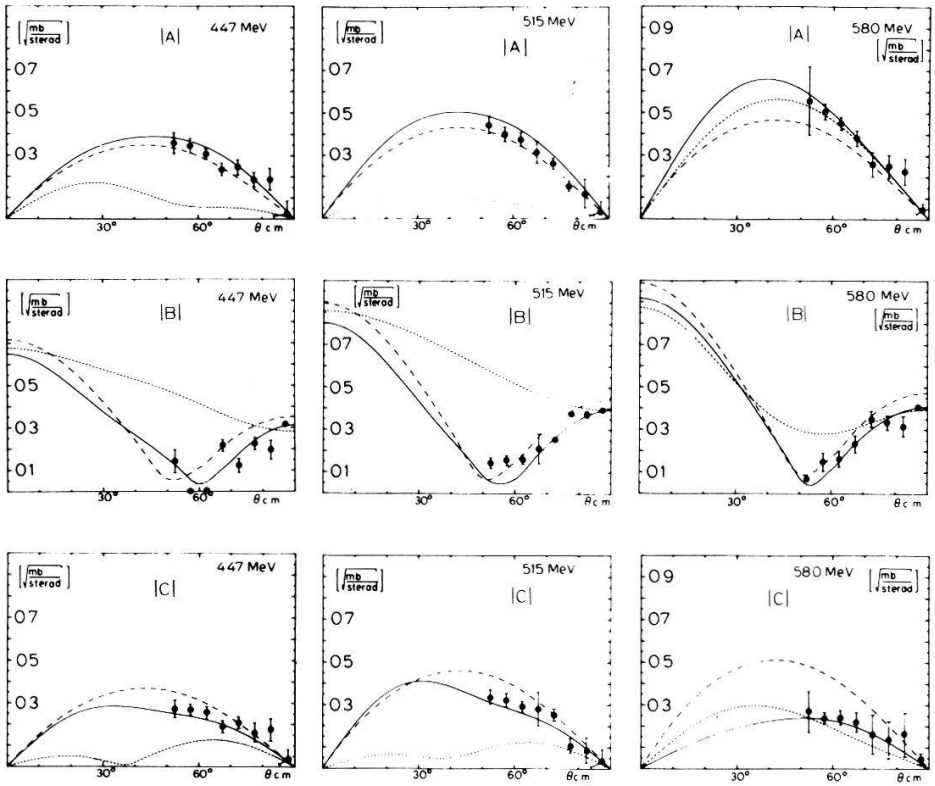

Figure 14
Moduli of the amplitudes *A*, *B*, *C* at 447, 515 and 580 MeV. The full and dotted lines are our 2 partial wave analysis solutions referred as sol. 1 and sol. 2 respectively for illustration, but we believe that the solution found in the amplitude analysis is the good one. The dashed line is the theoretical prediction by Locher [[4] and [70]].

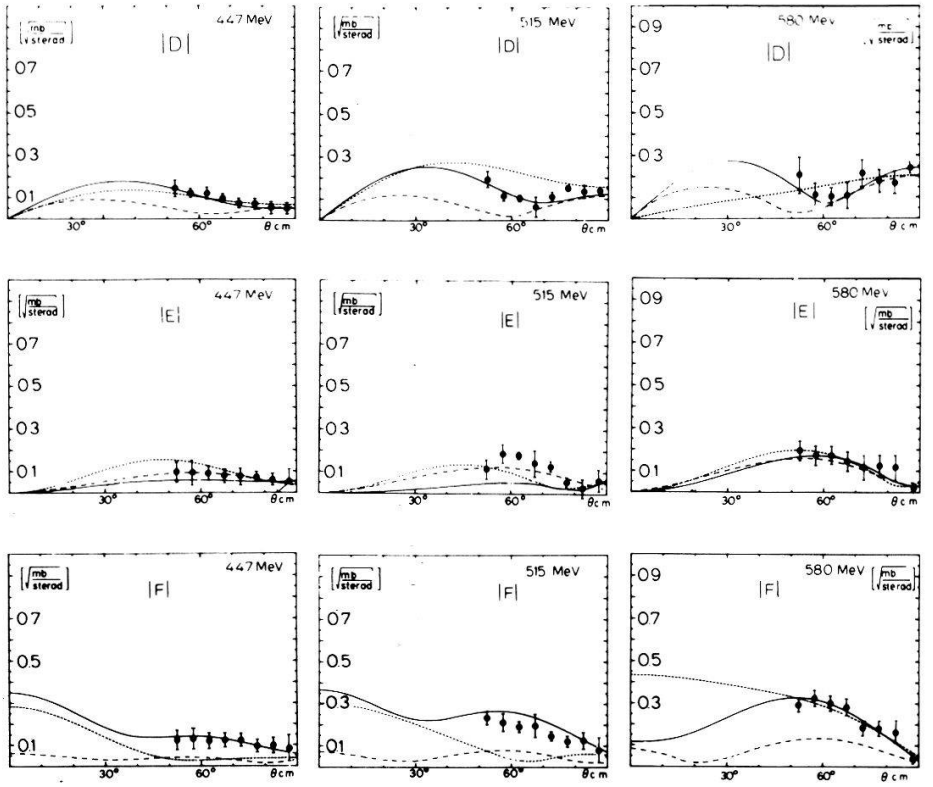

Figure 15 Same as Fig. 14 but for amplitudes *D*, *E* and *F*.

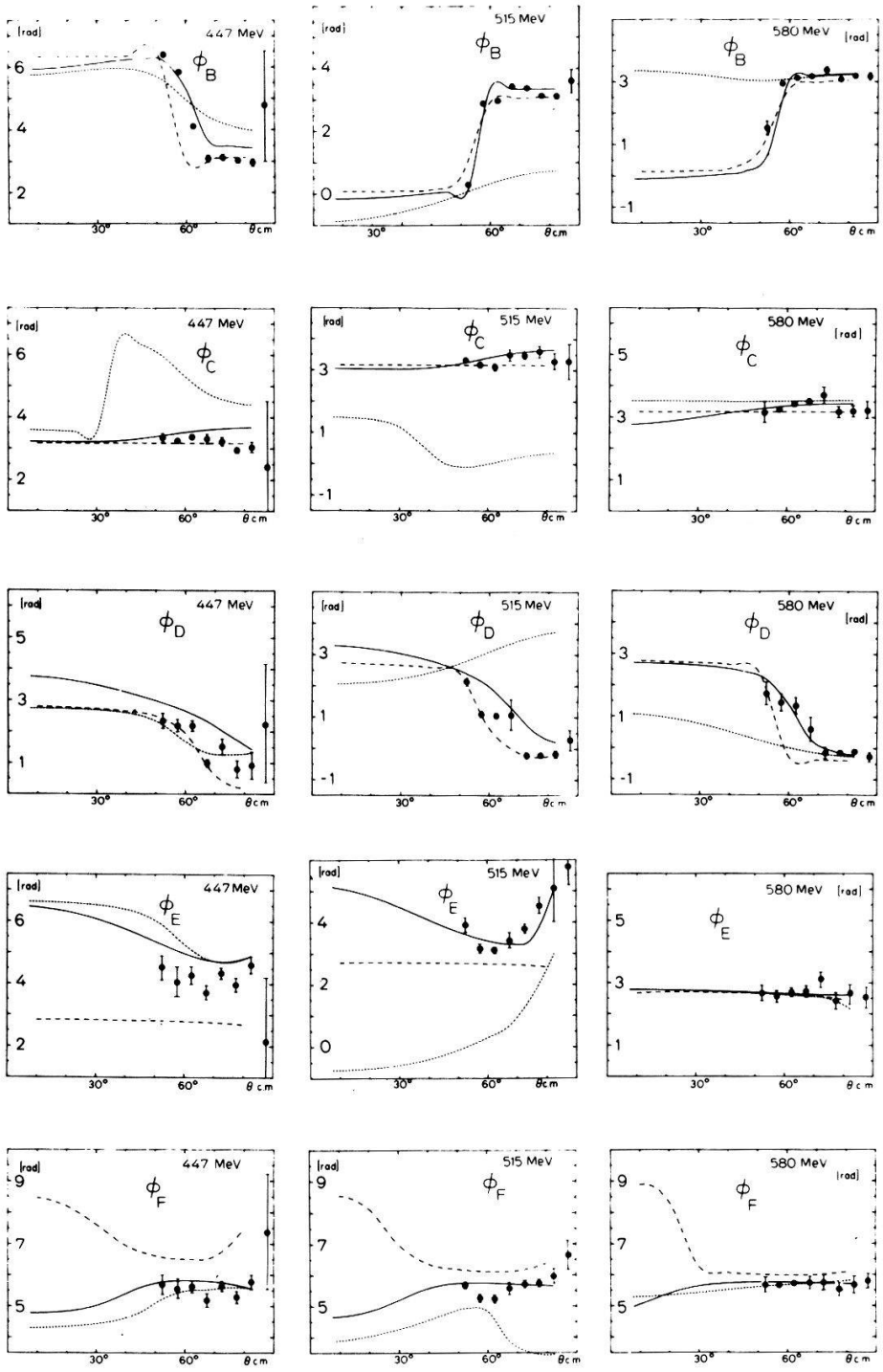

Figure 16
Phases of the 6 complex amplitudes at 447, 515 and 580 MeV. The other symbols are defined in Fig. 14.

1. If one looks in details into the 6 amplitudes, one notices that for the D, E and F amplitudes only triplet states contributes, but for A, B and C singlet and triplet states are present but dominated by the singlet $^1D_2$.

2. If triplets are negligible, one obtains the symmetry relation $A = -C$. One notices in Fig. 14 that this symmetry is broken as the energy increases. On the other hand Locher's calculations follow better this relation.

Table 20
Numerical values of the moduli of the reconstructed scattering amplitudes at the three energies. Units are $\sqrt{\text{mb/sterad}}$.

T[MeV]	θ_{cm}[deg]	$\|A\|$	$\|B\|$	$\|C\|$	$\|D\|$	$\|E\|$	$\|F\|$
447	52.5	0.36 ± 0.05	0.14 ± 0.06	0.27 ± 0.04	0.14 ± 0.04	0.10 ± 0.05	0.12 ± 0.05
	57.5	0.35 ± 0.03	0.00 ± 0.01	0.27 ± 0.03	0.12 ± 0.03	0.09 ± 0.07	0.13 ± 0.05
	62.5	0.31 ± 0.03	0.00 ± 0.01	0.25 ± 0.03	0.12 ± 0.03	0.09 ± 0.04	0.12 ± 0.04
	67.5	0.23 ± 0.03	0.22 ± 0.02	0.19 ± 0.03	0.10 ± 0.02	0.08 ± 0.03	0.12 ± 0.03
	72.5	0.24 ± 0.04	0.12 ± 0.04	0.21 ± 0.03	0.07 ± 0.03	0.07 ± 0.04	0.12 ± 0.03
	77.5	0.19 ± 0.04	0.22 ± 0.03	0.16 ± 0.05	0.07 ± 0.03	0.07 ± 0.03	0.09 ± 0.03
	82.5	0.19 ± 0.05	0.20 ± 0.05	0.17 ± 0.06	0.05 ± 0.03	0.06 ± 0.03	0.10 ± 0.04
	87.5	0.02 ± 0.06	0.32 ± 0.01	0.04 ± 0.05	0.05 ± 0.03	0.05 ± 0.06	0.09 ± 0.06
515	52.5	0.44 ± 0.05	0.14 ± 0.03	0.33 ± 0.03	0.20 ± 0.04	0.12 ± 0.05	0.23 ± 0.03
	57.5	0.40 ± 0.04	0.16 ± 0.03	0.32 ± 0.03	0.12 ± 0.03	0.19 ± 0.05	0.21 ± 0.04
	62.5	0.37 ± 0.04	0.16 ± 0.03	0.29 ± 0.03	0.11 ± 0.02	0.18 ± 0.02	0.19 ± 0.03
	67.5	0.31 ± 0.06	0.21 ± 0.07	0.28 ± 0.08	0.06 ± 0.05	0.14 ± 0.07	0.20 ± 0.06
	72.5	0.26 ± 0.02	0.25 ± 0.01	0.25 ± 0.03	0.11 ± 0.02	0.13 ± 0.02	0.15 ± 0.02
	77.5	0.15 ± 0.02	0.38 ± 0.01	0.11 ± 0.03	0.15 ± 0.02	0.06 ± 0.02	0.12 ± 0.02
	82.5	0.12 ± 0.07	0.37 ± 0.02	0.09 ± 0.06	0.14 ± 0.04	0.03 ± 0.05	0.12 ± 0.04
	87.5	0.04 ± 0.05	0.39 ± 0.01	0.04 ± 0.06	0.14 ± 0.02	0.06 ± 0.05	0.09 ± 0.05
580	52.5	0.56 ± 0.16	0.07 ± 0.01	0.27 ± 0.10	0.20 ± 0.09	0.19 ± 0.05	0.29 ± 0.04
	57.5	0.51 ± 0.04	0.15 ± 0.05	0.24 ± 0.03	0.11 ± 0.06	0.17 ± 0.05	0.32 ± 0.04
	62.5	0.45 ± 0.03	0.16 ± 0.04	0.24 ± 0.04	0.10 ± 0.05	0.17 ± 0.05	0.30 ± 0.04
	67.5	0.38 ± 0.04	0.23 ± 0.04	0.22 ± 0.05	0.11 ± 0.07	0.14 ± 0.05	0.28 ± 0.04
	72.5	0.26 ± 0.06	0.35 ± 0.04	0.16 ± 0.09	0.21 ± 0.07	0.12 ± 0.06	0.18 ± 0.04
	77.5	0.25 ± 0.06	0.33 ± 0.04	0.14 ± 0.08	0.18 ± 0.06	0.12 ± 0.05	0.18 ± 0.04
	82.5	0.22 ± 0.07	0.31 ± 0.05	0.16 ± 0.10	0.17 ± 0.06	0.12 ± 0.07	0.17 ± 0.06
	87.5	0.05 ± 0.02	0.41 ± 0.02	0.05 ± 0.02	0.24 ± 0.03	0.02 ± 0.02	0.04 ± 0.02

Table 21
Numerical values of the phases of the reconstructed scattering amplitudes for the three energies. Units are radians with $[0 \leq \phi \leq 2\pi]$.

T[MeV]	θ_{cm}[deg]	ϕ_B[rad]	ϕ_C[rad]	ϕ_D[rad]	ϕ_E[rad]	ϕ_F[rad]
447	52.5	0.13 ± 0.09	3.34 ± 0.14	2.34 ± 0.24	4.52 ± 0.39	5.69 ± 0.31
	57.5	5.86 ± 0.03	3.24 ± 0.03	2.18 ± 0.16	4.00 ± 0.52	5.55 ± 0.30
	62.5	4.10 ± 0.03	3.37 ± 0.08	2.18 ± 0.17	4.27 ± 0.29	5.62 ± 0.19
	67.5	3.09 ± 0.10	3.32 ± 0.16	0.99 ± 0.11	3.73 ± 0.22	5.20 ± 0.17
	72.5	3.12 ± 0.09	3.23 ± 0.13	1.52 ± 0.25	4.35 ± 0.18	5.64 ± 0.16
	77.5	3.02 ± 0.08	2.95 ± 0.09	0.80 ± 0.28	3.98 ± 0.22	5.29 ± 0.20
	82.5	2.96 ± 0.12	3.04 ± 0.17	0.92 ± 0.43	4.62 ± 0.27	5.77 ± 0.23
	87.5	4.74 ± 1.84	2.47 ± 2.01	2.27 ± 1.88	2.18 ± 2.01	1.11 ± 1.86
515	52.5	0.29 ± 0.04	3.34 ± 0.05	2.14 ± 0.13	3.92 ± 0.24	5.68 ± 0.11
	57.5	2.88 ± 0.06	3.18 ± 0.09	1.11 ± 0.09	3.17 ± 0.15	5.27 ± 0.13
	62.5	2.96 ± 0.08	3.10 ± 0.11	1.06 ± 0.09	3.11 ± 0.10	5.24 ± 0.13
	67.5	3.44 ± 0.09	3.48 ± 0.18	1.09 ± 0.49	3.43 ± 0.25	5.57 ± 0.20
	72.5	3.38 ± 0.05	3.49 ± 0.08	6.07 ± 0.05	3.81 ± 0.12	5.73 ± 0.07
	77.5	3.13 ± 0.03	3.61 ± 0.16	6.08 ± 0.04	4.56 ± 0.26	5.77 ± 0.10
	82.5	3.11 ± 0.09	3.29 ± 0.25	6.12 ± 0.12	5.09 ± 1.07	5.97 ± 0.23
	87.5	3.60 ± 0.36	3.28 ± 0.65	0.30 ± 0.37	5.78 ± 0.61	0.35 ± 0.51
580	52.5	1.52 ± 0.22	3.18 ± 0.34	1.74 ± 0.36	2.67 ± 0.25	5.67 ± 0.23
	57.5	2.94 ± 0.04	3.26 ± 0.04	1.46 ± 0.28	2.55 ± 0.19	5.65 ± 0.09
	62.5	3.12 ± 0.04	3.43 ± 0.08	1.36 ± 0.26	2.70 ± 0.15	5.69 ± 0.09
	67.5	3.16 ± 0.03	3.50 ± 0.10	0.61 ± 0.38	2.72 ± 0.18	5.66 ± 0.09
	72.5	3.38 ± 0.11	3.71 ± 0.27	6.14 ± 0.18	3.11 ± 0.22	5.85 ± 0.20
	77.5	3.08 ± 0.07	3.18 ± 0.18	6.15 ± 0.07	2.42 ± 0.27	5.50 ± 0.14
	82.5	3.20 ± 0.05	3.21 ± 0.15	6.19 ± 0.08	2.66 ± 0.34	5.60 ± 0.22
	87.5	3.16 ± 0.09	3.31 ± 0.22	5.96 ± 0.10	2.52 ± 0.29	5.83 ± 0.25

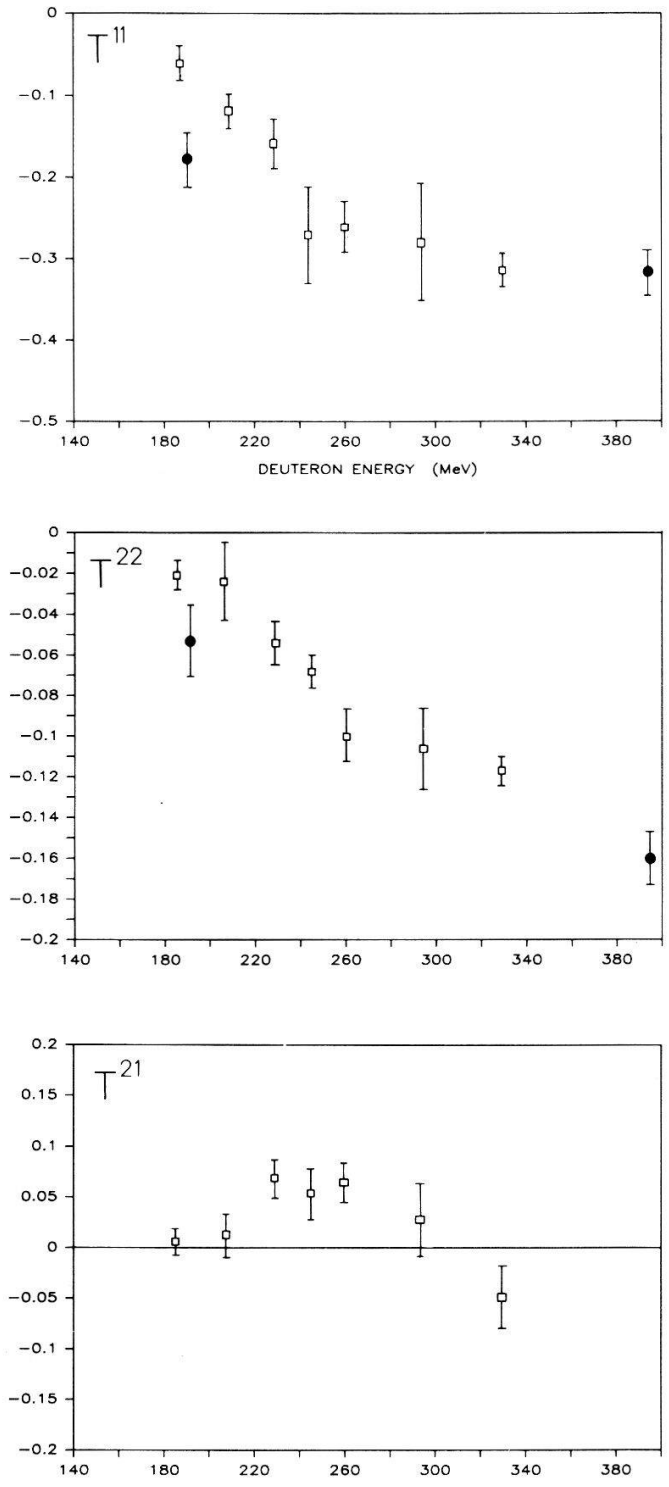

Figure 17
Deuteron-Carbon analyzing powers T^{11}, T^{22} and T^{21} as a function of the deuteron kinetic energy in MeV. The full circles are taken from Ref. [17]. As mentioned in paragraph 1.6 our definition of deuteron analyzing power is a factor of 2 larger than the one in Ref. [22].

Table 22
Numerical values for the 3 carbon analyzing powers T^{11}, T^{21} and T^{22} as a function of the deuteron laboratory energy. As mentioned in paragraph 1.6 our definition of deuteron analyzing power is a factor 2 larger than the one in Ref. [22] (see eq. 3.15 to 3.22).

T_d(MeV)	T^{22}	T^{21}	T^{11}
185	-0.02 ± 0.01	0.01 ± 0.02	-0.06 ± 0.02
209	-0.02 ± 0.02	0.01 ± 0.02	-0.12 ± 0.02
228	-0.05 ± 0.01	0.07 ± 0.02	-0.16 ± 0.03
244	-0.07 ± 0.01	0.05 ± 0.03	-0.27 ± 0.06
260	-0.10 ± 0.02	0.07 ± 0.02	-0.26 ± 0.03
295	-0.11 ± 0.02	0.03 ± 0.04	-0.28 ± 0.07
330	-0.12 ± 0.01	-0.05 ± 0.03	-0.31 ± 0.02

3. If triplet states are underestimated, the norm of amplitude F will be too small (see Fig. 15).

From remarks 2) and 3) one can conclude that in Locher's calculations the triplet states are underestimated. From a study of solution 1 one gets the following contributions as illustrated below.

	447	515	580	MeV
$^3P_2 \rightarrow d_2$	0.413	0.597	1.810	$\sqrt{mb/sr}$
$^3F_2 \rightarrow d_2$	0.642	0.597	0.548	$\sqrt{mb/sr}$
$(c_2 - a_2)/2$	0.310	0.343	0.793	$\sqrt{mb/sr}$
e_2	0.209	0.230	0.479	$\sqrt{mb/sr}$

VII. Conclusion

We have demonstrated that a double scattering experiment, to measure the vector and tensor polarisation of the scattered deuteron in the $pp \rightarrow d\P$ reaction can be performed, producing important and useful results. This is due essentially to the excellent polarimeter of our group, together with a good knowledge of its properties resulting from its long use in pp elastic scattering experiments.

The significant non zero asymmetries (especially for $\cos\phi_C$ and $\cos 2\phi_C$) prove that the dominant analysing powers T^{11} and T^{22} are non zero for $d^{12}C$ scattering. Unfortunately the non-existence of measured analysing powers imply that a more sophisticated analysis was necessary to obtain a complete knowledge of the $pp \rightarrow d\P^+$ observables.

Three years after the first direct reconstruction of the scattering amplitudes of the elastic scattering channel $pp \rightarrow pp$ (see Refs. [42] and [43]), it has been possible to do the same type of analysis in the inelastic channel $pp \rightarrow d\P^+$ at three different energies, and this independently of any theoretical input.

At the same time, analysing powers evaluations of T^{11}, T^{22}, T^{21} for $d^{12}C$ scattering have been done for the first time over a wide energy range. Unfortunately, it was not possible to obtain useful information on T^{20}.

An astonishing agreement for the $pp \to d\pi$ amplitudes is observed with Locher's work. This is extremely satisfactory as the approaches are completely different and independent. This adds confidence to the results for the analysing powers that we have obtained.

We have demonstrated that $pp \to d\P^+$ is no longer an inaccessible reaction, and that the $d^{12}C$ analysing powers are sufficiently different from zero to deserve being systematically measured and used.

To end this work we ask an ingenuous question: why do the amplitudes in both the pp elastic and $pp \to d\P^+$ systems have so flat an angle and energy behaviour but need such a complicated microscopical description to explain them?

Acknowledgements

We would like to thank the Swiss Institute for Nuclear Research for its invaluable technical assistance during the experiment and express our special gratitude to Professor J.-P. Blaser. We would like to thank Prof. J. Davies for lending us his LH_2 target, as well as G. P. Gregory from the CERN H_2 target group for construcing the appendix. During the course of this program, support from Prof. E. Baumgartner, G. H. Lamot, D. Measday and J. R. Scherrer was greatly appreciated. We also thank Dr. M. Locher for providing us with numerical values of the πd amplitudes as derived from his calculation. We would also like to thank the technical staff of the University of Geneva in particular the electronic (Mr Richeux), mechanical (Mr Perrin), and typing workshops (especially Mrs C. Bayala). This work was supported by the Swiss National Science Foundation and the Convention Intercantonale d'Enseignement du 3e Cycle de la Physique en Suisse Romande and the Computing Service of the Geneva Hospital.

REFERENCES

[1] E. K. Biegert et al., Phys. Lett. *73B* (1978) 235.
[2] I. P. Auer et al., Phys. Rev. Lett. *41* (1978) 354.
[3] W. Watari, Preprint Osaka University OCUPWA-004 (1985).
[4] M. P. Locher and A. Svarc, J. Phys. G: Nucl. Phys. 11, 183 (1985).
[5] D. Bugg, J. Phys. G: Nucl. Phys. *10* (1984) 717.
[6] M. P. Locher, Journal de Physique Colloque C2 Tome *46* (1985), p. C2–319.
[7] K. Seth, Proc. Ins. Int. Conf. on Photonuclear and related Physics, Tokyo 1983.
[8] E. Aprile et al., Nucl. Phys. *A415* (1984) 365.
[9] J. Hoftiezer et al., Nucl. Phys. *A412* (1984) 273 and *A412* (1984) 286.
[10] G. D. Smith et al., Phys. Rev. *C30* (1984) 980.
[11] E. Turpin et al., *Few Body . . .*, Karlsruhe 1983, ed. by B. Zeinitz 1984.
[12] R. D. Tripp, Phys. Rev. *102* (1956) 862.

[13] Yu K. Akimov, Sov. Phys. JEPT *37* (1960) 33.
[14] J. Baldwin et al., Phys. Rev. *103* (1956) 1502.
[15] J. Button and R. Mermod, Phys. Rev. *118* (1960) 1333.
[16] B. H. Silvermann et al., contributed paper to 6th Int. Symp. on High Energy Spin Physics, Marseille, Sept. 1984.
[17] M. Garçon, private communication CENS Feb. 1984.
[18] R. Aprile et al., Phys. Rev. Lett. *46* (1981) 1047.
[19] R. Hausammann, Ph.D. Thesis No 2038, University of Geneva 1982.
[20] M. Simonius, in '*Pol. Nucl. Phys.*', Lect. Notes in Phys. 30, Springer-Verlag (1974).
[21] G.G. Ohlsen, Rep. Progr. Phys. *35* (1967) 727.
[22] F. Mandl and T. Regge, Phys. Rev. *99* (1955) 1478.
[23] L. Darden, Ann. Jour. Phys. *35* (1967) 727.
[24] C. Bourrely, E. Leader, J. Soffer, Phys. Rep. *59* (1980) 95.
[25] B. M. Brink and G. R. Satchler, *Angular momenta,* Oxford University Press (1968).
[26] W. Lakin, Phys. Rev. *98* (1955) 139.
[27] Madison convention, Pol. Phenomena in Nucl. Reaction Univ. Wisconsin Press (1971) p. XXV.
[28] H. P. Stapp, Phys. Rev. *103* (1956) 425.
[29] E. Aprile et al., Nucl. Phys. *A379* (1982) 369.
[30] E. Aprile, Ph.D. Thesis No 2066, University of Geneva (1982).
[31] F. Foroughi, J. Phys. G: Nucl. Phys. *8* (1982) 1345.
[32] F. Foroughi, J. Phys. G: Nucl. Phys. *10* (1984) 617.
[33] F. Foroughi, J. Phys. G: Nucl. Phys. *10* (1984) 617.
[34] B. Blankleider and I. R. Afnan Phys. Rev. *C31* (1984) 1380.
[35] D. Besset et al., Nucl. Instr. Meth. *136* (1976) 331.
[36] D. Besset et al., Phys. Rev. *D21* (1980) 580.
[37] D. Rapin et al., Rapports University of Geneva (1971, 1972).
[38] D. Besset, Ph.D. Thesis No 1882, University of Geneva (1978).
[39] Ph. Sormani Rapport int. University of Geneva (1983).
[40] E. Aprile et al., in *Polarisation Phenomena in Nucl. Phys.* 1980", edited by G. Ohlsen, AIP Cong. Proc. 69, N.Y., 1981.
[41] E. Heer, Int. Communication Version *2*, 79–08.
[42] D. Besset et al., Nucl. Phys. *A345* (1980) 435.
[43] E. Aprile et al., Proc. of the 1981 Top. Conf., CERN Yellow Report 81-07, 124.
[44] E. Aprile et al., Phys. Rev. Lett. *47* (1981) 1360.
[45] D. Rapin, Ph.D. Thesis No 1884, University of Geneva (1979).
[46] B. E. Bonner et al., *Few Body . . .* , Karlsruhe 1983, ed. by B. Zeinitz 1984.
[47] E. Aprile et al., Phys. Rev. D27 (1983) 2600.
[48] M. L. Goldberger and K. M. Watson, *Collision theory* by J. Wiley & Son (1964).
[49] D. M. Brink and G. R. Satchler, '*Angular momentum*', Oxford University Press (1968).
[50] M. Jacob and G. C. Wick, Ann. Phys. (NY) *7* (1959) 404.
[51] W. Grein and M. P. Locher, J. Phys. G: Nucl. Phys. *7* (1981) 1355.
[52] W. Grein et al. Annals of Phys. *153* (1984) 301.
[53] D. Bugg, J. Phys. G: Nucl. Phys. *10* (1984) 47.
[54] D. Bugg, Preprint Queen Mary College, July 1984.
[55] H. Kamo and W. Watari, Prog. Th. Phys. *62* (1979) 1035 and Lett. Nuovo Cimento *29* (1980) 289. H. Kamo et al. Prog. Th. Phys. *64* (1980) 2144. W. Watari, Osaka Report OCUPWA-003 (1983) and OCUPWA-004 (1984).
[56] B. Blankleider, J. Phys. G: Nucl. Phys. *6* (1981) 171.
[57] B. Blankleider, Ph.D. Thesis FIAS-R-72 Nov. 1980.
[58] C. C. Dolnick, Nucl. Phys. *B22* (1970) 461.
[59] M. Simonius, *Theory of polarisation measurements I,* Preprint Feb. 1969 Cargene-Millon University (unpublished).
[60] M. Simonius, '*Theory of polarisation measurements II,* Preprint Feb. 1969.
[61] M. Simonius, Phys. Rev. Lett. *19* (1967) 279.
[62] H. A. Bethe, Ann. Phys. (NY), *3* (1958) 190.
[63] W. O. Amrein, *Non-Relativistic Quantum Dynamics,* in Math. Phys. Studies 2, ed. by D. Reidel Publishing Company, (1981).
[64] E. J. Stephenson et al., Nucl. Instr. and Meth. *178* (1980) 345.
[65] J. Baldwin et al., Phys. Rev. *103* (1956) 1502.

[66] J. BUTTON and R. MERMOD, Phys. Rev. *118* (1960) 1333.
[67] D. AEBISCHER et al., Nucl. Phys. *B106* (1976) 214.
[68] J. HOFTIEZER et al., Nucl. Phys. *A402* (1983) 429.
[69] F. JAMES, MINUIT routine CERN library.
[70] M. P. LOCHER, Private communication Nov. 1985.
[70] M. P. LOCHER, Private communication Nov. 1985.
[71] G. Cantale, PhD thesis n° 2175 (1986) University of Geneva.